Technical Report Documentation Page

1. Report No.	2. Government Accession No.	3. Recipient's Catalog No.
FHWA/TX-97/1338-1F		

4. Title and Subtitle	5. Report Date
RECYCLED CONTENT SIGN BLANKS	October 1996
	6. Performing Organization Code

7. Author(s)	8. Performing Organization Report No.
Paul N. Roschke, Ben F. Harrison IV, and Fred Benson	Research Report 1338-1F

9. Performing Organization Name and Address	10. Work Unit No. (TRAIS)
Texas Transportation Institute The Texas A&M University System College Station, Texas 77843-3135	11. Contract or Grant No. Study No. 0-1338

12. Sponsoring Agency Name and Address	13. Type of Report and Period Covered
Texas Department of Transportation Research and Technology Transfer Office P. O. Box 5080 Austin, Texas 78763-5080	Final: December 1994-September 1996
	14. Sponsoring Agency Code

15. Supplementary Notes

Research performed in cooperation with the Texas Department of Transportation and the U.S. Department of Transportation, Federal Highway Administration.
Research Study Title: Recycled Content Sign Blanks

16. Abstract

This report documents a study of the feasibility of using sign blanks constructed of reclaimed materials instead of conventional high-grade plywood and aluminum. Traditional sign substrates constructed of wood and aluminum currently are not designed according to engineering formulas. Lack of design and analysis procedures integrated with a set of performance specifications has made it difficult to apply results to field tests conducted by various highway departments. This study presents the engineering techniques necessary for judicious use of recycled materials in roadside sign applications.

Various types of recycled materials were solicited from commercial manufacturers and subjected to an array of laboratory tests and numerical simulations. Materials that were received were manufactured from a variety of materials including high-density polyethylene, polycarbonate, polyvinyl chloride, and calcium carbonate. This study discusses analysis, performance, and properties of tested materials. A total of seven recycled materials are tested in flexure, uni-axial tension, creep, free vibration, and exposure to ultraviolet radiation. Corollaries of this study are development of performance-based specifications and a new design procedure for sign blanks.

17. Key Words	18. Distribution Statement
Creep, Deflection, Failure, Finite Element, Nonlinear, Plastic, Plate, Recycled Material, Roadside Safety, Shear, Sign, Strain, Stress, Wind	No restrictions. This document is available to the public through NTIS: National Technical Information Service 5285 Port Royal Road Springfield, Virginia 22161

19. Security Classif.(of this report)	20. Security Classif.(of this page)	21. No. of Pages	22. Price
Unclassified	Unclassified	190	

RECYCLED CONTENT SIGN BLANKS

by

Paul N. Roschke, P.E.
Associate Research Engineer
Texas Transportation Institute

Ben F. Harrison IV
Graduate Research Assistant

and

Fred Benson
Assistant Professor
Texas A&M University at Kingsville

Research Report 1338-1F
Research Study Number 0-1338
Research Study Title: Recycled Content Sign Blanks

Sponsored by the
Texas Department of Transportation
In Cooperation with
U.S. Department of Transportation
Federal Highway Administration

October 1996

TEXAS TRANSPORTATION INSTITUTE
The Texas A&M University System
College Station, Texas 77843-3135

IMPLEMENTATION RECOMMENDATIONS

This report summarizes the results of a research program that evaluates the use of recycled materials in sign blanks for roadside signs. Opportunities for implementation of this research are detailed as follows:

1. The first objective was to write a performance specification for selection of candidate materials. Therefore, it is recommended that these specifications be adopted by TxDOT on an experimental basis.
2. A review of the design procedure for moderate-sized signs (especially checking the wind loads provisions) should be made by one or more engineers from the Design Division. If this procedure is deemed satisfactory, it should be implemented as a provisional standard for the engineering design of medium-sized roadside signs. The procedure should be updated to incorporate new failure criteria observed in field trials before it is updated to serve as a standard for design.
3. TxDOT should consider purchasing a shipment of UV-stabilized recycled sign blank material (preferably a UV-resistant form of GTHW) and manufacturing a large number of signs of various dimensions. These signs should be erected in a variety of geographical and climatic locations around the state. An evaluation of the performance and feasibility of their use should be made after two years of field observation. If in-service performance is judged to be satisfactory, the recycled sign blank material could be upgraded to the status of being an acceptable alternative to marine plywood and aluminum.
4. Other manufacturers of recycled materials should be required to show (through certified laboratory and/or field testing) that they meet or exceed the performance specifications for sign blanks. Trial installations of these materials should also be made in several locations in Texas.

DISCLAIMER

The contents of this report reflect the views of the authors who are responsible for the opinions, findings, and conclusions presented herein. The contents do not necessarily reflect the official views or policies of the Texas Department of Transportation, or the Federal Highway Administration. This report does not constitute a standard, specification, or regulation; it is not intended for construction, bidding, or permit purposes. The engineer in charge of this project is Dr. Paul N. Roschke, P.E. #53889.

ACKNOWLEDGMENT

This study was conducted under a cooperative program between the Texas Transportation Institute, the Texas Department of Transportation, and the Federal Highway Administration. Art Barrow, Rebecca Davio, and Samuel Reyes worked closely with the researchers, and their comments and suggestions are appreciated. Prof. Kishor C. Mehta and the Wind Engineering Research Center at Texas Technological University provided wind data.

TABLE OF CONTENTS

LIST OF FIGURES

LIST OF TABLES

TABLE PAGE

SUMMARY

This report documents a study of the feasibility of using sign blanks constructed of reclaimed materials instead of conventional high-grade plywood and aluminum. The researchers present the engineering techniques necessary for judicious use of recycled materials in roadside sign applications.

Various types of recycled materials were solicited from commercial manufacturers and subjected to an array of laboratory tests and numerical simulations. Materials that were received are manufactured from a variety of materials including high-density polyethylene (HDPE), polycarbonate, polyvinyl chloride, and calcium carbonate. Analysis, performance, and properties of tested materials are discussed. A total of seven recycled materials are tested in flexure, uni-axial tension, creep, free vibration, and exposure to ultraviolet radiation. Corollaries of this study are development of performance-based specifications and a new design procedure for sign blanks.

A preliminary design procedure is developed for two-pole supported and tee-pole supported sign substrates. The procedure is based on simple mechanics of materials bending formulae for a variety of deflection criteria. Design environmental loads are determined using ASCE 7-95 *Minimum Design Loads for Buildings and Other Structures.* A design example for a two-pole sign is performed for one of the recycled materials collected during the study. Adequacy of the preliminary design is checked using a finite element model of the structure in conjunction with a set of performance-based specifications.

Experimental results suggest that complex dynamic responses to wind loads may be closely simulated in a laboratory environment. The researchers have also shown that sign substrates made from recycled materials not only need to be durable for a variety of environmental conditions, but also perform best when they are ductile, efficient, and dissipate energy of vibration at a reasonable rate. A brief listing of estimated costs for some of the recycled materials that were tested in the laboratory is included for quantities varying by order of magnitude from 1,000 to 1,000,000 sheets.

1. INTRODUCTION

1.1 GENERAL

Highway signs are essential in communicating information to motorists. The sign blank, or sign substrate, is the structural element on which information is presented. Texas currently uses blanks for roadside signs made from high-grade plywood and aluminum materials. These signs, similar to those shown in Fig. 1, are currently in use throughout the state. However, costs for sign blanks made from pristine plywood and aluminum are increasing significantly. Moreover, disposal of these materials is contributing to landfill problems.

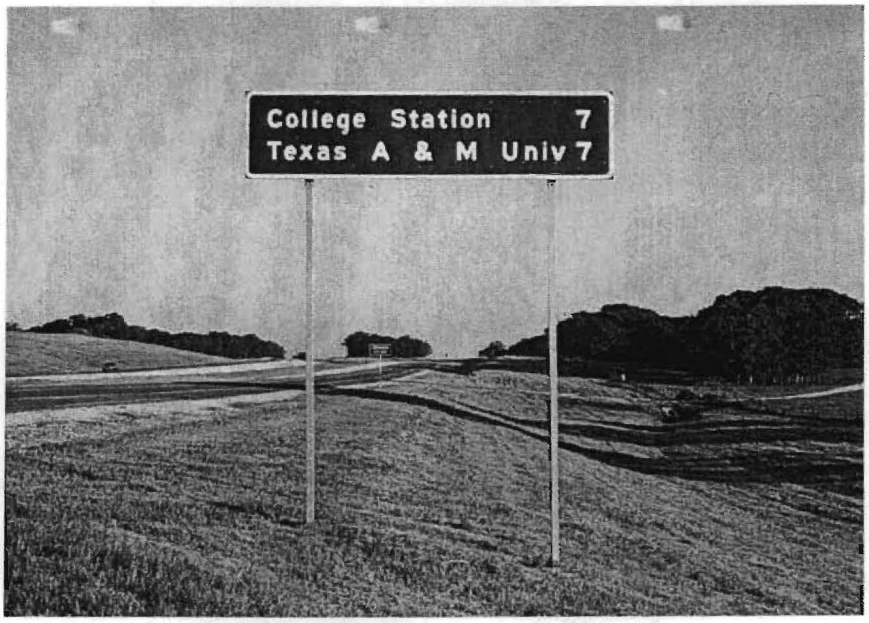

FIG. 1. Typical Roadside Sign Installation

Finding alternative materials for use as sign substrates that can reduce life cycle cost and aid the environment is becoming a high priority. Concomitant with increasing material costs, environmental factors are encouraging the use of recycled materials. If these materials are durable and possess the required performance criteria, their use not only benefits the

environment but also reduces the burden being placed on landfills. Therefore, this study seeks to carry out a comprehensive investigation to identify suitable alternative materials, especially those that are made from previously used materials, for use as sign substrates.

1.2 PRESENT STATUS OF THE QUESTION

A number of current and planned investigations involving recycled materials in various fields of highway engineering are underway. For example, the Federal Highway Administration is funding a study titled "Feasibility of Using Composite Materials in Construction" (FHWA), which seeks to identify commercially available composite and recycled materials that can be used in highway applications. Material properties and manufacturing methods are of special interest. Static and dynamic tests are to be performed on various composite recycled materials in order to establish their suitability for sign supports, frangible couplings, guardrail posts, and blockouts. Temperature effects are to be determined over a range of environments. Creep and long-term dead loads are also being considered. In other applications recycled and composite materials are being investigated for applications in noise walls, pavement additives, drain pipe, and flexible delineator posts (Smith 1996).

Numerous examples exist of the successful introduction of recycled materials into highway safety structures. For example, a recycled material currently in use as an offset block outperforms wood in impact experiments and requires little or no maintenance (Roads 1993). In roadside sign-related studies, the Department of Transportation (DOT) in Utah has been investigating a poly-fibre matrix material that Composite Technologies Corporation produces (Composite 1995). Their study includes extensive field testing of the material. The State of Utah is considering using the material in sign blanks that have a maximum dimension that is less than 1.2 m. The Florida Department of Transportation has an extensive field testing program for materials that are candidates for sign blanks. As described later, manufacturers seeking approval of material for use as a sign substrate in Florida must have a sample placed on a support at a beach that faces the ocean. The material must successfully survive the natural elements for one year.

In an annual report on highway safety programs and the highway environment as it relates to safety the National Safety Council Committee on Roadway Environment

(NSCCRE) reports improvements in traffic signing to have a very high benefit cost ratio (20.9 to 1) (1982). Research programs are underway in many states that seek to find alternative substrates for signs. The ultimate goal is to reduce material and maintenance costs. In response, industries have developed composite materials made of recycled plastic, fiber-reinforced plastics, and alloys made of recycled aluminum.

Two predominantly reclaimed materials have been investigated for use as sign substrates. The first, fiberglass reinforced plastic (FRP), was investigated by Utah. Problems associated with this material are: (1) glass fibers present constructability problems since workers must be protected from the fibers; and (2) delamination occurs after placing the material in the field. The second alternative is unreinforced recycled plastic. This material has not presented the constructability problems associated with FRP substrates; however, cracking due to oscillatory wind loads and creep due to temperature effects are problems. A review of current literature and state transportation departments has revealed that a formal study investigating the use and performance of alternative sign substrate materials has not yet been conducted.

In order to use a recycled material as a sign substrate, a method for determining the required thickness of a particular material must be available. However, the thickness dimension of sign blanks made from marine plywood or aluminum in current use along Texas highways is not designed according to engineering formulas. Rather, specifications to material suppliers are based on field experience over many years of installation. Newer materials, such as recycled plastics, have different properties than the traditional substrates and a database of practical experience is not available. Therefore, it is imperative that tests be conducted to characterize the behavior of several of these new materials. Knowledge of these properties, in turn, enables a design procedure to be developed. In this way a required thickness for a sign that is to be manufactured from virtually any suitable material can be specified. The design procedure should be flexible enough to take into account properties of the material as well as the geometry of the sign and its supports. Once a material has been designed for use as a sign blank, its performance must be analyzed in order to determine if the design is sufficient.

Due to a lack of experience and formal research into the use of recycled content sign blanks coupled with the pressing need to use materials more efficiently, a formal investigation into the design and analysis of recycled content sign blanks needs to be conducted.

1.3 OBJECTIVES AND APPROACH

The primary objective of this study is to develop a procedure by which candidate recycled materials may be evaluated, designed for use as sign blanks, and analyzed. As a first step toward achieving these ends, a thorough review of the literature in this field is conducted and a set of performance specifications is drafted. Following this phase, the four other components of the study are as follows: (1) gather and test materials that are viable candidates, (2) develop and perform a material testing program, (3) develop a design procedure based upon material properties, and (4) develop a laboratory procedure that may be used to analyze the performance of the substrate that has been designed.

In order to achieve the objectives of the research, a comprehensive experimental investigation is necessary. First, a battery of mechanical tests is performed to determine the elastic modulus, material behavior, percent critical damping, creep performance, and environmental effects of candidate materials. Second, a design procedure is derived that specifies the required thickness of the substrate. Finally, a technique for analyzing the design is achieved.

The research presented in this report is essentially a method by which candidate recycled content sign blanks may be compared, designed, and studied. In order to produce a substrate that is efficiently designed, it is necessary to have not only a method by which the design is produced, but also a set of performance based specifications that act as a guide to producing satisfactory sign blanks. When failures in the material occur, the design process and performance specifications may be reviewed and modified in order to accommodate the new criteria. Since sign substrates currently in use in Texas are designed to resist environmental loads based upon past experience instead of engineering analysis, a new design procedure is derived. Results of this investigation are intended to give experimental validity to an alternative design for sign materials.

2. LITERATURE REVIEW AND COMPLEMENTARY INVESTIGATIONS

2.1 INTRODUCTION

Routine operation and maintenance of the nation's highway system requires millions of tons of natural and manufactured construction materials. Environmental concerns arising from the disposal of waste materials generated during routine maintenance, constraints on land use, location of new landfill disposal sites, and increasing costs have necessitated that many state agencies become proactive in developing and implementing procedures for the reuse and recycling of waste materials.

An important candidate for the application of recycled materials is traffic sign substrates. Approximately $250 million is spent each year in maintaining 58 million traffic signs that are spread over 3.8 million miles of roads, streets, and highways in the United States (TRB 1992). Increasing the use of recycled materials for sign substrates could mean significant savings in direct replacement costs and reductions in detrimental environmental effects.

2.2 SIGN SUBSTRATES

In an annual report on highway safety programs and the highway environment as it relates to safety, the NSCCRE reports improvements in traffic signing have a very high cost benefit ratio (20.9 to 1) (1982). Sign vandalism costs taxpayers millions of dollars each year and is a contributing factor in a number of serious traffic accidents. Surveys of state and local agencies indicate that up to 30 percent of all sign repair and replacement is caused by vandalism.

Major reasons for sign deterioration include:

- Clouding and color fading due to exposure to ultraviolet (UV) rays that cause the deterioration of transparent plastic and the disappearance of the metallic layer resulting in loss of retro-reflectivity;
- Cracking due to differences in thermal expansion of materials;
- Delamination and peeling of laminate due to poor adhesion;
- Accumulation of dirt; and
- Vandalism and knockdown.

Signs can lose their property of retro-reflectivity in varying degrees because of accumulation of dirt, fungus, or mildew. A study of highway tort liability by the State of Pennsylvania showed that signing deficiencies are a primary factor for 20 percent of sampled tort actions. Therefore, performance and durability of traffic signs are very important in avoiding costs from tort actions.

Aluminum and wood are the substrates most frequently used for traffic signs. Grades 6061 (heat treatable) and 5052 (non-heat treatable) aluminum alloys are widely used. Currently, grade 3000 aluminum alloys, which are made primarily from recycled aluminum, are also being specified.

2.3 ALTERNATIVE SIGN SUBSTRATES AND MANUFACTURERS

Research programs are underway in many states that are seeking to find alternative substrates for signs. The ultimate goal is to reduce material and maintenance costs. In response, industries have developed composite materials made of recycled plastic, fiber-reinforced plastics, and alloys made of recycled aluminum. State and federal agencies are testing these new substrates in the field. Several industrial responses to these needs are briefly discussed below.

2.3.1 Signs and Blanks, Inc.

Signs and Blanks, Inc. (SABI), has performed research with the goal of using recycled aluminum sign substrates for use at ground level (Signs 1995). Their approach utilizes 3105-H191 grade aluminum that contains more than 99% recycled aluminum of which 80% is from post-consumer scrap. The processing of this material requires only 5% of the energy required to manufacture aluminum signs from ore.

The 3000 series aluminum materials are non-heat treatable, use manganese as the major alloying element, and incorporate magnesium as a secondary alloying element. SABI, considering the worst case scenario, has conducted tests on minimum strength requirements for aluminum signs by using a 91.4 cm octagonal for wind loading. Finite element analysis has shown that the material typically fails at 193.1 MPa. Their study also shows that single support posts fail at a 150 km/hr wind speed, while the recycled aluminum sign can withstand 30% more wind load than the post on which it is mounted.

2.3.2 Composite Technologies Company, Inc.

Composite Technologies Company, Inc. (CTC), is a commercial supplier of sign blanks manufactured from 100% recycled plastic. Polymer Fiber Matrix (PFM), a proprietary product, is comprised of 62% polymer, 35% glass reinforcement, 2% fillers, and 1% additives. Over 80% of the polymer content of the panel is Polyethylene Terapthalate (PET) plastic derived from post consumer beverage bottles. The panel is UV stabilized for outdoor weatherability. PFM substrate can be cut and reused or recycled as a whole.

Tests for weatherability have been conducted on PFM sign blanks. No significant deterioration occurred after 2,950 hours of exposure to UV light (340 MJ/m^2 at wavelengths less than 385 nm). Laboratory experiments on PFM substrate show satisfactory results. Field testing is still in progress. Salient mechanical properties of PFM substrate are given in Table 1.

2.3.3 Sequentia, Inc.

Sequentia, Inc., makes fiberglass reinforced plastic (FRP) panels. These FRP panels can be recycled mechanically. FRP panels are light in weight, easy to handle, and chemically resistant. According to the manufacturer, these Polyplate sign panels require no special tools for cutting and do not require learning new procedures for handling and fabrication. Mechanical and physical properties of Polyplate substrate are listed in Table 1.

TABLE 1. Specifications for Mechanical and Physical Properties of Recycled Plastic Sign Substrates

Property	Material		ASTM Standard
	PFM	Polyplate	
(1)	(3)	(2)	(4)
Mechanical			
Tensile strength	54.5 MPa	68.9 MPa	ASTM D638
Tensile modulus	7,170.5 MPa	8,273.7 MPa	ASTM D638
Flexural strength	117.9 MPa	137.9 MPa	ASTM D790
Flexural modulus	8,549.5 MPa	8,273.7 MPa	ASTM D790
Compression strength	106.9 MPa	220.6 MPa	ASTM D695
Compression modulus	#	9,652.7 MPa	ASTM D695
Punch shear	#	89.6 MPa	ASTM D732
Notched IZOD	1.63 m-N/cm	#	ASTM D256
Deflection temperature	87.2° C	#	ASTM D648
Physical			
Weather resistance	Grade II	Grade II	ASTM D3841
Coefficient of linear thermal expansion	3.24×10^{-5} °C^{-1}	1.44×10^{-4} °C^{-1}	ASTM D696
Squareness	<0.318 cm of square/3.66 m length	<0.318 cm of square/3.66 m length	ASTM D3841
Color	Pigmented black for added UV protection	Uniform gray	–

– Data not available

2.4 REVIEW OF RESEARCH ON RECYCLED SIGN BLANK SUBSTRATES

2.4.1 Aluminum

The Oregon Department of Transportation is currently recycling its aluminum signs by painting over existing sign faces to conceal the old letters from view (1994). Signs are initially washed with industrial detergent to remove dirt. An air brush spray gun is used to apply the paint. This produces a neutral backdrop when the process is finished. Painting is done by application of an epoxy primer coat. This produces a dry film that has a thickness of 5.08×10^{-8} m per coat. Silk-screened signs pose no problem with this method of recycling, but high intensity and engineering grade signs have letter silhouetting that has not been completely eliminated, even after application of several coats of primer. These layers are

covered by an acrylic urethane enamel coat. Acrylic urethane enamel and epoxy are environmentally stable and have good adhesive qualities.

Impact tests on a sign have been carried out by projecting 5.08 cm diameter steel balls at the sign from a given height and observing the degree of damage. All of the impacted signs had varying degrees of damage: cracking, splitting, chipping, and small sections of some signs were broken. However, in all cases the materials that failed were either the silk-screen paint surface or the plastic reflective sheeting and letters. The epoxy primer and acrylic urethane enamel finish remained tightly bonded to the materials that failed.

Temperature variation tests appear to have little or no adverse effect. Raised letters or numbers are removed by heat treatment during which the adhesive used for bonding becomes pliable and letters can easily be scraped off. The background material is then given a coat of epoxy primer followed by urethane enamel.

The cost of materials involved in Oregon's sign recycling are next described: One coat of epoxy primer producing a dry film thickness of 2.0 mm gives approximately 133.6 m^2 of coverage per liter. One coat of acrylic urethane enamel producing a dry film that is 1.5 mm thick gives approximately 8.1 m^2 of coverage per liter. The cost of epoxy primer is approximately \$0.54/m^2, and urethane coating costs \$0.86/m^2 of coverage. Thinner used for cleanup of acrylic urethane enamel and epoxy primer is not considered in the cost since only small quantities are used. This process appears to be cost effective in doubling the life expectancy of aluminum sign blanks in comparison with the conventional grinding process. However, questions about reusing signs for a second or third time are still unanswered. Thus, performance of the recycled signs is currently under evaluation.

2.4.2 Plastic and Fiberglass Reinforced Plastic Substrates

Plastic and fiberglass reinforced plastic sign substrates have limitations in comparison with wood or metal substrates. The physical and mechanical properties are sometimes marginally acceptable which makes them unsuitable for use in extreme climatic conditions. Therefore, information on low versus high temperature performance of the blanks is important in determining their suitability in different areas of the state.

Flammability, ignition, and possible generation of toxic fumes are important factors where a vehicle crash or brush fire may ignite plastic and fiberglass reinforced plastic

substrates. Mechanical properties of thermosetting plastics are highly dependent on temperature. For example, the modulus of elasticity of plastic decreases with an increase in temperature. Long term creep performance of plastics is highly temperature sensitive. In locations where there are sustained wind loads under varying temperature conditions, creep may be a problem. Compressive strength, bending strength, and modulus of elasticity decrease with increasing temperature. Manufacturers of sign substrates caution that these materials may fade over time despite the addition of UV stabilizers. Manufacturing processes and quality of raw materials effect the strength of the sign blanks. Moreover, the presence of contaminants such as dirt and paper in raw materials can cause the finished plastic to be brittle.

Plastic and fiberglass reinforced plastic substrates are currently available from a variety of manufacturers. State DOTs are evaluating their suitability to replace aluminum and wood signs. Table 1 gives a comparison of mechanical properties of two commercial plastic products.

The Ministry of Transportation Ontario has developed draft technical specifications for plastic lumber products that are to be used for highway applications (1993). Specifications for traffic sign blanks are given in Table 2.

A study conducted by the Virginia Department of Transportation compared field performance of aluminum and fiberglass panels between 1986 and 1989 (Shephard 1989). Periodic observations of the installations were made with an emphasis on durability and compatibility with reflectorized sheeting. Also vandalism, crash damage, warping, cracking, bubbles, and wrinkles were noted.

TABLE 2. Specifications for Plastic Sign Blanks Developed by Ministry of Transportation Ontario

Properties (1)	Testing Standard (2)	Minimum Test Performance (3)	Comments (4)
Physical			
Specific Gravity	ASTM D 792-91	0.7	
Softening Point	ASTM D 1525-91	>60 °C	
Flash Ignition	CAN/ULC*-S102.2-M88	>200 °C	Required for fire performance rating.
Flame Spread Classification	CAN/ULC-S102.2-M88	140 Maximum	Required for fire performance rating; equal to value of red pine.
Smoke Developed Classification	CAN/ULC-S102.2-M88	230 Maximum	Required for fire performance rating; equal to value of red pine.
Decay Resistance	ASTM D 2017	10% Maximum Weight Loss	Required for estimate of maintenance free life expectancy.
Termite Resistance	ASTM D 3345-74	10 Minimum Rating	Required for estimate of maintenance free life expectancy.
Carpenter Ant Resistance	ASTM D 3345-74	10 Minimum Rating	Test required for recycled plastic lumber with or without cellulose material. Carpenter ants are substituted for termites in the test procedure.
Coefficient of Thermal Expansion ($\times 10^{-6}$ per °C)	ASTM D 696M-91	<155	Expansion and contraction of material over service temperature will be required for detailed design.
Water Absorption	ASTM D 57-81	<10%	150 mm long specimens of 89 × 89 plastic lumber to be tested for both 24 hour and long term immersion.
U.V. Resistance	ASTM G 23-90	No blistering, cracking, or spalling after 1,000 h exposure.	Required to determine the effect of UV radiation on the material.
Mechanical			
Modulus of Rupture (MOR)	ASTM D 198-84	18.0 MPa	Required for wind load resistance set equal to MOR used for other applications.
Longitudinal Shear	ASTM D 198-84	2.0 MPa	Required for wind load resistance set equal to shear strength for other applications.
Compression Parallel	ASTM D 198-84	12.0 MPa	Set equal to lowest plastic lumber industry standard.
Modulus of Elasticity	ASTM D 198-84	3,100 MPa	Required for wind load resistance. Set equal to highest plastic lumber industry standard.
Peel Strength of Overlay	ASTM D 903-49	No adhesive bond failure	Required to assure that overlay bond is adequate.

*ULC - Underwriters Laboratory of Canada

Key findings from the study are as follows:

1. Splintering of sign material requires the use of safety glasses and hand gloves during fabrication.

2. Large signs require additional bracing members and assembly time to ensure rigidity, alignment, and adequate support.

3. Some large signs exhibit waviness that may adversely effect retro-reflective qualities of the sign.

4. Reclamation of a damaged sign may not be feasible unless the sign is cut into smaller sizes. Although FRP signs may not be sold as scrap, this is not the case for unusable aluminum.

5. FRP signs are light in weight in comparison with aluminum signs, and hence, they are easier to handle in the shop and field.

6. Sign reclamation by means of sanding, handling, and cutting is easier than for aluminum substrates. The sanding process for aluminum requires three to four passes with encapsulated sheeting, whereas FRP requires two or three passes.

7. The cost of FRP material is less than aluminum; however, the size of the sign and reclamation value influence the difference in cost.

The Ohio DOT has tested the following sign substrates:

1. 3004-H38 grade aluminum made from 100% recycled materials that are marketed by Signs and Blanks, Inc., Akron, Ohio;

2. Duraplate made from 100% recycled industrial plastics marketed by International Plastics Corporation, Lexington, Kentucky; and

3. Polymer Fiber Matrix made from 100% recycled plastic that is made and marketed by Modern Technologies Corporation, Dayton, Ohio.

The substrates were evaluated once every six months and compared with a control substrate. The thickness of the substrates varied. An interim report on field evaluation of recycled flat sheet sign substrates prepared by the Ohio DOT determined that impact of small objects on aluminum substrates can cause denting and cracking in FRP signs (Gallagher and Donnally 1995). Duraplate signs showed only gashes caused by impact. Thus, impact may cause deterioration of the performance of FRP signs. PFM was found to be more brittle than

other materials, while FRP is more susceptible to damage from impact. However, results are not conclusive enough to recommend a product. The field evaluation is to continue at six month intervals for one more year.

2.5 REUSE AND RECYCLING OF SIGN SUBSTRATES IN STATE DOTS

In order to understand state DOT programs that are directed toward the use of sign substrates made from recycled materials, a telephone survey was conducted. The following discussion reports the current practices of reuse, experimental evaluation of alternative substrates, and monetary aspects of recycling.

2.5.1 Aluminum Substrate Recycling

Aluminum constitutes a major share of sign substrates in most states. Typically, aluminum signs are stripped of their old faces by machine grinding, chemical dipping, or chemical scraping. However, the latter two methods have been discontinued because of problems associated with the treatment and disposal of the wastewater generated. Also, because of stringent environmental regulations the chemical methods were found to be uneconomical. The machine grinding method involves running the old sign through a machine that sands off markings.

Another way of refurbishing an old sign is to overlay a new sign face onto its damaged or faded predecessor. A study conducted by the Federal Highway Administration (FHWA) on aluminum scrap in Arkansas revealed that 77% of the scrap can be salvaged, if an overlay technique is used (TRB 1992). However, if a stripping method is used, only 61% can be salvaged. The study also determined that 22% of the signs are unsalvageable.

2.5.2 Alabama DOT

Alabama DOT has been reusing deteriorated aluminum sign substrates (grades 5052H38 and 6061T6). Damaged sign substrates are collected by regional offices and transported to the central sign refurbishing facility in Montgomery, Alabama. They are sorted into reusable and non-reusable scrap. The reflective sheeting of the reusable signs is removed by a sanding process.

The cost of reuse is $\$7.53/m^2$ excluding the retro-reflective sheeting. Refurbished sign blanks contribute 30% of the annual sign requirement by the state. Alternative sign substrates have been tried in the field, but the study was informal and no report has been

made. The performance of plastic and FRP substrates was deemed to be poor in comparison with aluminum. This prompted Alabama DOT to continue with aluminum as the substrate of choice.

2.5.3 Arizona DOT

Aluminum and wooden signs are both used in Arizona. Recycling of aluminum signs has been done for the past 5 years. Damaged signs are collected by regional offices and transported to a central facility in Phoenix. Sign blanks are segregated according to size and extent of damage. Signs that cannot be used again are sold as scrap. Previously, reflective sheeting was removed by a grinding process. At present, a high pressure water jet is being used as a replacement for grinding. A 110.3 MPa water jet is directed at the used signs in a fully enclosed booth. Water is drained from the booth and goes to a centrifuge where the cut plastic sheets are removed. The water is then filtered and recycled. This method can handle 0.93 m^2 of signs per hour and does not affect the surface of the sheet. Signs can be reused many times by this method of refurbishing, whereas grinding the signs removes material and leads to disposal of the substrate after one or two reuses.

The present cost of a new aluminum sign blank is \$14.96/m^2. Recycling by grinding costs \$6.46/m^2 for engineering grade and \$9.15/m^2 for high-intensity grade sheets. However, use of the water jet method reduces the refurbishing cost to \$3.55/m^2. The water jet method has been tried for the past six months. Arizona DOT has entered into a contract agreement with Correctional Industries, Inc., who have tentatively agreed to recycle the material at a cost of \$2.69/m^2.

Arizona DOT has also experimented with FRP signs. The extreme high temperature conditions within the state cause FRP signs to expand and contract and do not permit the use of sign materials made from plastics or FRP.

2.5.4 Connecticut DOT

Only aluminum sign substrates are used in Connecticut. Reuse of substrate is done once every 5 years since Connecticut is a small state and there are fewer signs in comparison with other states. Stripping of the reflective sheeting is done mechanically by contractors. The

cost of contracting mechanical stripping is $\$7.64/m^2$ whereas the cost of new aluminum blank material is $\$18.84/m^2$.

The state has experimented with plastic signs, but temperatures during the winter season average -9.44° C or less, and hence, the problem of plastic becoming brittle is profound. Connecticut has discontinued use of plastic signs.

2.5.5 Florida DOT

Florida is currently testing the use of plastic sign substrates, sign posts, and guard-rails at 11 different sites. Plastic products are obtained from the manufacturer under the condition that these materials are used for test purposes. If any damage to the substrate occurs, the manufacturer replaces the sample without cost to the state. Currently, only signs of sizes less than 0.6 m × 0.6 m are being tested.

One of the most important test sites is Marathon, Florida, which is 64.4 km east of Key West, Florida. This site provides a worst case scenario in that it is 2.74 m from the edge of the ocean and there is direct sunlight throughout the year.

Initial screening of plastic substrates is done by testing for bonding of reflective sheeting. Most substrates have no problem in bonding. Florida DOT also calls for testing of warping and contraction, which is currently in progress.

2.5.6 Idaho DOT

Aluminum used in sign blanks in Idaho has a grade of 5052H38. The state has recycled aluminum sign blanks for the past thirty years. Materials used for sign blanks include aluminum (75%) and Simpson high-density plywood (25%). All old or damaged signs are returned to a central storage facility. These signs are segregated into salvageable and non-salvageable categories based on the extent of damage. Unsalvageable signs are sold in a public auction.

Storage and stock piling of salvageable signs is done for 3 to 4 years or for a time sufficient to accumulate a large truck load. Bids are invited from various refurbishing companies that are registered with Idaho DOT. Although aluminum signs were previously recycled by a chemical process, a mechanical process of grinding and removing the reflective sheeting is now used.

Several problems and limitations in recycling sign substrates in Idaho are as follows:

1. Aluminum blanks are printed with transparent ink. Grinding causes roughness of the surface which is visible if transparent ink is used; this does not affect the visibility or quality of a sign.

2. Reduction in thickness of aluminum sheets causes it to be used only once or twice after the first recycling, after which it is stockpiled as scrap and sold at auction.

3. It is difficult to ensure that a contractor gives back the same sign blanks that were sent for recycling. This occurs because contractors sometimes recycle signs from several other state agencies concurrently.

The cost of new sign blank material is $\$16.15/m^2$. The recycling or refurbishing operation was costing $\$5.17/m^2$ in 1991. Inventory of various sizes of sign blanks is taken before any signs are sent for recycling. Orders for new sign blanks are based on the required number minus the available number of recycled sign blanks. Hence, it is difficult to estimate the annual percentage contribution of the recycled sign blanks. The last batch sent for recycling contributed 5,110 m^2.

2.5.7 Illinois DOT

Aluminum substrates are used in traffic signs in Illinois and have been recycled since 1979. Old, damaged, and obsolete signs are recycled by removing the reflective sheeting by means of a sanding process. IDOT has successfully used a mechanical abrading process to refurbish over 700,000 aluminum sign blanks since 1979. Recycling is done in a state owned sign shop. 68% of signs replaced statewide (70,000 annually) are fabricated from blanks refurbished by the central sign shop. Reuse of a sign substrate is allowed a maximum of two times. IDOT has not explored use of materials such as plastic or FRP.

2.5.8 Massachusetts DOT

Aluminum is predominantly used as the substrate for signs in Massachusetts. There is currently no recycling or reuse of sign blanks in the state. Although Massachusetts attempted to use an FRP substrate, it did not perform well because of wind loads in coastal areas and large temperature stresses. The study was informal, and there is no written report on performance of FRP sign substrates.

2.5.9 Missouri DOT

Missouri uses aluminum for 90% of its sign blanks; the remaining blanks are comprised of wood and steel materials. Large aluminum sheets are reused by cutting, sanding, and re-sheeting. No experimentation has been carried out with FRP or plastic substrates.

2.5.10 Montana DOT

Sign substrates made from aluminum are widely used in Montana. Recycling of signs is not done by the state. Damaged signs are sold as scrap. The state is currently experimenting with 55.7 m^2 of plastic sign substrate (Polyplate made by Sequentia, Inc.).

2.5.11 Oregon DOT

The Department of Transportation in Oregon mainly uses aluminum sign substrates. They have been reusing and recycling the substrate since October, 1994. Signs with no pin holes or substantial damage are reused by painting epoxy and polyurethane on the front face where reflective sheeting was originally present and using the rear face as a new front face. Cost of refurbishing the substrate is approximately \$3.23/m^2 which is less than the cost of grinding to remove reflective sheeting as done by other DOTs. The first batch of recycled sign substrates under this new system is currently being installed in the state.

A two part epoxy coating is applied to the face of the sign in accordance with instructions from an epoxy manufacturer. The epoxy coating is followed by the polyurethane coating. Impact tests done by using steel balls show that urethane adds strength to the aluminum sheeting. Also coating with urethane offers resistance to graffiti. There is no detrimental out-of-plane warping of the sign when it is subjected to outdoor temperature stresses.

Aluminum signs are collected from various districts in Oregon and brought to the central sign workshop in Salem. The process of refurbishing the signs is carried out in a state prison, where the cost of labor is minimal. Material cost is estimated to be \$1.08 to \$1.61 /m^2 and labor cost is \$1.18 to \$1.83/m^2. Grade 5052H38 aluminum is used as sign blank material. Previously Oregon used 6061HT6 grade aluminum, but because of deformity and poor strength, it was replaced with grade 5052H38. Oregon DOT has not used FRP or plastic substrates.

2.5.12 Tennessee DOT

Aluminum is exclusively used as a traffic sign substrate in Tennessee. Damaged signs are not recycled. An informal study was conducted to determine the suitability of using plastic signs. The study found unacceptable warping of plastic signs that are 0.76 m × 0.76 m.

2.5.13 Utah DOT

Aluminum and plywood are used as sign blank materials by the Utah DOT (1995). The state does not currently recycle damaged aluminum signs; the scrap value of the materials is reclaimed by public auction. The primary reason for damage to aluminum signs is vandalism.

Utah DOT is currently investigating use of plastic signs. Plastic sign blanks have been installed in two areas that have high and low exposure to vandalism. Plastic substrate materials are heavier than aluminum signs. Some fiberglass reinforced plastic sign blanks were tested three years ago and were found to be damaged easily by winds and vandalism.

Plastic and reinforced fiberglass sign blanks were installed on a trial basis in Utah in 1988. Testing was done by installing 6 sign blanks of different sizes at various places; performance was evaluated after a 6 month period. The study was informal, and no report was made. Key findings were as follows:

1. There was no problem of bonding reflective sheeting to plastic or fiberglass substrate.
2. Curling of plastic signs was observed during the 6 month trial period. Up to 5.1 cm of bowing of the plastic sheets was observed.
3. Reflecting sheets peeled away from FRP substrate on exposure to sunlight.
4. Vertical cracking and flexing of sheets has been observed due to thermal stresses and wind loads.
5. The main reason for damage to traffic sign substrates in Utah was vandalism (gunshots or spray painting).

In a brief statement concerning the above findings, the New Product Testing Committee in Utah DOT did not recommended using plastic or FRP substrates.

3. EVALUATION OF CANDIDATE MATERIALS

3.1 GENERAL

The thickness dimension of sign blanks made from marine plywood or aluminum in current use along Texas highways is not designed according to engineering formulas. Rather, specifications to material suppliers are based on experience with these materials over many years of installation. Newer materials, such as recycled plastics, have different properties than the traditional substrates, and a database of practical experience is not available. Therefore, it is imperative that tests be conducted to characterize the behavior of these new materials. Knowledge of these properties, in turn, will enable a design procedure to be developed. In this way TxDOT can specify a required thickness for a sign that is to be manufactured from virtually any suitable material. The design procedure needs to be flexible enough to take into account properties of the material such as density, stiffness, strength, as well as the geometry of the sign and its supports.

Recycled material suppliers were solicited for purposes of obtaining candidate materials for use as recycled content sign blanks (see Table 3).

TABLE 3. Collected Materials and Designations

Material Designation (1)	Company (2)	Content (3)
Plywood	—	—
AQ	Aquanalogy, Inc.	—
CTC	Composite Technologies Corp.	—
RENW	Renewed Materials, Inc.	Rubber, HDPE, Misc. Plastic
CMB	Pellatech, Inc.	HDPE
GTHW	Pellatech, Inc.	Polyvinyl Chloride (PVC) and Calcium Carbonate
SPAB	Pellatech, Inc.	HDPE, Polycarbonate
VIWB	Pellatech, Inc.	HDPE

In order to design a substrate of sufficient thickness and subsequently evaluate the design, certain fundamental material properties had to be determined. These properties include the flexural modulus (E), damping coefficient (ξ), and creep. In this report the flexural modulus is evaluated by a four-point flexure test. This procedure is discussed in section 3.2. The damping coefficient is evaluated by observing free vibration of candidate materials. Vibration characteristics are discussed in further detail in section 3.3. Susceptibility to creep for each material was evaluated by performing a short term creep and recovery test as discussed in section 3.4.

3.2 FOUR-POINT FLEXURE TEST

Flexural modulus is a function of the state of the extreme fiber in a material. In an outdoor environment it is the extreme outer fibers that are in direct contact with the elements of nature. Therefore, an understanding of the flexural behavior of a particular candidate material is necessary for both design and performance evaluations. A four-point bend test was used to determine the flexural modulus of elasticity for candidate materials. This value can be compared qualitatively with the flexural modulus of plywood. Additionally, the modulus of elasticity in conjunction with other information, such as the unit weight, was necessary for design evaluation with the performance specifications.

3.2.1 Laboratory Procedure

For experimental determination of the flexural modulus, a four-point bend test was chosen over a three-point bend test. The test is based on ASTM D790-92, "Standard Test Methods for Flexural Properties of Unreinforced Plastics and Electrical Insulating Materials." In a four-point bend test the moment is constant between two loads (see Fig. 2). In contrast, the highest moment occurs only at the location of the middle support for a three-point bend test. This concentrated force can cause failure at the center of the specimen resulting in a modulus of elasticity that may not be truly indicative of the material. The constant moment in the four-point bend test is distributed over a larger volume of the material. Since the majority of the recycled materials are not entirely homogeneous, the four-point test provides more consistent results.

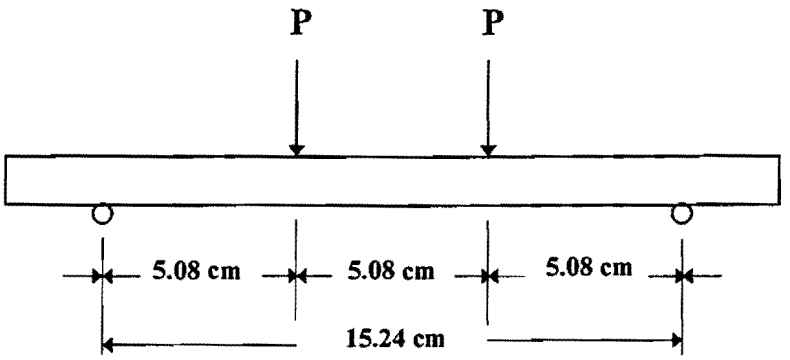

FIG. 2. Common Flexure Test Support Conditions and Dimensions

Each specimen was in the form of a bar that was approximately 20.3 cm long and had a rectangular cross section. Supports were placed 15.2 cm apart. The two loads were 5.08 cm from either end and 5.08 cm from each other (see Fig. 2).

A Schaevitz Engineering 100-MHR linear variable differential transformer (LVDT) (S/N 43458) was placed beneath the specimen at mid-span and used to continuously monitor displacement during loading (see Fig. 3). This LVDT had a ±0.254 cm stroke. All specimens were tested in an Instron model 1125 machine with a 22.2 kN Instron load cell (CAT #2511-325) with full range set at 2.22 kN. The crosshead speed was set at 0.254 cm/min. Data from the load cell and the LVDT were recorded using a microcomputer-based data acquisition system (see Fig. 4). The test was run until stroke on the LVDT reached approximately 0.254 cm. This provided data for the modulus of elasticity but not additional information such as modulus of rupture.

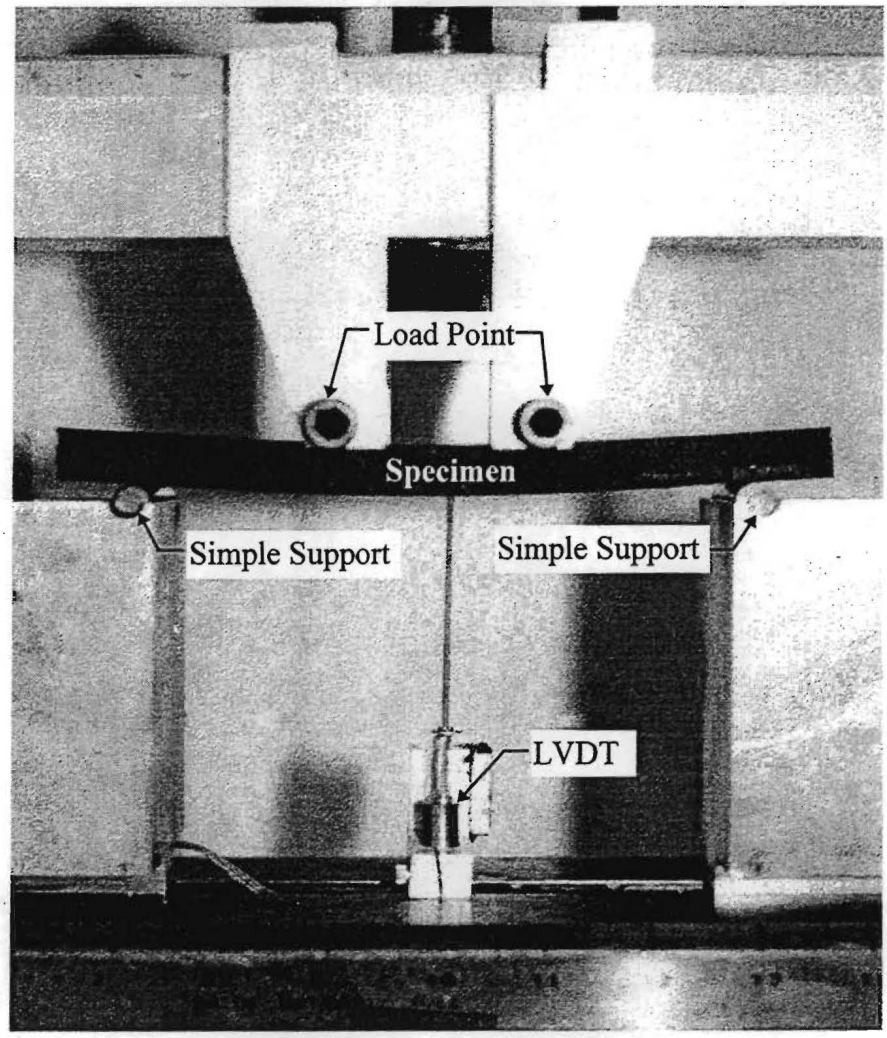

FIG. 3. Four-Point Bending Test in Progress

FIG. 4. Data Acquisition and Microcomputer for Flexure Tests

3.2.2 Calculations

The modulus of elasticity was determined using load-deformation relationships. For a simply supported member with two equal evenly distributed concentrated loads (see Fig. 2), the relationship between load and displacement at the center is:

$$\Delta_c = \frac{Pa}{24EI}\left(3l^2 - 4a^2\right) \tag{1}$$

where Δ_c is the mid-span deflection, P is the applied load at each point, E is the modulus of elasticity, I is the moment of inertia, l is the unsupported length of the specimen, and a is the spacing of the loads (see Fig. 5).

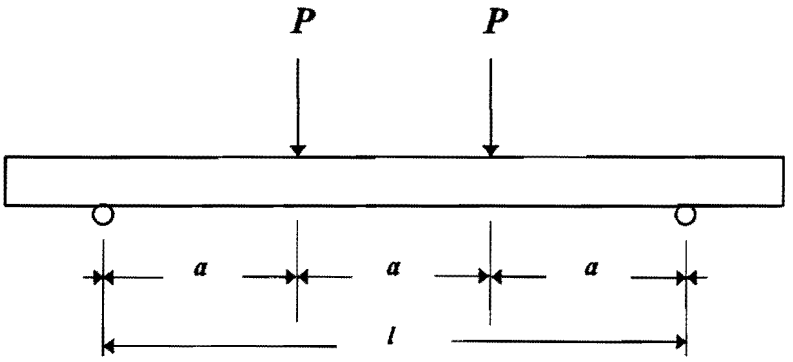

FIG. 5. Load-Deformation Variables

Rearranging Eq. 1 to isolate the modulus:

$$E = \frac{Pa}{24\Delta_c I}\left(3l^2 - 4a^2\right) \tag{2}$$

For this test, a = 5.08 cm and l = 15.24 cm. Since each specimen had a rectangular cross-section, the moment of inertia is given by:

$$I = \frac{(w)(t)^3}{12} \tag{3}$$

where w represents the width of the specimen, and t is the thickness (see Fig. 6). The load deformation relationships used to develop Eq. 2 idealized the supports as perfectly pinned. Perfectly simple supports are difficult to achieve and as a result this idealization may introduce a slight error.

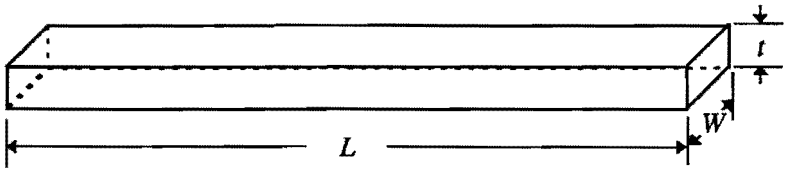

FIG. 6. Flexure Specimen Geometry and Dimensions

3.2.3 Results

Six candidate materials were tested in flexure by the four-point method. Data were acquired at a rate of 2 Hz for the duration of the test. For each load-displacement measurement, a modulus was determined using Eq. 2; an average of these values was taken to be the modulus for that particular test. Two tests were performed on two specimens for each material. The average modulus from the two tests on each specimen was averaged with the average from the second specimen to produce a final modulus.

Results of the flexure tests are shown graphically in Fig. 7 and also are listed in Table 4. CTC has a slightly higher modulus than wood, while the other materials are at least 50% lower. The weakest material is Aquanology (AQ) with a modulus that is 84% less than that of wood. However, the modulus of elasticity does not necessarily indicate the efficiency of a material.

TABLE 4. Results of Flexural Modulus Tests

Material (1)	Average Value for E (kN/m^2) (2)	Unit Weight (kN/m^3) (3)	Equivalent Thickness (4)
Plywood	5.76×10^6	6.07	1.000
AQ	9.22×10^5	9.23	1.770
CTC	6.53×10^6	9.23	0.951
RENW	1.11×10^6	15.08	1.826
CMB	1.56×10^6	9.37	1.533
GTHW	1.37×10^6	5.83	1.601
SPAB	1.33×10^6	9.55	1.617
VIWB	2.73×10^6	11.99	1.272

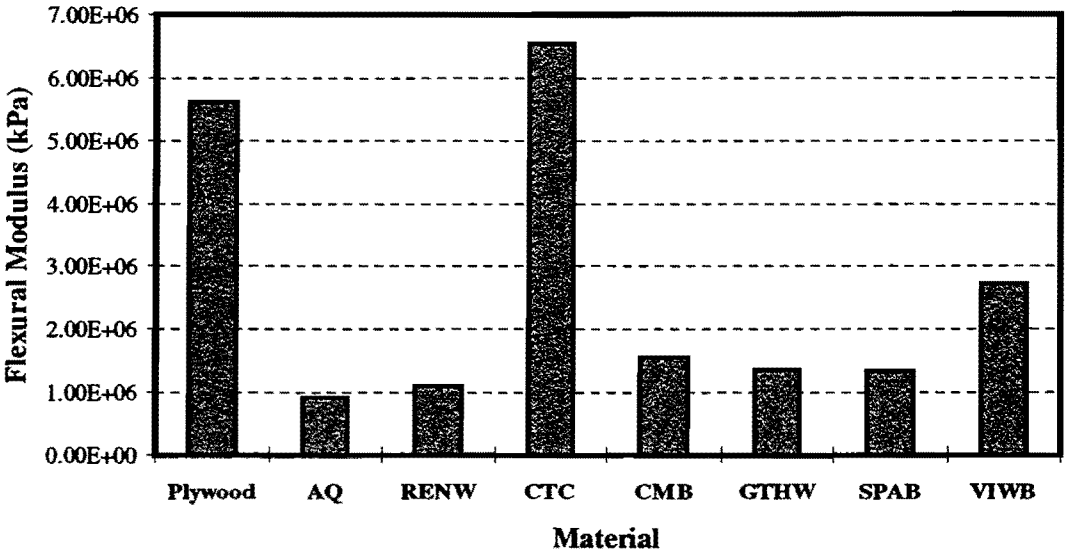

FIG. 7. Comparison of Flexural Modulus for Various Materials

The unit weight of each material was determined simply by measuring the three dimensions of each specimen, weighing the specimen, and dividing the weight by the total volume (see Fig. 8).

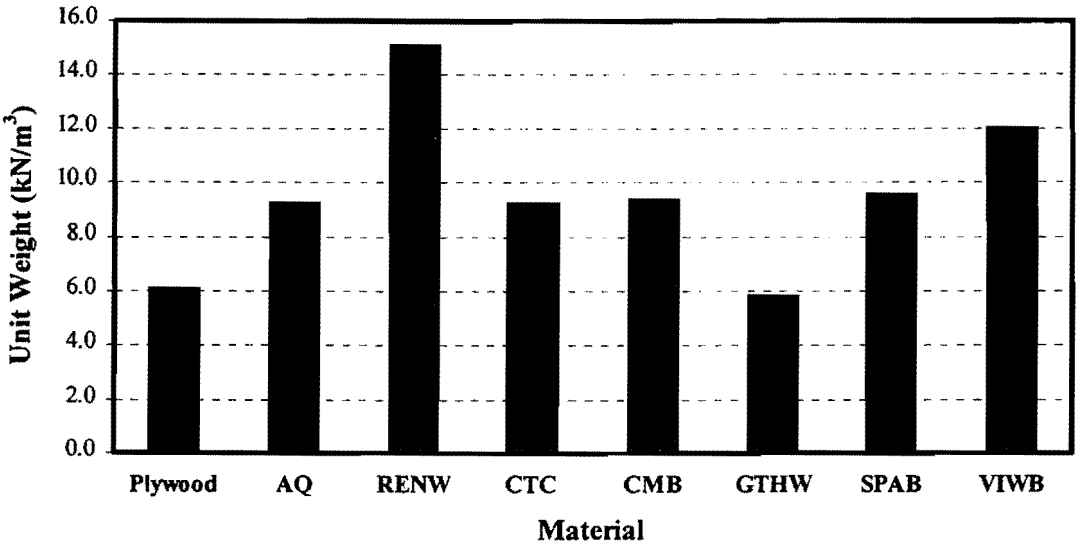

FIG. 8. Unit Weight of Substrate Materials

Performance of the materials may be compared qualitatively to plywood. Consider a simply supported beam of unit thickness and width that is subjected to a concentrated load at the center (see Fig. 9). If each material is to produce an equivalent deflection under the same load and support conditions, and the width of each specimen is identical, each beam will, in general, have a different thickness. This thickness is referred to as the equivalent thickness since it produces an equivalent deflection under the load. Materials that are more efficient than plywood will have an equivalent thickness less than unity, and less efficient materials will have an equivalent thickness that exceeds unity. The moment of inertia of a rectangular cross-section of unit-width is:

$$I = \frac{t^3}{12} \tag{4}$$

and the deflection at the center of the beam is:

$$\Delta = \frac{Pl^3}{48EI} \tag{5}$$

where P is the applied static load, and l is the length of the beam. If a beam constructed of recycled materials is to produce an identical deflection as a wood beam of unit thickness and

width, and E_w is the modulus of wood then Eq. 4 and Eq. 5 may be used to determine the equivalent thickness of the recycled beam. The equivalent thickness (t_{eq}) is given by:

$$t_{eq} = \left(\frac{E_w}{E}\right)^{\frac{1}{3}} \tag{6}$$

where E is the flexural modulus of the material being compared to plywood. Equivalent thicknesses of the recycled materials tested in this study are presented in Table 4 and Fig. 10. CTC is the stiffest material tested and has an equivalent thickness less than 1. Of the remaining materials, GTHW and CMB are the most stiff. Even though GTHW does not have a relatively high modulus of elasticity and must be approximately 60% thicker than plywood to produce an identical deflection, it is the lightest material tested and is therefore relatively efficient.

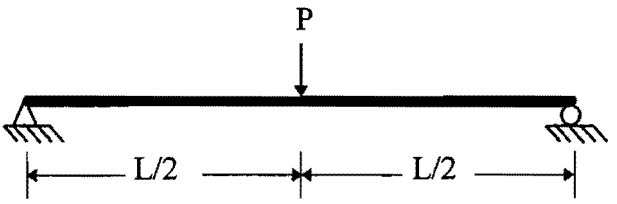

FIG. 9. Simply Supported Beam of Unit Cross-Sectional Dimensions

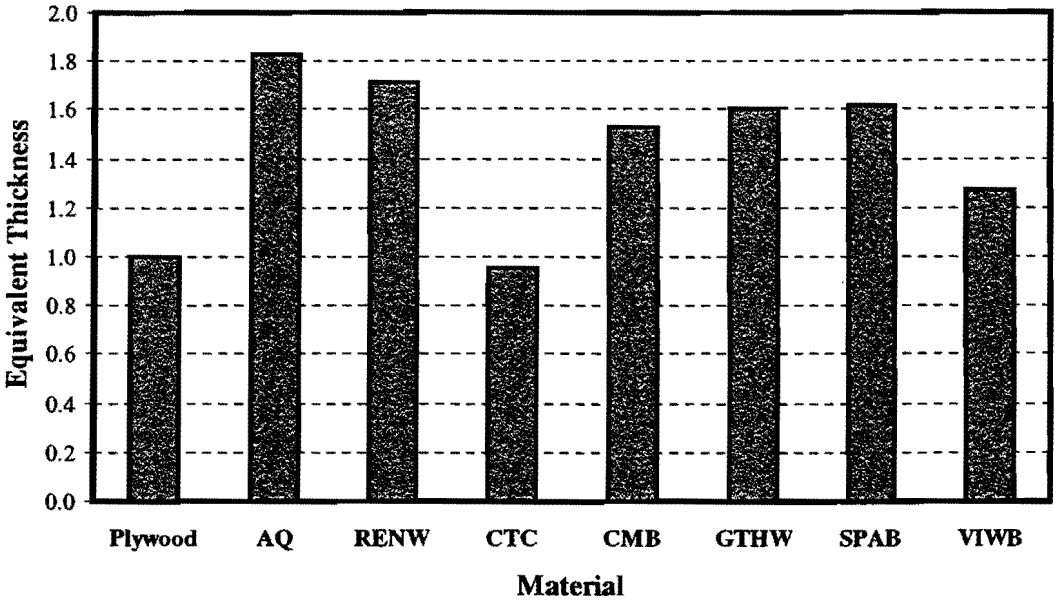

FIG. 10. Equivalent Thickness of Substrate Materials

3.3 UNI-AXIAL TENSION TEST

After each specimen was subjected to a flexural test, it was machined into the shape shown in Fig. 11 in preparation for a uni-axial tension test. Tension tests were performed in this study to validate the modulus of elasticity produced in section 3.2 and to determine the tensile modulus. Plywood was not tested in tension due to grip limitations caused by the large thickness of the material.

3.3.1 Laboratory Procedure

Uni-axial tension tests were performed on specimens whose cross-sectional areas had been reduced in the test region to insure failure occurred away from the grips (see Fig. 11). The intention was to minimize the effects of boundary conditions on the data.

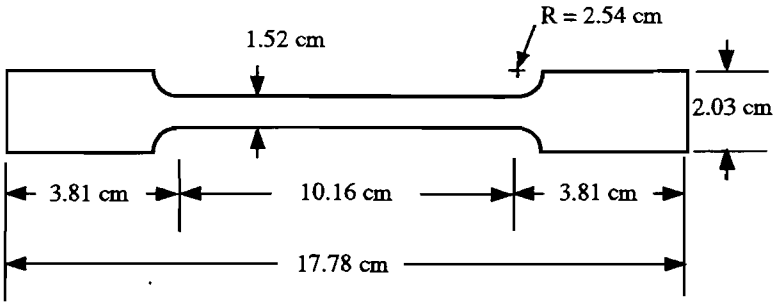

FIG. 11. Dimensions of Tension Test Specimen

Specimens were tested in an Instron Model 1125 that is identical to the machine described in section 3.2. An Instron 89 kN load cell, catalog number 2511-305, was used to measure load on the specimen. An MTS model 632, 11B-20 extensiometer was placed at the center of the test coupon (see Fig. 12). The extensiometer had an initial gage length of 2.54 cm. This allowed the device to output strain directly as it measured displacement across the gage. Use of the extensiometer instead of the crosshead displacement compensates for any slipping that may occur in the grips. All specimens were strained at a rate of 1.27 mm/min. Since the strength of plastic materials is a function of the strain rate, all specimens were tested at the same rate.

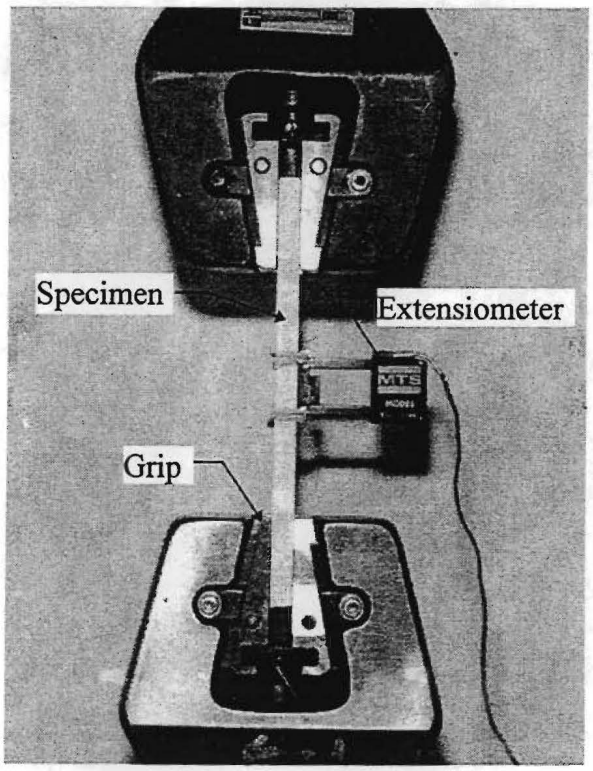

FIG. 12. Uni-Axial Tension Test

3.3.2 Calculations

Normal stress in the material is the load, P, divided by the cross-sectional area, A:

$$\sigma = \frac{P}{A} \tag{7}$$

The modulus of elasticity is determined from the slope of the linear elastic region of the stress-strain diagram:

$$E = \frac{\Delta\sigma}{\Delta\varepsilon} \tag{8}$$

where E represents the modulus, $\Delta\sigma$ is the change in normal stress acting on the specimen, and $\Delta\varepsilon$ is the respective change in strain.

3.3.3 Results

A total of six candidate materials were tested in uni-axial tension. Data were acquired at a rate of 2 Hz for the duration of the test. Each specimen was tested until failure, or until the test had taken over 20 minutes and was terminated due to effects of creep. Materials CMB and SPAB exhibited a great amount of ductility recording strains in excess of 0.08 m/m

when the test was terminated (see Fig. 13). Material GTHW exhibited linear elastic behavior up to a stress of 1.05×10^4 kPa and then excellent ductility to failure. Materials VIWB and CMB have high strength but low ductility.

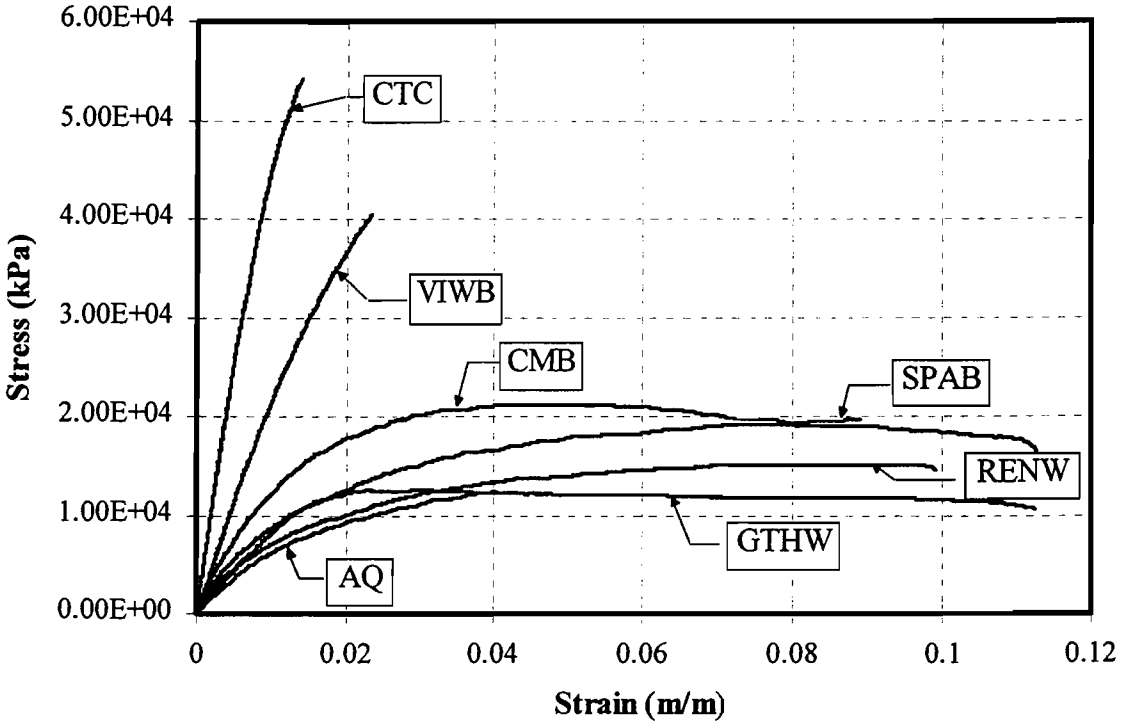

FIG. 13. Stress versus Strain for Uni-Axial Tension

A tensile modulus for each material was determined by performing linear interpolation in the linear-elastic region of the stress-strain diagram. Results are given in Table 5 and Fig. 14. Moduli range from 6.011×10^6 for CTC, which exceeds that of wood, to less than 1.0×10^6 for AQ, RENW, and SPAB. All moduli are approximately identical to those obtained in Table 4, given the small number of specimens tested. The exception is GTHW which differs by 50%. One explanation for this discrepancy may be the non-uniformity of the cross-section in the test region of the tensile specimen. A small chip or other internal flaw can reduce the cross-section within the test area. This would result in a higher actual state of stress existing within the test area in comparison with the assumed

average normal stress. In addition, the manufacturing process introduces some degree of non-homogeneity into the material in that the outer layers are less porous than the core.

TABLE 5. Elastic Modulus for Uni-Axial Tension

Material (1)	Modulus of Elasticity (kPa) (2)
AQ	6.805×10^{5}
CTC	6.011×10^{6}
RENW	8.959×10^{5}
CMB	1.246×10^{6}
GTHW	7.764×10^{5}
SPAB	1.076×10^{6}
VIWB	2.507×10^{6}

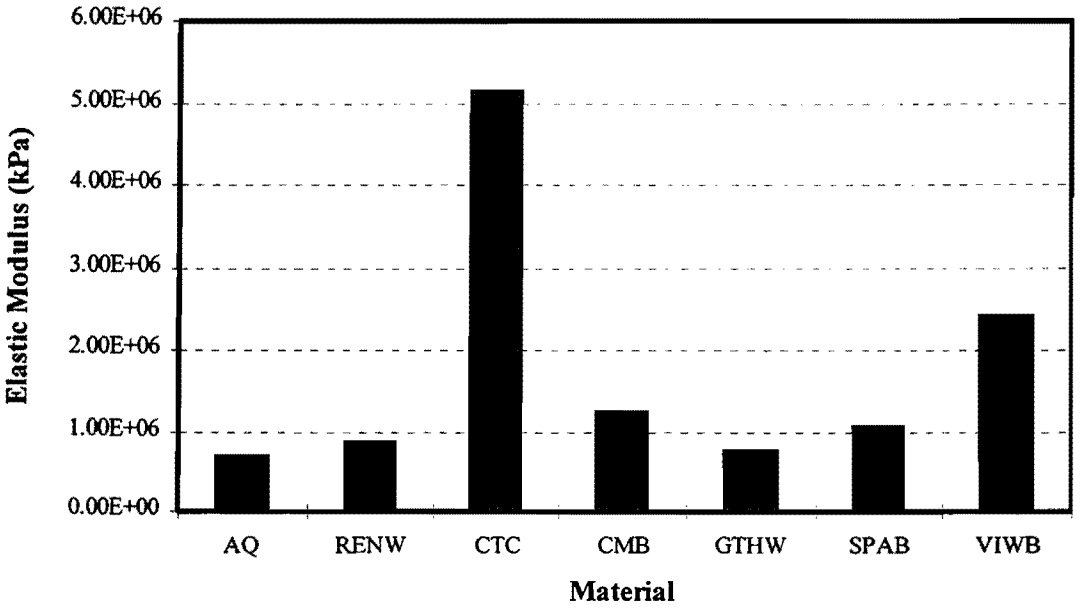

FIG. 14. Elastic Modulus for Uni-Axial Tension

3.4 FREE VIBRATION TEST

It is mentioned in Chapter 2 that some problems arose when state DOTs field tested sign substrates manufactured from recycled materials. These problems included failures in the substrate induced by oscillating wind. In several instances cracking was observed at the hardware connections between the sign substrate and the sign support. Materials with a low damping ratio and low ductility have a tendency to exhibit this behavior. Since highway roadside signs are frequently subjected to random oscillatory loads from large highway vehicles and wind, dynamic response characteristics play a role in the fatigue life of the structure.

To this end, free vibration tests were performed on the candidate substrate materials in order to determine damping characteristics such as the damping ratio. Determination of the damping ratio (ξ) as described in this section was based on the logarithmic decrement (δ) which represents the rate of decay of motion of a freely vibrating structure (Chopra 1995). As ξ increases, the rate of decay of motion also increases, and the sign substrate undergoes fewer cycles of high level stress thereby increasing the service life of the sign.

An optimum material would have relatively high values for damping and ductility in order to improve its resistance to fatigue damage. To determine a material damping ratio experimentally, it is necessary to perform experiments under conditions of free vibration. In the following subsections, damping characteristics of each candidate material are compared on a qualitative basis to those of a plywood specimen that currently qualifies as an acceptable substrate material. Specimens which have values of ξ that are conspicuously low can be eliminated from consideration as a substrate due to their inability to dissipate energy.

3.4.1 Laboratory Procedure

A free vibration test was carried out in the laboratory by clamping a small beam-shaped specimen of each material type to a large structural column using a C-channel clamp and chair, two bolts, and a torque wrench (see Fig. 15). The specimen was placed in a clamping device with the edge of the end flush with the opposite end of a C-channel. After leveling the sample, the bolts were turned by hand and then tightened with a torque wrench to 13.6 N-m of torque. A PCB accelerometer (model number 309A) with a voltage sensitivity of 1.8%, resolution of 0.02 g, resonant frequency of 120kHz, and a range of ±1,200 g was

attached to the free end of the specimen (see Fig. 15). The specimen was given an initial displacement by hand and suddenly released in order to set the sample into free vibration. Acceleration data were recorded electronically at a rate of 1,200 Hz. This procedure was repeated five times for each specimen.

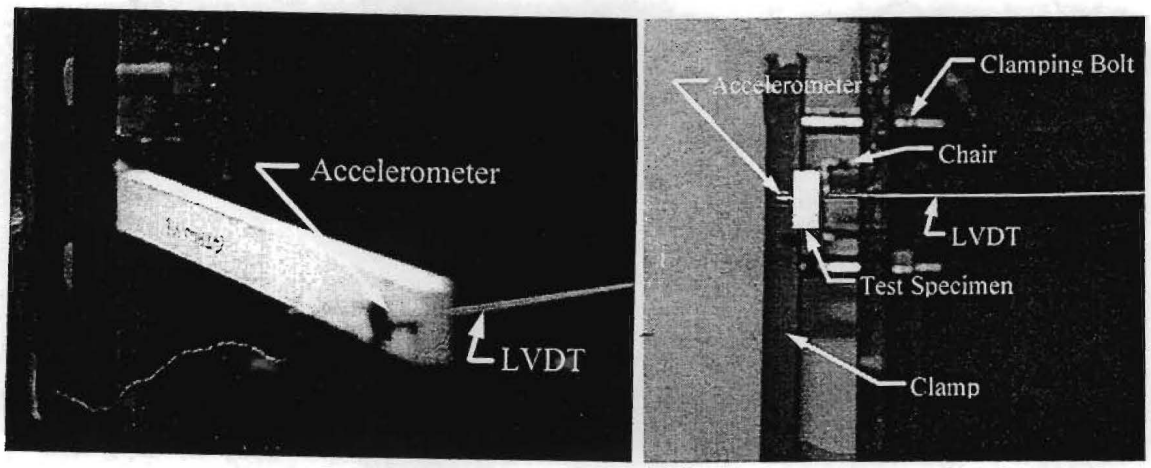

(a) (b)

FIG. 15. Free Vibration Specimen Ready for Testing: (a) Isometric View; and (b) End View

Data recorded during the experiment were subjected to electronic noise from various types of machinery in the laboratory. A digital filtering technique was used to remove noise and higher modes of vibration from the data to closely approximate the true acceleration time history of the fundamental mode. This is accomplished by the use of a Butterworth low and high pass filter (Tokarczyk 1996).

3.4.2 Calculations

The damping coefficient (ξ) was determined experimentally using the logarithmic decrement method (Chopra 1995). The logarithmic decrement (δ) is defined by:

$$\delta = \frac{1}{j} \ln \frac{u_i}{u_{i+j}} \tag{9}$$

where u_i is the displacement amplitude at the i^{th} peak, and j represents the number of cycles that separate the peaks. This relationship represents the rate of decay of vibration between

two peaks, u_i, and u_{i+j}. The logarithmic decrement, δ, is related to the damping coefficient, ξ, by the following relationship (Chopra 1995):

$$\delta = \frac{2\pi\xi}{\sqrt{1-\xi^2}} \tag{10}$$

If $\xi << 1$, then $\xi^2 \cong 0$, and Eq. 10 reduces to:

$$\xi \cong \frac{\delta}{2\pi} \tag{11}$$

For values of ξ that are less than 0.2 (see Fig. 16), Eq. 11 yields a reasonably accurate approximation of the exact relationship given by Eq. 10 (Chopra 1995).

Eq. 11 is used to calculate damping coefficients for material samples in this study since the damping ratios (ξ) are well below 0.2 (see Table 6).

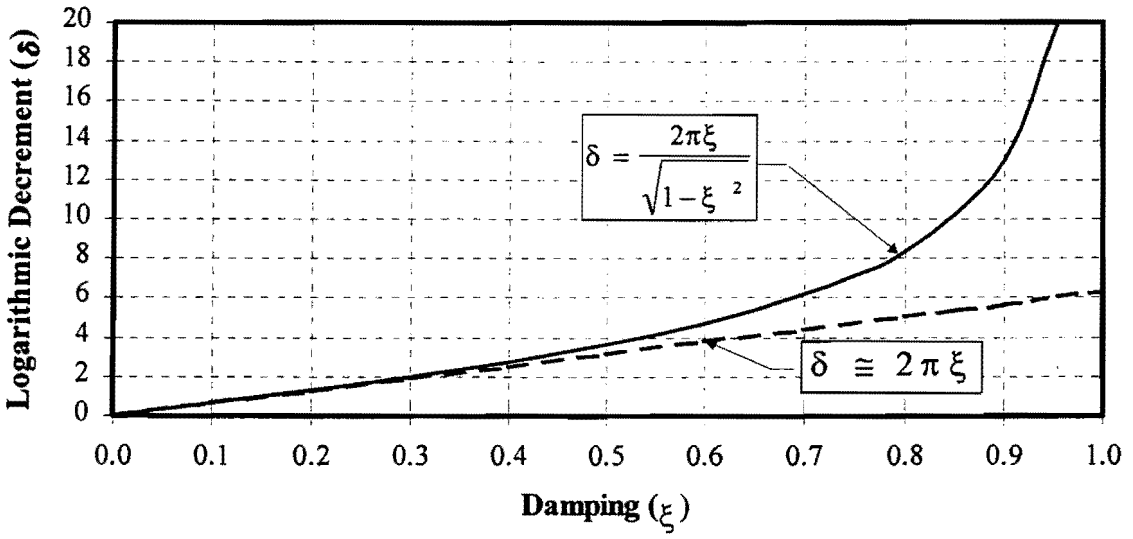

FIG. 16. Exact and Approximate Evaluation of Logarithmic Decrement (Chopra 1995)

3.4.3 Results

Figs. 17-23 illustrate a typical unfiltered and filtered first mode acceleration time history for each material. Effects of filtering can clearly be seen in Fig. 18. The figures are plotted to the same identical scale so that differences in the rate of decay of the motion may

be observed. For instance, GTHW (see Fig. 21) absorbs strain energy of free vibration much faster than VIWB (see Fig. 23).

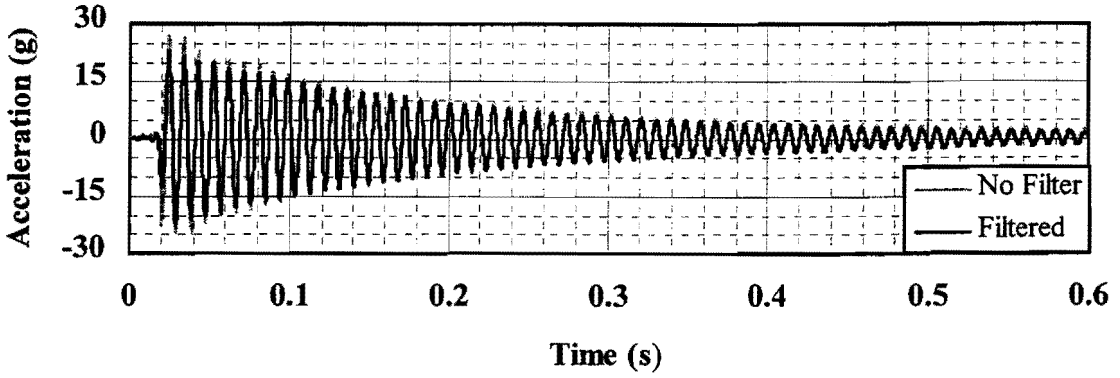

FIG. 17. Typical Free Vibration of Plywood

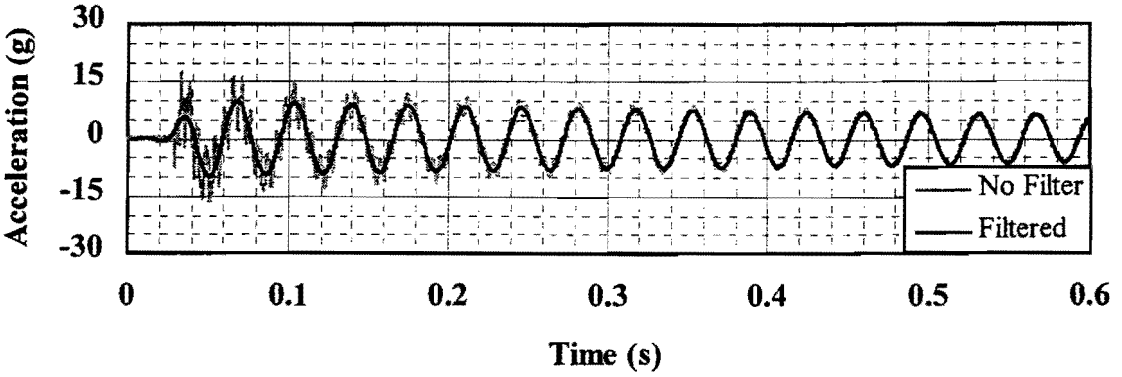

FIG. 18. Typical Free Vibration of CTC

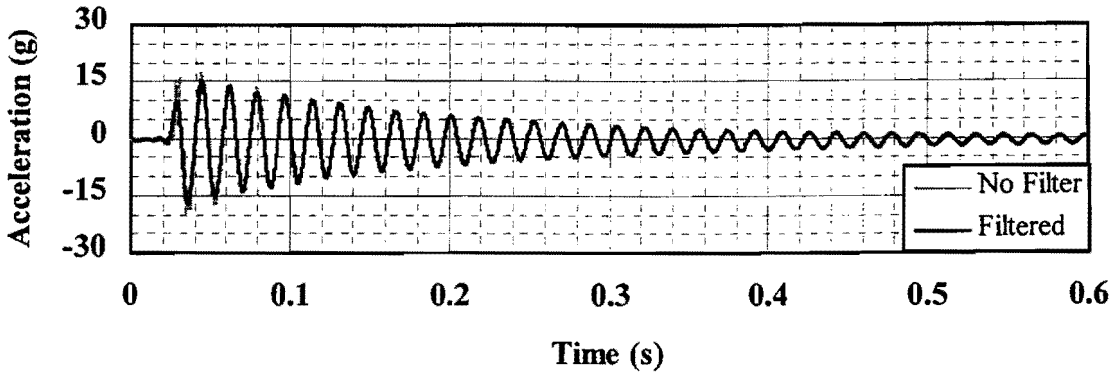

FIG. 19. Typical Free Vibration of RENW

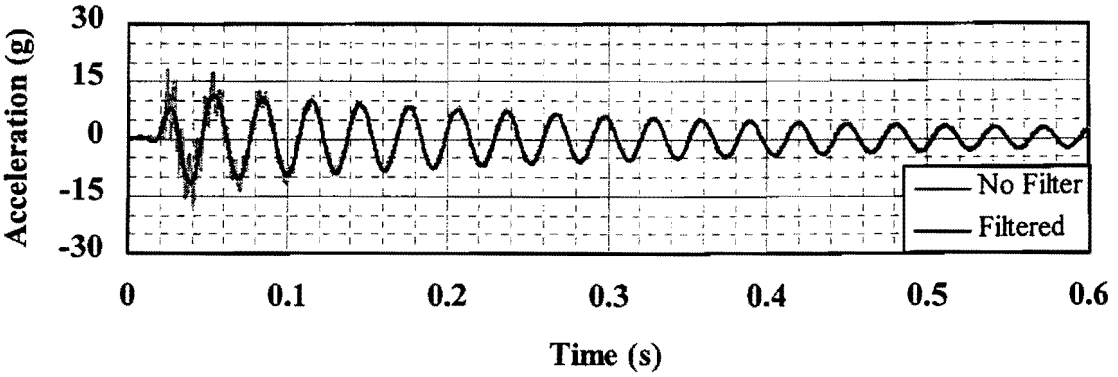

FIG. 20. Typical Free Vibration of CMB

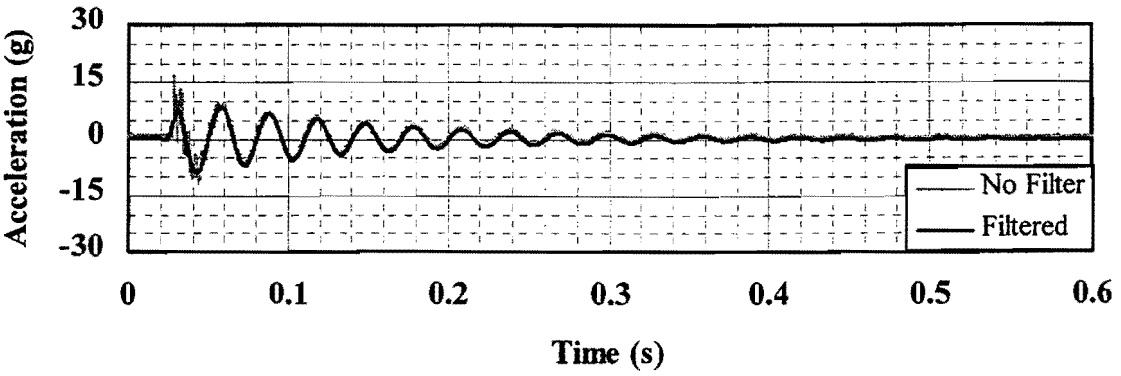

FIG. 21. Typical Free Vibration of GTHW

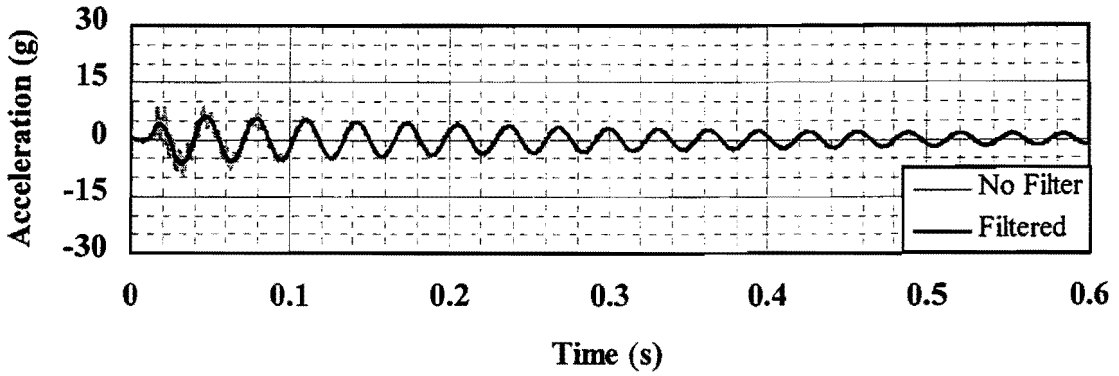

FIG. 22. Typical Free Vibration of SPAB

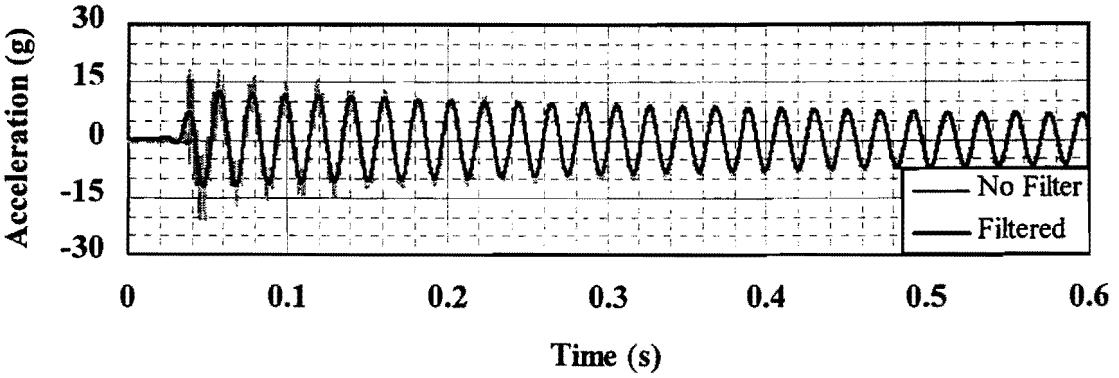

FIG. 23. Typical Free Vibration of VIWB

Results from free vibration tests for the six candidate materials show that some recycled materials compare favorably to plywood (see Table 6). For instance, the material in this test with the highest damping coefficient (3.81%) is GTHW. A sample from a plywood sign substrate produced a damping coefficient of 0.79%. By comparison, the material in this test with the lowest damping coefficient (0.40%) is VIWB (see Table 6 and Fig. 24). The relatively wide range in damping values may be attributed to differences in material structure. For instance, as shown in Table 4, VIWB is relatively dense and has a relatively high modulus. The high density may reduce the amount of internal friction, thus inhibiting energy dissipation and exhibiting poor damping. In contrast, GTHW is relatively light; its cross-section has an air entrained matrix and a rigid shell. During vibration the matrix flexes and

dissipates energy. As a result, materials with internal mechanisms for dissipating energy, such as the matrix in GTHW or cross-lamination of wood fibers in plywood, exhibit improved damping characteristics.

TABLE 6. Free Vibration Damping Coefficient (ξ)

Material (1)	Specimen Thickness (cm) (2)	Average Value for ξ (%) (3)
Plywood	1.636	0.79
CTC	0.537	0.47
RENW	1.732	1.53
CMB	0.904	1.41
GTHW	1.245	3.81
SPAB	0.914	1.29
VIWB	1.466	0.40

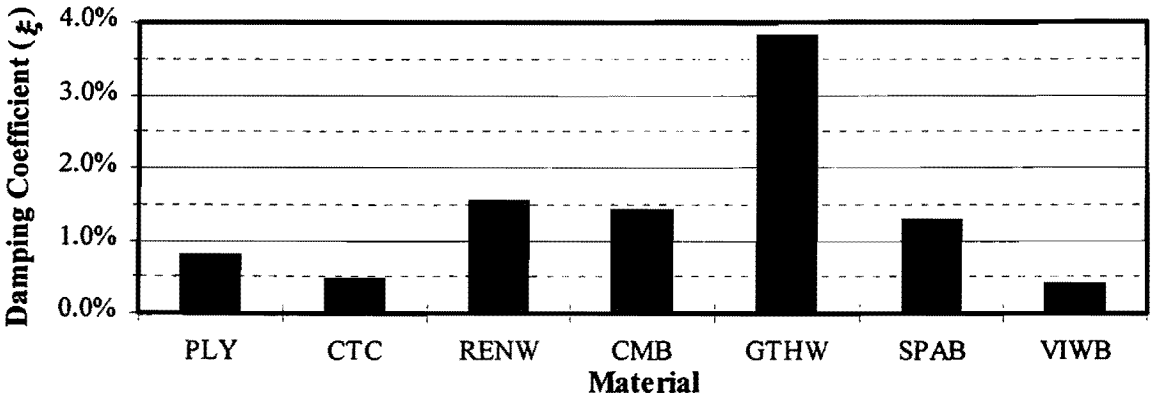

FIG. 24. Free Vibration Results (ξ)

3.5 CREEP TEST

Materials with an excessive tendency to creep may begin to sag when mounted as traffic control devices. This could make the sign more difficult to read and induce stress concentrations around the bolt holes, thus shortening the life of the sign. Therefore, a short term creep test was performed to determine the rate of deformation and recovery of the recycled materials. Each specimen was tested at a room temperature of 22° C and at 60° C. The latter temperature was used to simulate behavior when the substrate is heated by the sun

in a outdoor environment. Each test produced a displacement versus time chart that showed behavior of the specimen with the load applied (creep) and with the load removed (recovery).

3.5.1 Laboratory Procedure

Creep tests were performed in bending on a cantilevered specimen. Each specimen was 2.54 cm wide and 30.48-cm long. The small beam-shaped specimen was clamped to a large structural column using a C-channel clamp and chair, two bolts, and a torque wrench (see Fig. 25). An edge of the specimen was clamped flush with an end of a C-channel. After leveling the sample, the bolts were turned by hand and tightened with a torque wrench to 13.6 N-m of torque. The load was then applied uniformly to the free end of the specimen using a special hanger (see Fig. 25). Strain was recorded using strain gages that were placed 25.4 cm from the free end. Temperature effects were eliminated by zeroing the strain gage reading at the inception of each experiment.

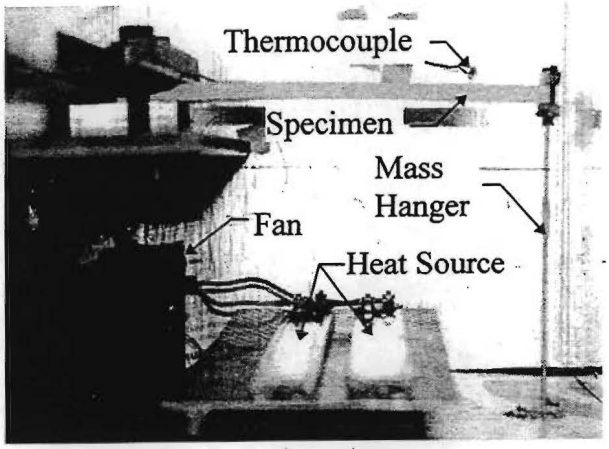

FIG. 25. Creep Specimen Ready for Testing

3.5.2 Calculations

Each specimen was loaded to an identical stress. Since dimensions of the specimens varied, each specimen had to be loaded with a different mass based on the cross-sectional dimensions of the specimen. Maximum bending stress in the sample was computed using the beam bending formulae:

$$\sigma = \frac{My}{I} \tag{12}$$

and,

$$I = \frac{wt^3}{12} \tag{13}$$

$$M = Pl \tag{14}$$

$$y = \frac{t}{2} \tag{15}$$

where σ is the bending stress, y is the distance from the neutral axis to the extreme fiber, I is the moment of inertia about the axis of bending, w is the width of the specimen, t is the thickness of the specimen, M is the moment at the location the strain is being measured, P is the applied load at the free end, and l is the distance from the applied load to the strain gage. Eqs. 12-15 determined the load, P, that was applied to each specimen in order to achieve an identical state of maximum extreme fiber normal stress for each experiment as follows:

$$P = \frac{\sigma wt^2}{6l} \tag{16}$$

A strain gage was placed 0.1905 m from the applied load. Stress at the gage was 1.079×10^3 kPa. Cross-sectional properties of each creep specimen and the applied mass are given in Table 7.

TABLE 7. Applied Mass for Creep Test

Material (1)	Moment of Inertia (m^4) (2)	Flexural Modulus (kPa) (3)	Thickness (m) (4)	Applied Mass (g) (5)
Plywood	9.806×10^{-9}	5.76×10^6	1.635×10^{-2}	692.69
AQ	4.060×10^{-9}	9.22×10^5	1.278×10^{-2}	366.94
CTC	3.292×10^{-10}	6.53×10^6	5.367×10^{-3}	70.90
RENW	1.109×10^{-8}	1.11×10^6	1.732×10^{-2}	739.93
CMB	1.640×10^{-9}	1.56×10^6	9.042×10^{-3}	209.48
GTHW	4.388×10^{-9}	1.37×10^6	1.245×10^{-2}	407.25
SPAB	1.823×10^{-9}	1.33×10^6	9.144×10^{-3}	230.25
VIWB	7.564×10^{-9}	2.73×10^6	1.465×10^{-2}	584.15

3.5.3 Results

Figs. 26-33 show the time dependent behavior of the materials under constant stress. Wood and CTC did not experience a great amount of creep, and they did not experience a change in stiffness at the elevated temperature (see Figs. 26 and 28). The initial strain recorded for plywood was approximately equal to the strain predicted by Hooke's law. Most of the recycled materials experienced greater than predicted initial strains at 22° C. This may be attributed to the high strain rate in the creep experiment since the stress was applied instantaneously and behavior of plastic materials was known to be strain rate dependent.

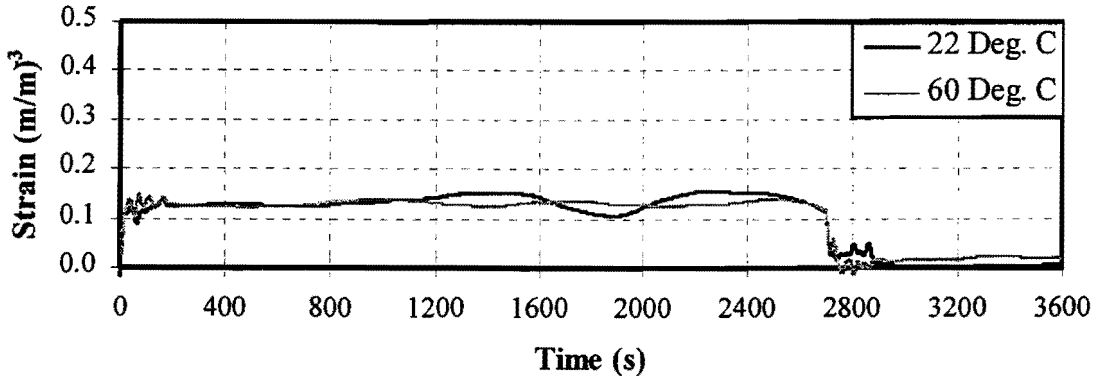

FIG. 26. Creep and Recovery of Plywood

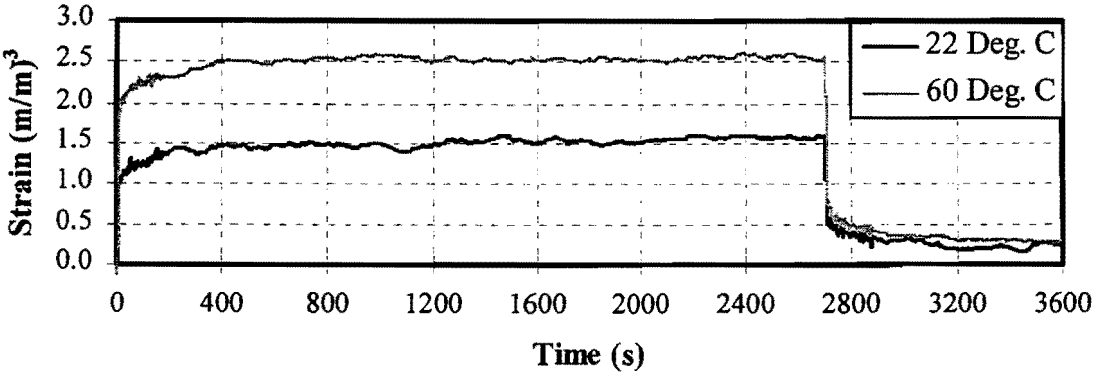

FIG. 27. Creep and Recovery of AQ

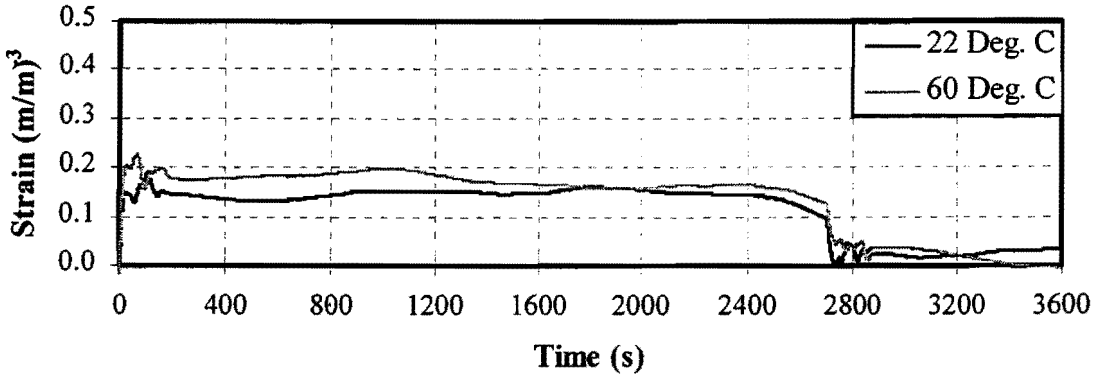

FIG. 28. Creep and Recovery of CTC

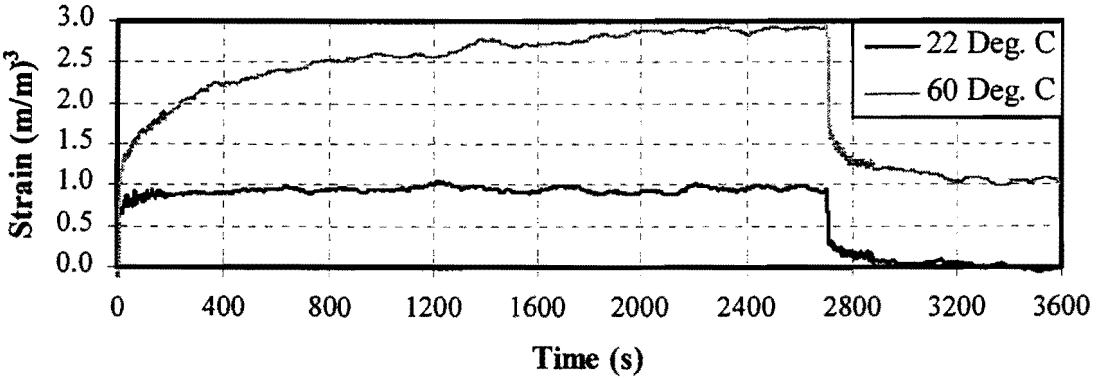

FIG. 29. Creep and Recovery of RENW

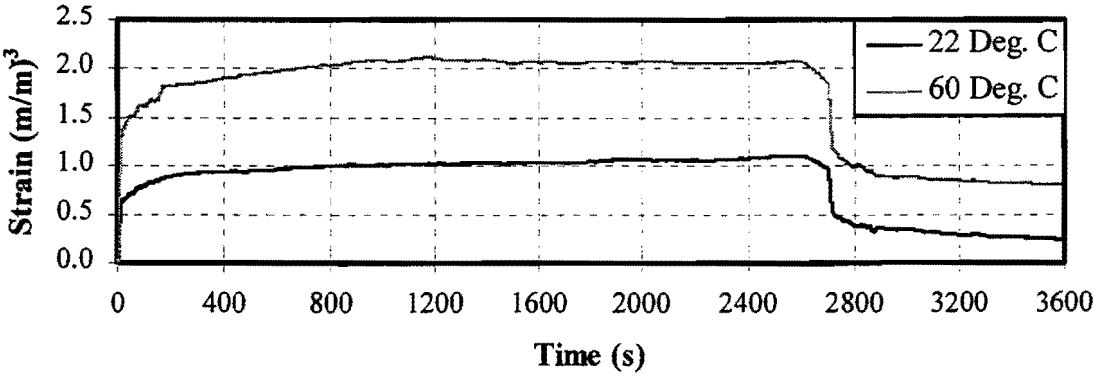

FIG. 30. Creep and Recovery of CMB

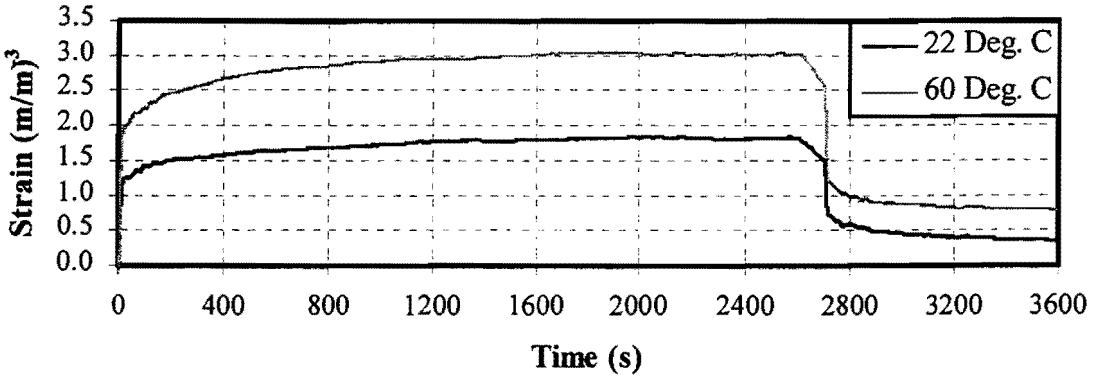

FIG. 31. Creep and Recovery of GTHW

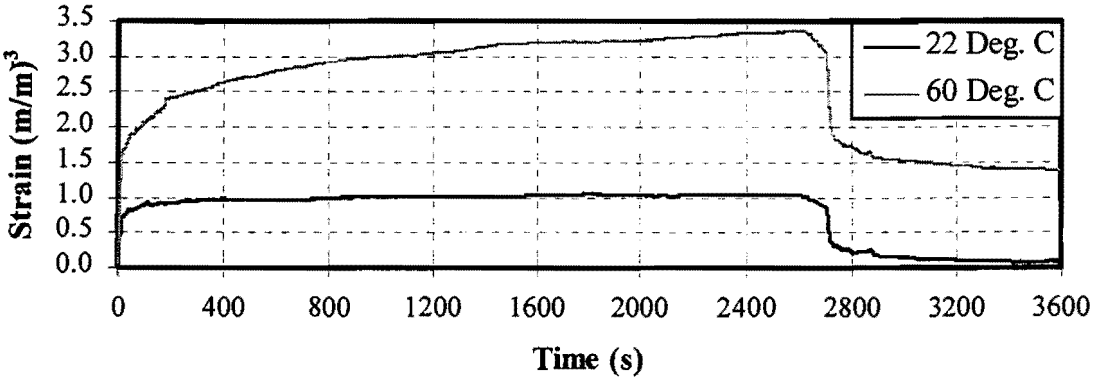

FIG. 32. Creep and Recovery of SPAB

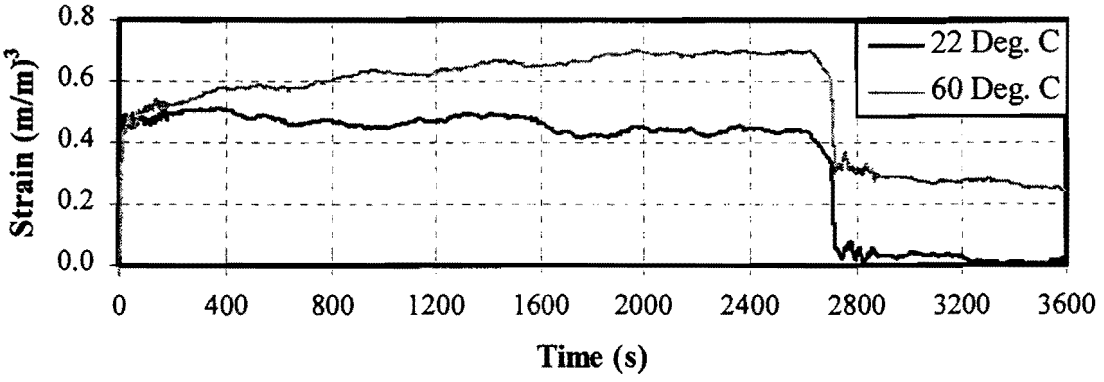

FIG. 33. Creep and Recovery of VIWB

A measure of the amount of creep was made by determining the percent increase in strain during the creep portion of the experiment (see Tables 8 and 9). Thermal effects were quantified by measuring the percent increase in maximum strain (see Table 10). Creep is defined for purposes of this discussion as the non-linear portion of displacement that occurs over time after the initial static displacement. This quantity may be expressed as the percent difference between the initial and maximum strain. CMB experienced a high level of creep at room temperature experiencing a 126% increase in strain. VIWB was extremely stable with just a 9% increase at room temperature. At an elevated temperature of 60° C RENW, SPAB, and CMB exhibited high propensity for creep, and GTHW performed as it did at room temperature with a 70% strain. Plywood and CTC performed well with relatively low creep values. RENW and SPAB both experienced approximately a 100% increase in maximum strain due to the elevation of the testing temperature to 60° C.

TABLE 8. Creep Results 22° C

Material (1)	Initial Strain (m/m) (2)	Maximum Strain (m/m) (3)	Creep (%) (4)
Plywood	1.29×10^{-4}	1.34×10^{-4}	15%
AQ	9.39×10^{-4}	1.61×10^{-3}	70%
CTC	2.23×10^{-4}	2.50×10^{-4}	12%
RENW	6.17×10^{-4}	1.04×10^{-3}	68%
CMB	5.04×10^{-4}	1.14×10^{-3}	126%
GTHW	1.14×10^{-3}	1.87×10^{-3}	65%
SPAB	6.47×10^{-4}	1.08×10^{-3}	67%
VIWB	4.71×10^{-4}	5.11×10^{-4}	9%

TABLE 9. Creep Results 60° C

Material (1)	Initial Strain (m/m) (2)	Maximum Strain (m/m) (3)	Creep (%) (4)
Plywood	1.35×10^{-4}	1.48×10^{-4}	10%
AQ	1.69×10^{-3}	2.62×10^{-3}	55%
CTC	2.04×10^{-4}	2.11×10^{-4}	4%
RENW	9.38×10^{-4}	2.96×10^{-3}	215%
CMB	1.11×10^{-3}	2.18×10^{-3}	97%
GTHW	1.82×10^{-3}	3.09×10^{-3}	70%
SPAB	1.26×10^{-3}	3.38×10^{-3}	169%
VIWB	4.28×10^{-4}	7.03×10^{-4}	64%

TABLE 10. Temperature Effect on Material Stiffness

Material (1)	Percent Increase in Maximum Strain (23° C to 60° C) (2)
Plywood	*
AQ	47.48 %
CTC	*
RENW	98.69 %
CMB	62.57 %
GTHW	49.41 %
SPAB	104.71 %
VIWB	31.54 %

* Negligible increase in strain

3.6 ENVIRONMENTAL STUDY

One of the important characteristics of a sign substrate material is that it must withstand continuous exposure to outdoor weather. Deterioration of outdoor materials is the result of exposure to ultraviolet (UV) light, rain, wind, and freeze-and-thaw cycles. In order to determine the influence, if any, that environmental conditions have on the mechanical properties and serviceability of a sign blank, samples collected for this study were exposed to UV light in a simple test stand (see Fig. 34). Effects of UV and weathering were determined

by comparing results of uni-axial tension and four-point bending tests on exposed samples with the same tests performed on samples in their virgin state.

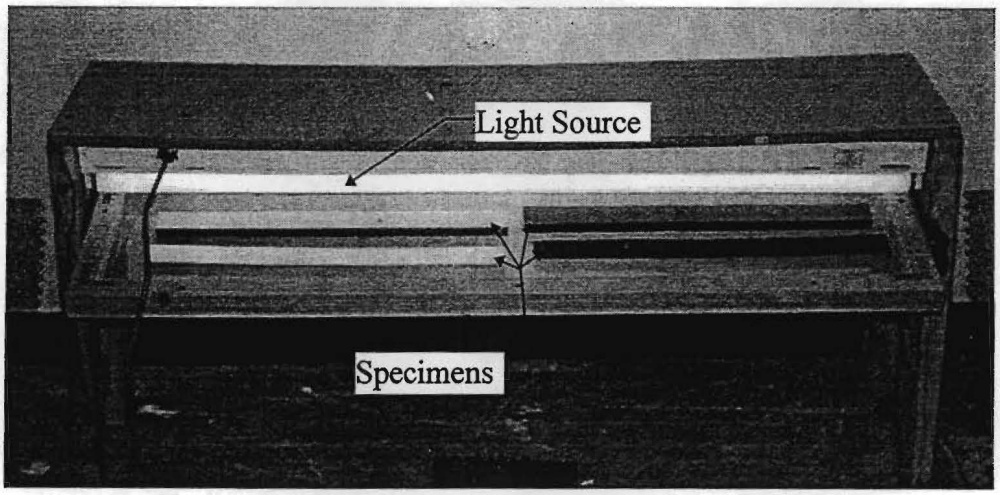

FIG. 34. UV Test Stand

3.6.1 Environmental Tests

A 0.038 m × 0.203 m coupon of each specimen was subjected to a UV exposure test that was intended to approximate exposure to sunlight. The test was performed using procedures outlined in ASTM G53-94. Standard practice suggests the use of four fluorescent UV-B light bulbs rated at 40 watts each. However, for this study, the samples were placed in a custom-built stand (see Fig. 34) that contained only two 40 watt bulbs. Each coupon was placed on a shelf that was 50 mm directly below the UV-B light source.

3.6.2 Results

Eight samples of material, two specimens of each material type, were tested in a UV-B stand (see Fig. 34). After 45 days three of the samples showed discoloration on the surface. This is thought to be a result of the relatively short wavelength of light used in this particular test. The wavelengths ranged between 280 nm and 315 nm.

To describe the effects of exposure to UV-B rays, the uni-axial stress-strain diagrams are provided for both the virgin and exposed specimens (see Figs. 35-40).

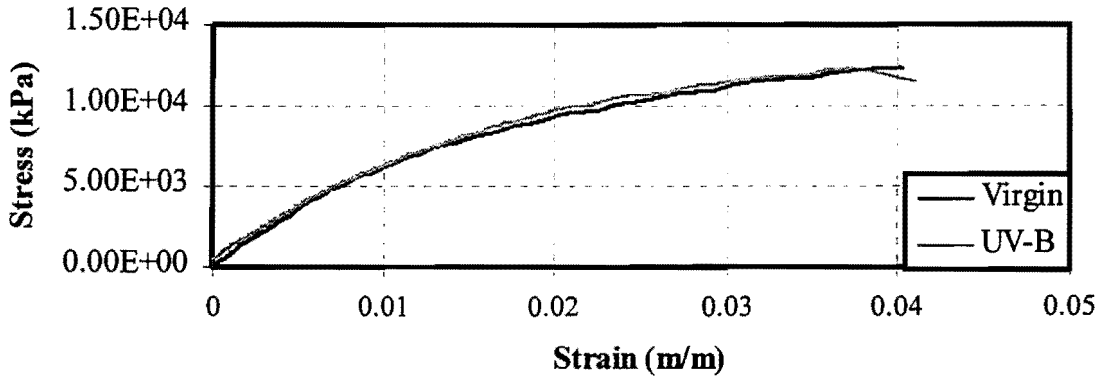

FIG. 35. Environmental Effect on AQ

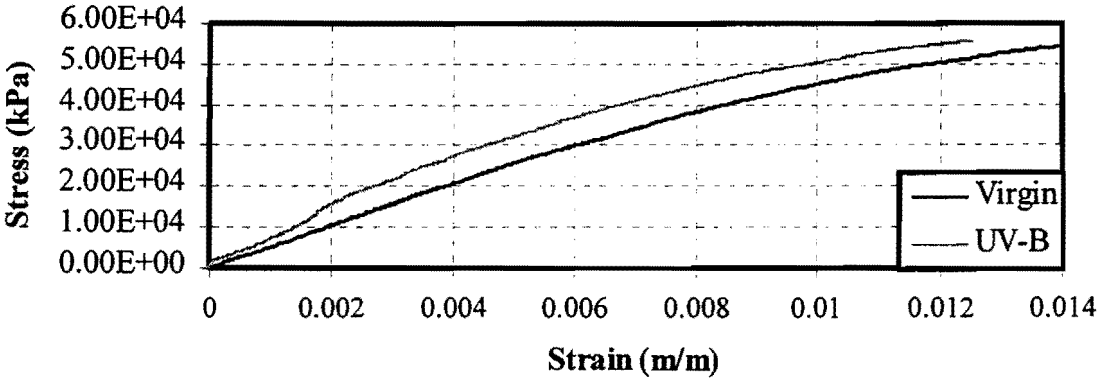

FIG. 36. Environmental Effect on CTC

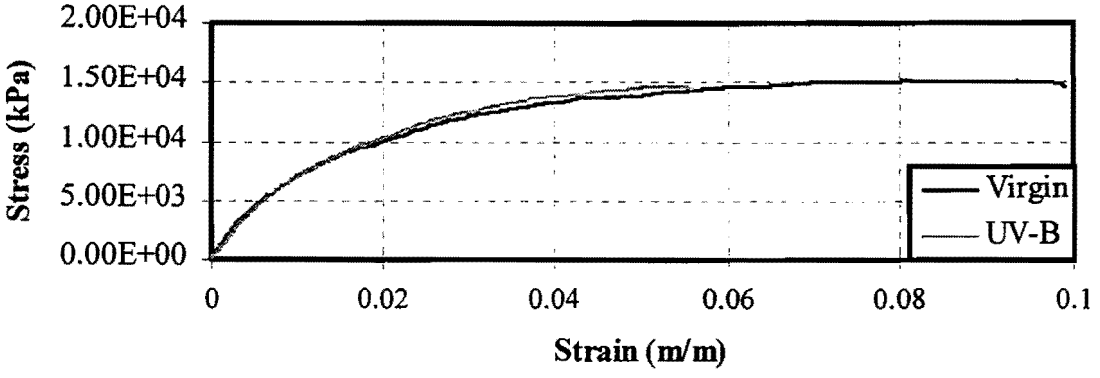

FIG. 37. Environmental Effect on RENW

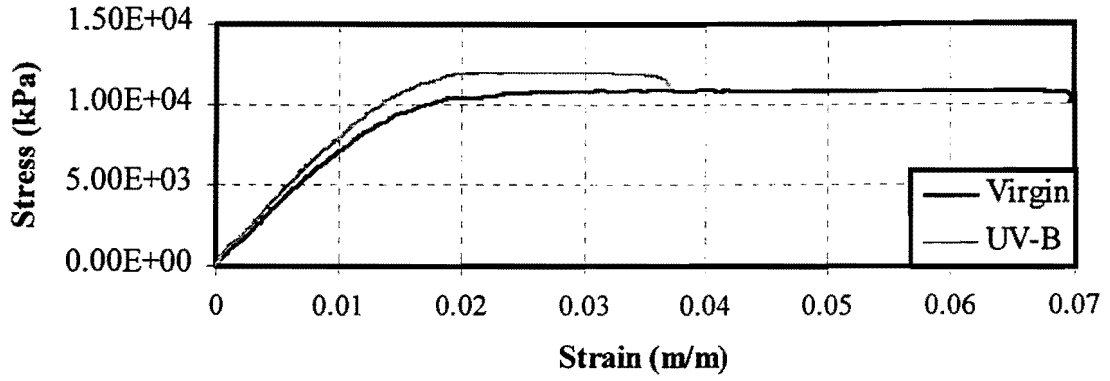

FIG. 38. Environmental Effect on GTHW

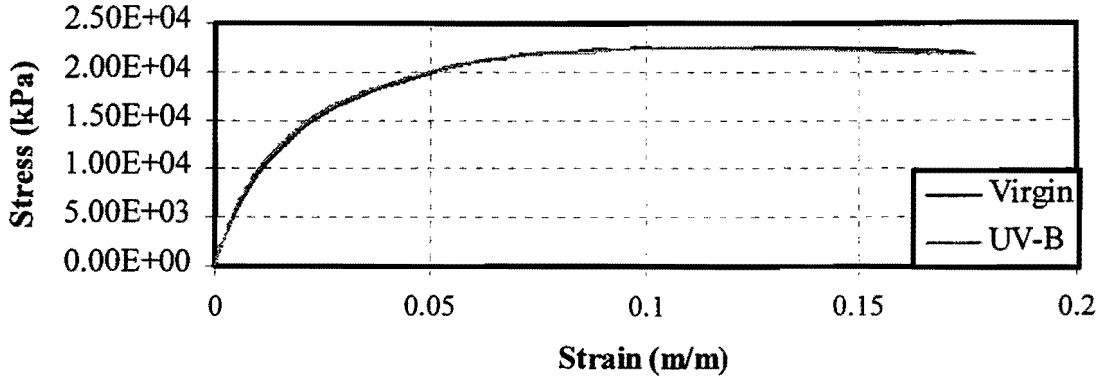

* Test terminated due to onset of creep

FIG. 39. Environmental Effect on SPAB

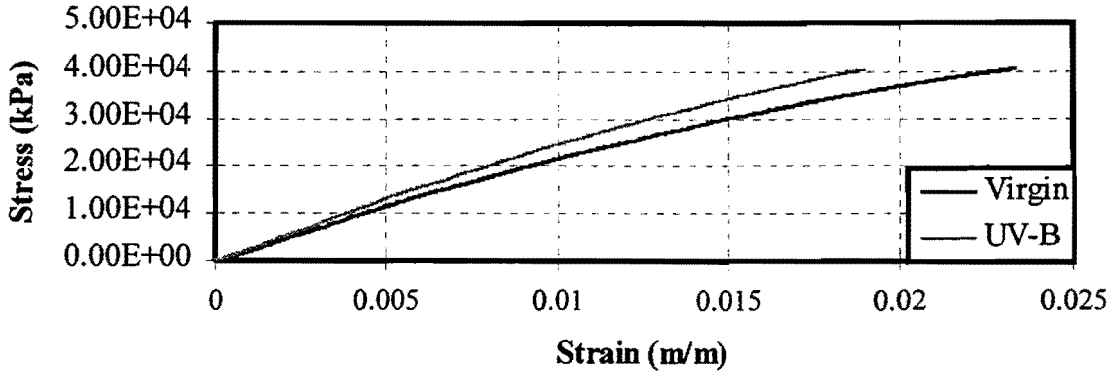

FIG. 40. Environmental Effect on VIWB

Marine plywood showed considerable discoloration of the edges. The Renewed Materials sample (RENW) was discolored and faded. Lastly, the Composite Technologies Corporation product (CTC) showed no physical sign of UV damage.

Results of the UV-B specimens are mixed. Plywood experienced a significant reduction in strength of 16%, while recycled specimens retained their strength or, in some cases, became stiffer but less ductile. CTC experienced a negligible change in its flexural modulus that may be attributed to experimental variance. GTHW and SPAB samples were not UV stabilized during manufacturing and became approximately 7% stiffer after being exposed to UV-B rays (see Table 11 & Fig. 41).

TABLE 11. Summary of Environmental Effects

Material	Flexural Modulus		
	Virgin kPa	UV-B kPa	Change (%)
(1)	(2)	(4)	(5)
Plywood	5.62×10^6	4.77×10^6	-16.31%
AQ	9.22×10^5	9.40×10^5	1.86%
CTC	6.53×10^6	6.43×10^6	-1.65%
RENW	1.11×10^6	1.14×10^6	3.04%
GTHW	1.37×10^6	1.47×10^6	7.33%
SPAB	1.33×10^6	1.42×10^6	6.84%
VIWB	2.73×10^6	2.78×10^6	1.82%

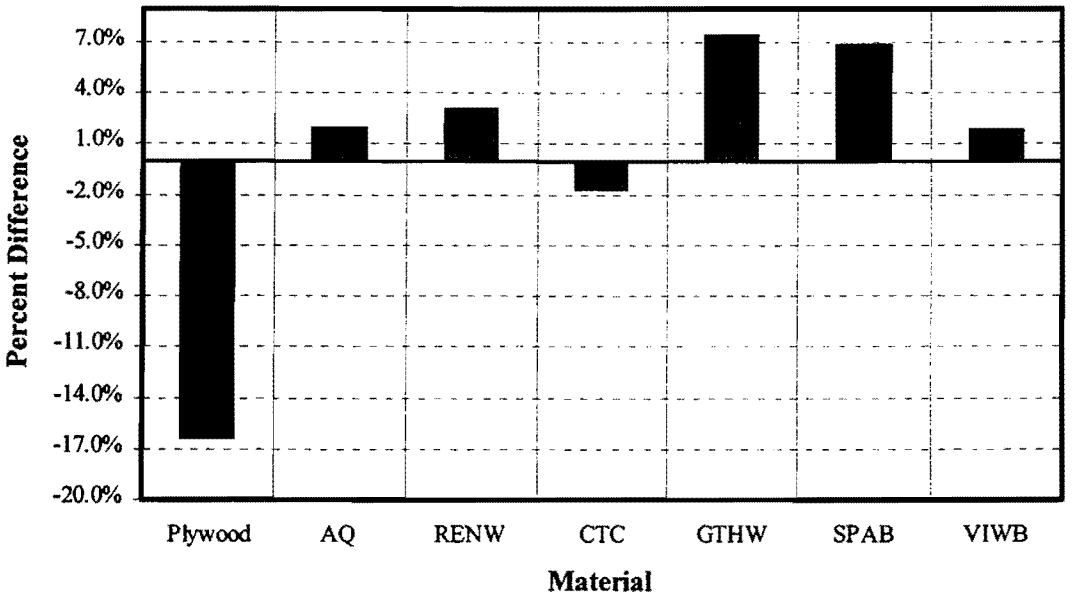

FIG. 41. Change in Flexural Modulus Due to UV-B Exposure

4. DESIGN METHOD FOR ROADSIDE SIGN BLANKS

4.1 GENERAL

In order to procure sign blanks made from recycled material that conform to a minimum standard of performance, it is necessary to develop a procedure by which the blanks may be designed and certified. A need for a design procedure that is independent of the material results from the variability in densities, mechanical properties, and serviceability of substrates produced by manufacturers of recycled products. As recycling technologies advance and the quality of recycled materials improves, a design procedure for roadside signs will enable a material supplier to closely match the material properties and serviceability of their products with those required for a specified size and performance at a given site within Texas.

The following sections describe how to determine the required thickness of a candidate material, or evaluate suitability of an existing material. The goal of this procedure is to reduce the development time and expense of producing an efficient design for recycled materials. This chapter, in conjunction with the performance specifications outlined in Appendix A, provides the necessary information for performing the design process presented in Fig. 42.

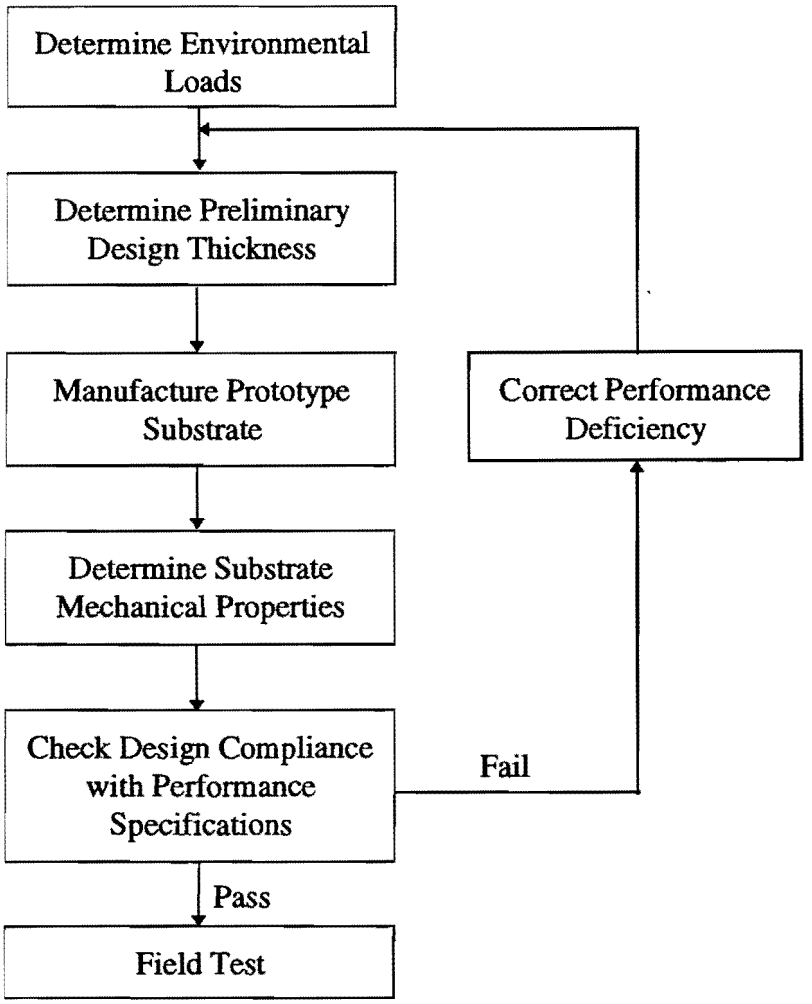

FIG. 42. Design Process

4.2 LOADING PROCEDURE

As a preliminary step, environmental loads for a sign are determined from a design code or recommended design guide. One of the most widely used guidelines for roadside hardware, "Structural Supports for Highway Signs, Luminaires and Traffic Signals" (SSHS), states that for design purposes, the four types of loads to be considered are dead, live, ice, and wind. Each type of load and its relationship to roadside signs are discussed in the following sections.

Two types of loads are predominant in the design of sign blanks: dead and wind loads. Dead load is due to the self-weight of the sign substrate itself. Wind loads that act

on the face of the sign can create both drag and lift (AASHTO 1994). In what follows, a procedure for application of wind loads is applied from "ASCE Standard 7-95: Minimum Design Loads for Buildings and Other Structures" (1995). ASCE 7-95 is chosen over AASHTO because ASCE 7-95 is a more recent code with a more in-depth gust factor approximation.

4.2.1 Dead

The dead load of a highway sign is taken to be the weight of the sign blank itself. In a simplified static analysis the dead load is applied vertically at the centroid of the sign (see Fig. 43(a)). For more complicated approaches, such as static and dynamic finite element analysis (FEA), a continuum approach more accurately represents distribution of mass. In the latter approach the mass and inertial properties of the material are evenly distributed throughout the sign panel (see Fig. 43(b)), which is important for an accurate simulation of dynamic behavior.

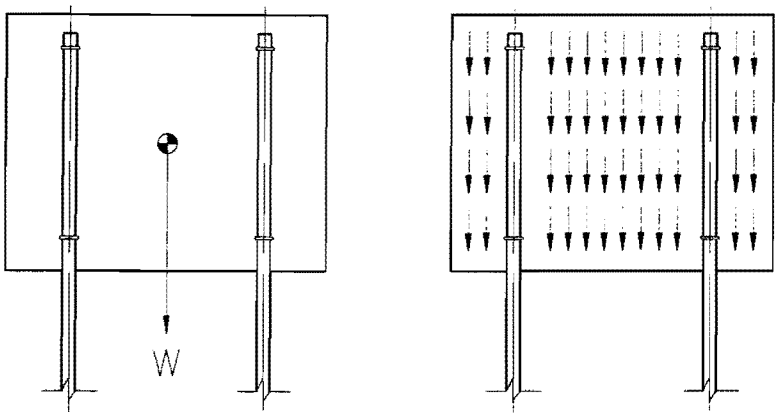

FIG. 43. Sign Panel Weight: (a) Simplified Static Analysis; and (b) Continuum Approach

4.2.2 Live

Live loads as defined in SSHS are specified only for the design of walkways and service platforms (AASHTO 1994). Therefore, live loads are not applicable in the design of sign panels.

4.2.3 Ice

According to section 1.2.3 of SSHS and section 3.2.1 of "Review of Structural Design Criteria for Noise Walls" (RSDC), ice loads are applied to only one face of the sign panel and on surfaces of structural supports. SSHS specifies the ice load to be 143.6 Pa for locations within Texas. Distribution of this added mass is readily accomplished by a finite element analysis code.

4.2.4 Wind

In general, strong winds provide the most significant forces that a roadside sign blank must resist. SSHS governs design wind pressures for roadside structures. Key elements of this code are based upon design approaches that have since been superseded by ASCE 7-95 "Minimum Design Loads for Buildings and Other Structures." ASCE 7-95 was written with a focus on buildings and other traditional three-dimensional structures. However, the code does have provisions for other less traditional structures, including signs.

4.2.4.1 Wind Pressure Formulae

ASCE 7-95 contains a refined method for determining wind pressures on objects based upon wind speed. It defines a flexible building or other structure as one that has a fundamental frequency less than one hertz or a ratio of height to the least horizontal dimension greater than 4. Sign substrates meet this criterion due to the insignificance of the through-thickness dimension in comparison to the height of the sign above ground. Signs may also be designated as "other structures." In accordance with these definitions, the equation to be used for velocity pressure is:

$$P = q_z G_f C_f \tag{17}$$

where G_f is the gust factor, C_f is the force coefficient (see ASCE 7-95, Table 6-8), and q_z is the wind velocity pressure (in units of Pa) given by:

$$q_z = 0.613 K_z K_{zt} V^2 I \tag{18}$$

where K_z is the exposure coefficient (see ASCE 7, Table 6-3 and Table 12), K_{zt} is a speed factor for hills and escarpments (see ASCE 7, Fig. 6-2), V is the basic wind speed based upon a 50-year mean recurrence interval (see ASCE 7, Fig. 6-1), and I is the importance factor of the structure (see ASCE 7, Table 6-2). For purposes of this study, roadside signs are taken to be category I structures with an importance factor of 0.87.

Determination of the gust factor G_f involves a detailed procedure outlined in section 6.6 of the ASCE 7-95 code. As discussed previously, due to the high aspect ratio of a sign substrate, G_f should be determined according to a classification as a flexible or dynamically sensitive structure. ASCE 7-95 classifies this type of structure as Category III for determination of the gust effect factor (1995). The calculation for G_f is rather lengthy and complex. Details of this procedure are given in the following sections.

TABLE 12. Velocity Pressure Exposure Coefficient K_z for ASCE 7-95

Height above ground level, z(m)	Exposure Category			
	A	B	C	D
(1)	(2)	(3)	(4)	(5)
0-4.6	0.32	0.57	0.85	1.03
6.1	0.36	0.62	0.90	1.08
7.6	0.39	0.66	0.94	1.12

Category C exposure is defined as open terrain with scattered obstructions having heights generally less than 9.1 m (ASCE 7-95). Exposure D is limited to structures exposed to winds that have an over water fetch of at least 1.61 km and extend only 457.2 m inland (ASCE 7-95). Since only a small percentage of roadside signs meet the criteria for exposure D, exposure C is taken to be the applicable category for a sign blank in most regions. Exposure D must still be considered in coastal areas or alongside other open

bodies of water that meet the criterion. Categories A and B are not considered since they produce lower exposure coefficients and wind pressures.

4.2.4.2 Gust Factor for Dynamically Sensitive Structures

ASCE 7-95 calls for a rational analysis in order to determine gust factors for flexible buildings or other dynamically sensitive structures. The gust factor is a non-dimensional multiplicative constant. Although no analysis procedures are given in the standard, the commentary provides equations that can be used to determine a gust factor. The basic steps of this approach are outlined in this section. ASCE 7-95 does not give a procedure that uses SI units for the determination of this constant; therefore, English units are used here.

Values for the variables listed in Table 13 must be known to begin evaluating the gust effect factor. The notation in this table is consistent with that used in ASCE 7-95.

TABLE 13. Required Parameters for G_f

Variable (1)	Definition (2)
b	Width of sign
Exposure	Category C or D (ASCE 7-95, Sec. 6.5.3)
h	Height to centroid of sign from ground
$\hat{V}_{ref}$	Design wind speed (ASCE 7-95, Fig. 6-1)
β	Percent critical damping
n_1	Fundamental frequency

The depth of the sign substrate is considered to be insignificant in relation to its width and height; here, it is set equal to zero. As a preliminary calculation, the following quantities are required:

$$I_{\bar{z}} = c\left(\frac{33}{\bar{z}}\right)^{\frac{1}{6}} \tag{19}$$

$$L_{\bar{z}} = l\left(\frac{\bar{z}}{33}\right)^{\varepsilon} \tag{20}$$

$$\overline{V}_{\bar{z}} = \bar{b}\left(\frac{\bar{z}}{33}\right)^{\bar{\alpha}} \hat{V}_{ref} \tag{21}$$

where $I_{\bar{z}}$ is the intensity of turbulence at height $\bar{z}$, $L_{\bar{z}}$ is the integral length scale of turbulence at the equivalent height, and $\overline{V}_{\bar{z}}$ is the mean hourly wind speed in ft/s at height $\bar{z}$ where $\bar{z}$ is the equivalent height of the structure ($\bar{z} \geq 0.6h$ and $\bar{z} \geq z_{min}$). The exposure constants c, $\bar{b}$, and l are given in Table 14 and defined in ASCE 7-95.

TABLE 14. Exposure Constants for G_f

Exposure (1)	$\hat{\alpha}$ (2)	$\hat{b}$ (3)	$\overline{\alpha}$ (4)	$\bar{b}$ (5)	c (6)	l(ft) (7)	ε (8)	z_{min}(ft) (9)
C	1/9.5	1.00	1/6.5	0.65	0.20	500	1/5.0	15
D	1/11.5	1.07	1/9.0	0.80	0.15	650	1/8.0	7

Several secondary calculations are also necessary:

$$N_1 = \frac{n_1 L_{\bar{z}}}{\overline{V}_{\bar{z}}} \tag{22}$$

$$\eta_b = 4.6\frac{n_1 b}{\overline{V}_{\bar{z}}} \tag{23}$$

$$\eta_h = 4.6\frac{n_1 h}{\overline{V}_{\bar{z}}} \tag{24}$$

where h is the height of the centroid of the sign substrate above ground, and b is the width. Components of R, the resonant response factor, are:

$$R_l = \begin{cases} \dfrac{1}{\eta_l} - \dfrac{1}{\eta_l^2}\left(1 - e^{-2\eta_l}\right) & for\ \eta_l > 0 \\ 1 & for\ \eta_l = 0 \end{cases} \tag{25}$$

where l can take the values of h or b, and:

$$R_n = \frac{7.465N_1}{\left(1 + 10.302N_1\right)^{\frac{5}{3}}} \tag{26}$$

The square of the resonant response factor is defined to be:

$$R^2 = \frac{1}{\beta} R_n R_b R_h \tag{27}$$

The square of the background response, Q^2, is given by:

$$Q^2 = \frac{1}{1 + 0.63\left(\frac{b+h}{L_{\bar{z}}}\right)^{0.63}} \tag{28}$$

Finally, the gust factor for a dynamically sensitive structure is given by:

$$G = \frac{1 + 7I_{\bar{z}}\sqrt{Q^2 + R^2}}{1 + 7I_{\bar{z}}} \tag{29}$$

The procedure ASCE 7-95 outlines for calculating the gust effect factor is complicated. In order to simplify the procedure, an approximate approach that combines the use of equations and graphs is discussed in the following section.

4.2.4.3 Derivation of Graphic Approach to Gust Factor Approximation

A relatively simple way to determine the gust factor for a sign blank from equations and graphs is given in this section. First, dimensions of the sign are simplified. Since the depth of a sign is a relatively insignificant dimension, it is set equal to zero. However, by also eliminating the width dimension, one introduces a conservatism of 10-15%. That is, a conservative value of G is determined by assuming that the width (b) and depth (d) are zero. As later shown, the gust factor can be determined graphically for each exposure based on the design wind speed (V) the natural frequency of the structure (n) and the damping ratio (β).

In assuming that dimensions b and d are zero, this method produces an inherent conservatism for determining the gust factor. For applications to the design of luminaries and poles, this method should prove to be accurate since width and depth are minimal. However, roadside signs embody at least two dimensions of significance; therefore, this method provides a conservative value for G. Elimination of this conservatism may be realized by the procedure outlined in section 4.2.4.2.

First, a ratio of the basic wind speed (V) and the natural frequency (n_1) is computed; this enables determination of an equation for the square of the resonant response factor. Substituting Eq. 21 into Eq. 24 gives:

$$\eta = \frac{4.6 n_1 h}{\bar{b}\left(\frac{\bar{z}}{33}\right)^{\bar{\alpha}} \hat{V}_{ref}} \tag{30}$$

Substituting Eqs. 20 and 21 into Eq. 22 produces:

$$N_1 = \frac{n_1 l \left(\frac{\bar{z}}{33}\right)^{(\varepsilon-\bar{\alpha})}}{\bar{b}\hat{V}_{ref}} \tag{31}$$

Substituting Eq. 31 into Eq. 25 produces:

$$R_h = \frac{\bar{b}\left(\frac{\bar{z}}{33}\right)^{\bar{\alpha}} \hat{V}_{ref}}{4.6 n_1 h} - \left(\frac{\bar{b}\left(\frac{\bar{z}}{33}\right)^{\bar{\alpha}} \hat{V}_{ref}}{9.2 n_1 h}\right)^2 \left(1 - \exp\left(\frac{-9.2 n_1 h}{\bar{b}\left(\frac{\bar{z}}{33}\right)^{\bar{\alpha}} \hat{V}_{ref}}\right)\right) \tag{32}$$

Substituting Eq. 31 into Eq. 26 produces:

$$R_n = \frac{7.465\left(\frac{n_1 l \left(\frac{\bar{z}}{33}\right)^{(\varepsilon-\bar{\alpha})}}{\bar{b}\hat{V}_{ref}}\right)}{\left(1+10.302\left(\frac{n_1 l \left(\frac{\bar{z}}{33}\right)^{(\varepsilon-\bar{\alpha})}}{\bar{b}\hat{V}_{ref}}\right)\right)} \tag{33}$$

$$\Psi = R_n R_h \tag{34}$$

The product of Eq. 32 and Eq. 33 (ψ) is a function of $\hat{V}_{ref}$, n_1, h, and exposure (see Eq. 34). For any given exposure, this product may be plotted as a function of h for different $\frac{\hat{V}_{ref}}{n_1}$

ratios (see Fig. 44). When the output of this function is divided by the percent critical damping (β), the result is R^2 (see Eq. 27 and Fig. 45).

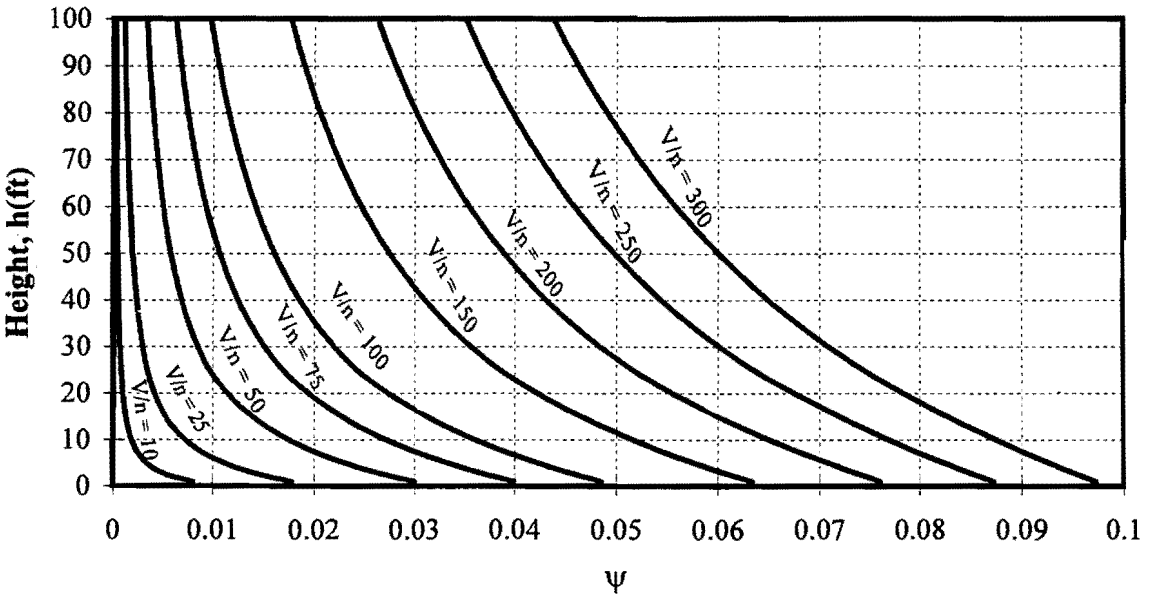

FIG. 44. ψ versus h for Various $\frac{\hat{V}_{ref}}{n_1}$ Ratios

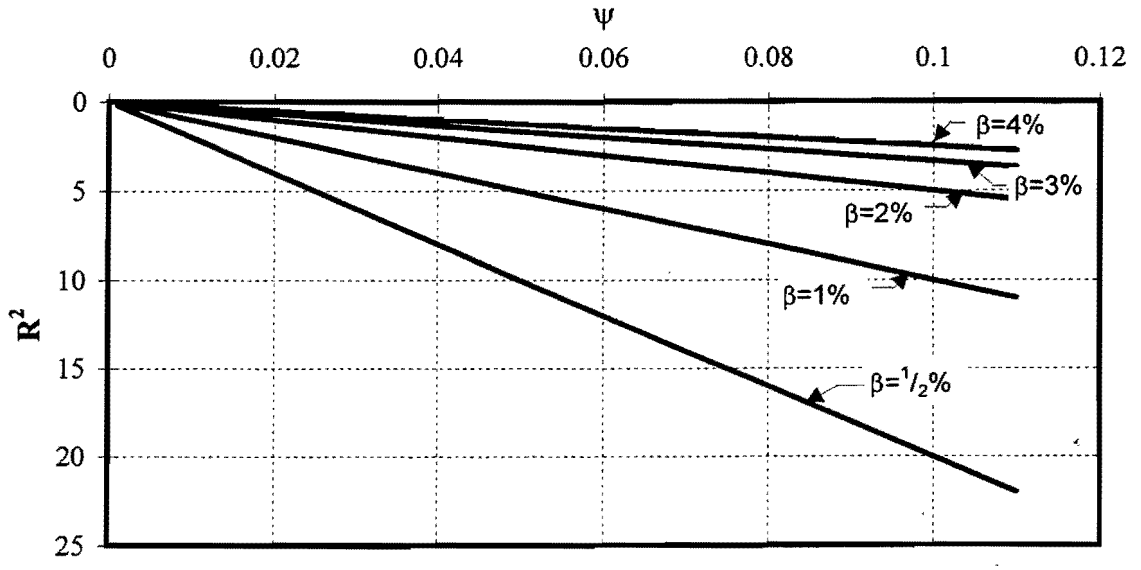

FIG. 45. Graphical Division of ψ by β

Eq. 29 shows that G is a function of I_z, R^2, and Q^2. Q^2 in Eq. 35 may be simplified as follows, since $b = 0$:

$$Q^2 = \frac{1}{1 = 0.63\left(\frac{h}{L_{\bar{z}}}\right)^{0.63}} \tag{35}$$

From Eqs. 19 and 29, G can be written as a function of R^2, h, and exposure:

$$G = \frac{1 + 7c\left(\frac{33}{\bar{z}}\right)^{\frac{1}{6}}\sqrt{Q^2 + R^2}}{1 + 7c\left(\frac{33}{\bar{z}}\right)^{\frac{1}{6}}} \tag{36}$$

Fig. 46 shows the relationship between R^2 and G for different values of h. Height has little effect on G until $h \geq h_{min}$ at which point a non-negligible error propagates. In order to maintain a purely graphical approach for the determination of G, it is necessary to remove the dependence of this relationship on h. Fig. 46 shows that the gust factor is inversely

proportional to the height. If $h \leq h_{min}$, no correction is necessary and the line for minimum height may be used. However, if $h > h_{min}$, a correction must be made.

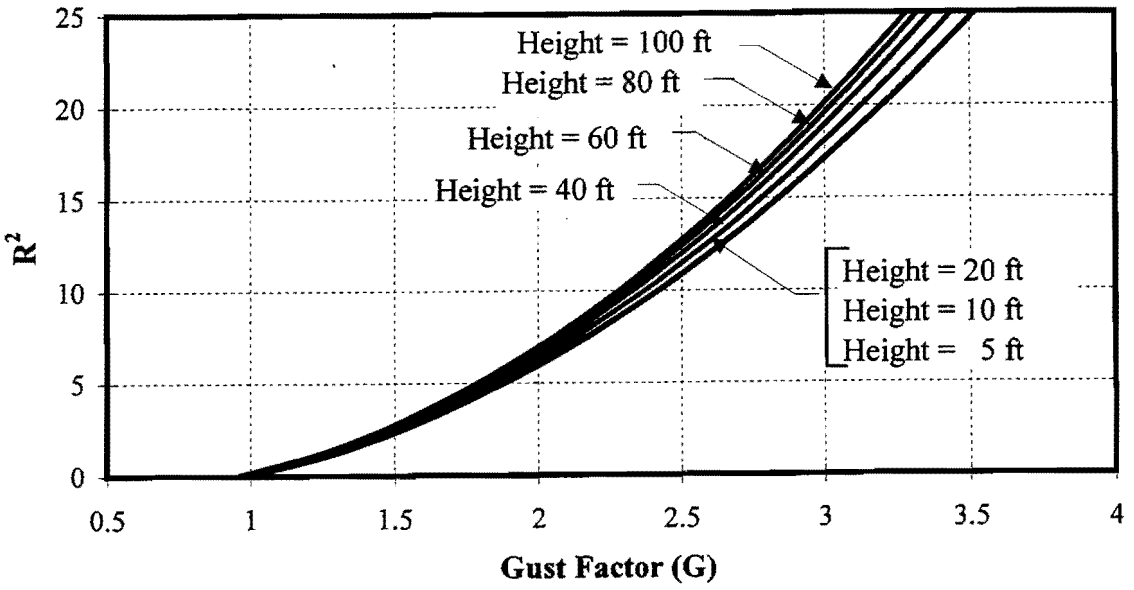

FIG. 46. R^2 versus G for Exposure C

To determine the proper correction for G, a plot of the difference between values of G is presented (see Fig. 47 and 48). This difference is nearly linear, and therefore, the slopes of these relationships are plotted as a function of G (see Fig. 49). A fit of this data with a logarithmic function shows the correction for the gust factor:

$$Slope = 0.0553\log_e(h) - 0.1708 \tag{37}$$

Fig. 48 shows that the linearized gust factor corrections intersect at an uncorrected gust factor of 0.9. To obtain the gust factor correction ΔG, the difference between 0.9 and the original gust factor, G_{max}, is multiplied by the slope:

$$\Delta G = \left(G_{\max} - 0.9\right)\left(0.0553\log_e(h) - 0.1708\right) \tag{38}$$

The corrected gust factor is:

$$G = G_{\max} - \Delta G \tag{39}$$

The final form of the gust factor for exposure C is:

$$G = 1.1708G_{\max} + (0.0498 - 0.0553G_{\max})\log_e(h) - 0.1537 \tag{40}$$

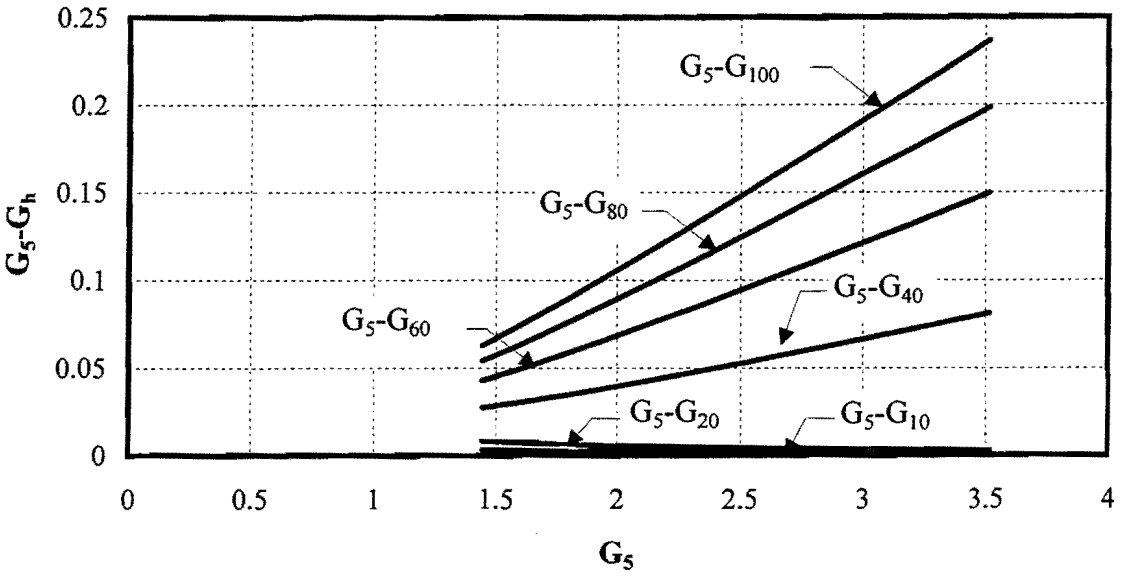

FIG. 47. Gust Factor Error

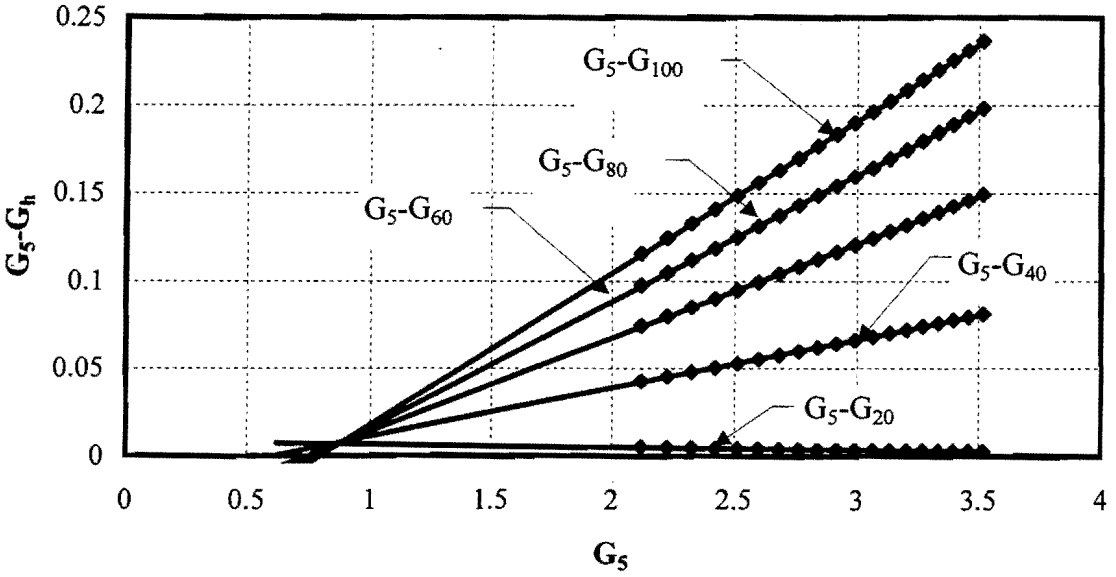

FIG. 48. Linearization of Gust Factor Error

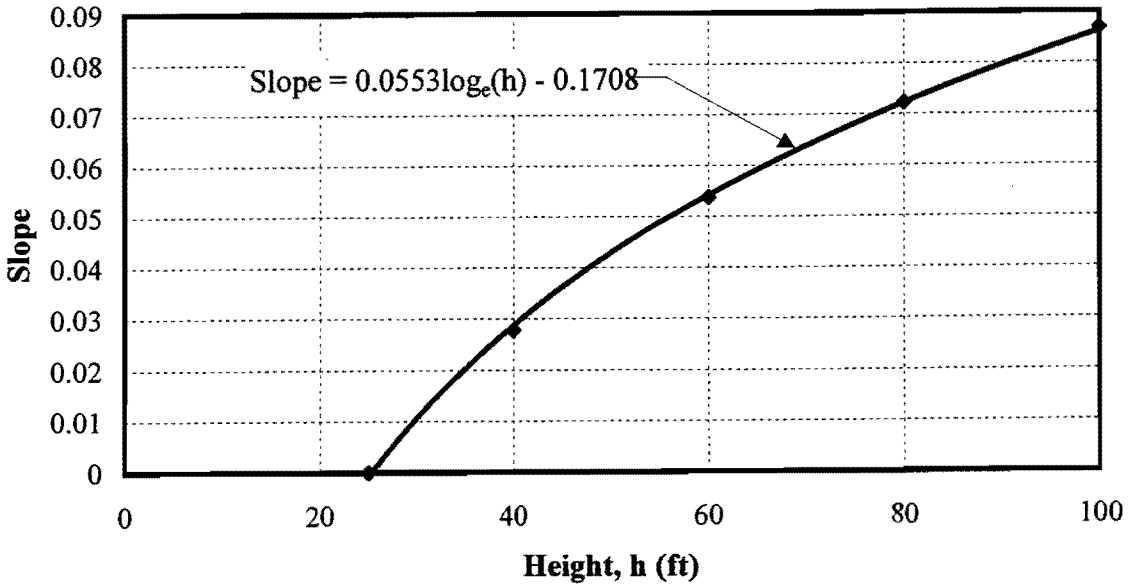

FIG. 49. Slope of Error with Height

The derivation for the correction equation for exposure D follows a similar procedure. The correction equation for exposure D is:

$$G = 1.167G_{\max} + (0.0618 - 0.0687G_{\max})\log_e(h) - 0.15 \tag{41}$$

4.2.4.4 Graphical Approach to Gust Factor Approximation

The graphical procedure that approximates the gust factor is relatively simple. First, determine the variables listed in Table 15. Next, determine the ratio $\hat{V}_{ref}/n_1$. By referring to the figure corresponding to the correct exposure category (see Figs. 50 and 51), locate the structure height, h. Use interpolation to find the point on this graph where a horizontal projection of the height intersects the appropriate $\hat{V}_{ref}/n_1$ ratio. Next, draw a vertical line from this point until it intersects the appropriate damping ratio, β. Finally, draw a horizontal line from this point to the gust factor curve. The value on the upper abscissa at this intersection is the maximum gust factor, G_{max}.

Next, z_{min} is obtained from Table 16. If $0.6h \leq z_{min}$, then $G=G_{max}$. If $0.6h > z_{min}$, then use the appropriate equation in Table 17 to determine the gust factor.

TABLE 15. Required Variables

Variable (1)	Definition (2)
β	Percent critical damping expressed as a decimal.
Exposure	Category C or D.
n_1	Natural frequency of the structure expressed in Hz.
$\hat{V}_{ref}$	Basic wind speed obtained from ASCE 7-95.
h	Height to center of area on which wind is acting.

TABLE 16. z_{min} for Exposures (ASCE 7-95, Table C6-6)

Exposure (1)	z_{min} (ft) (2)
C	15
D	7

TABLE 17. Corrected Gust Factor Formula

Exposure (1)	Gust Factor (2)
C	$G = 1.1708G_{max} + (0.0498 - 0.0553G_{max})\log_e(h) - 0.1537$
D	$G = 1.167G_{max} + (0.0618 - 0.0687G_{max})\log_e(h) - 0.15$

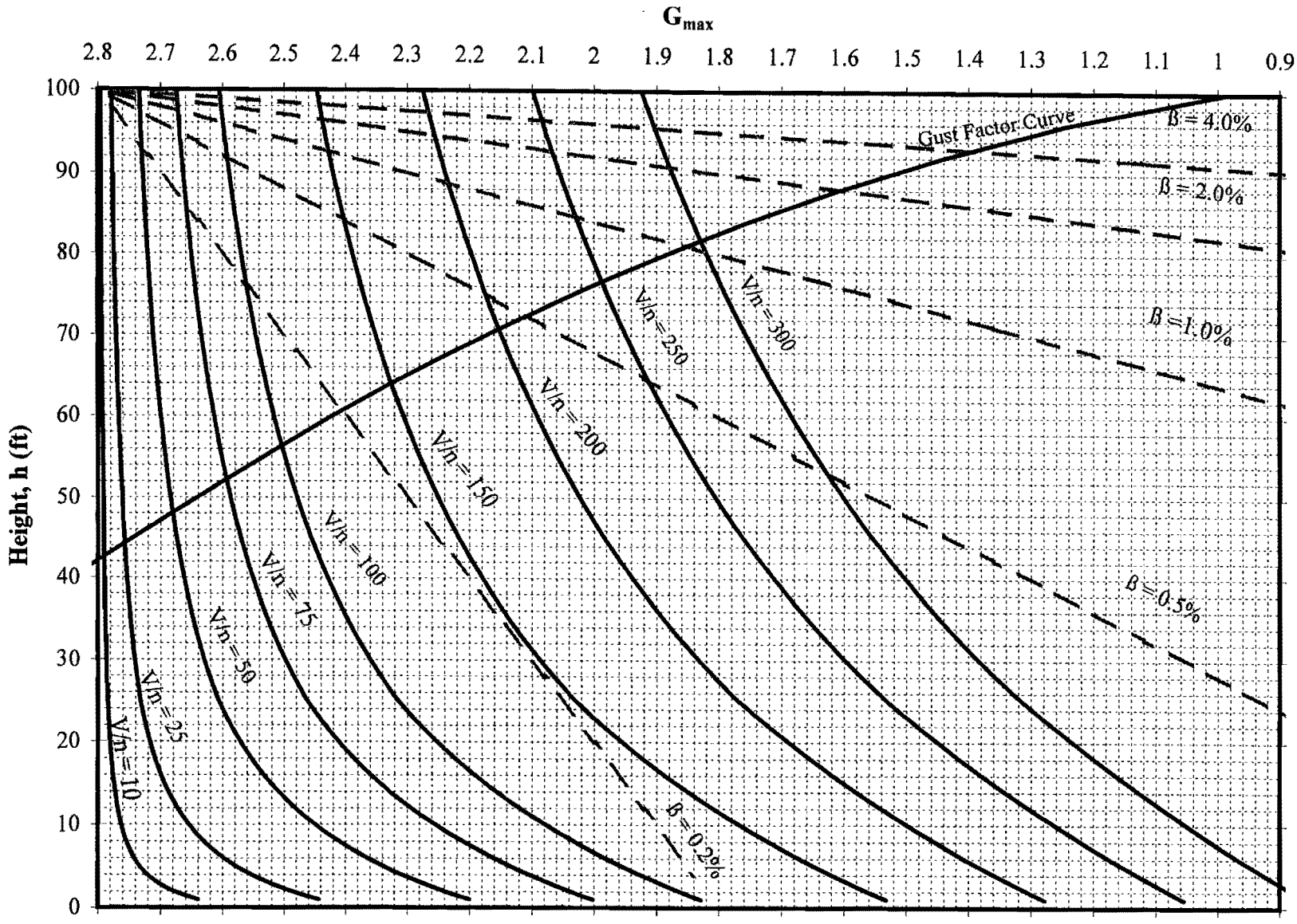

FIG. 50. Graphical Solution of G_{max} for Exposure C

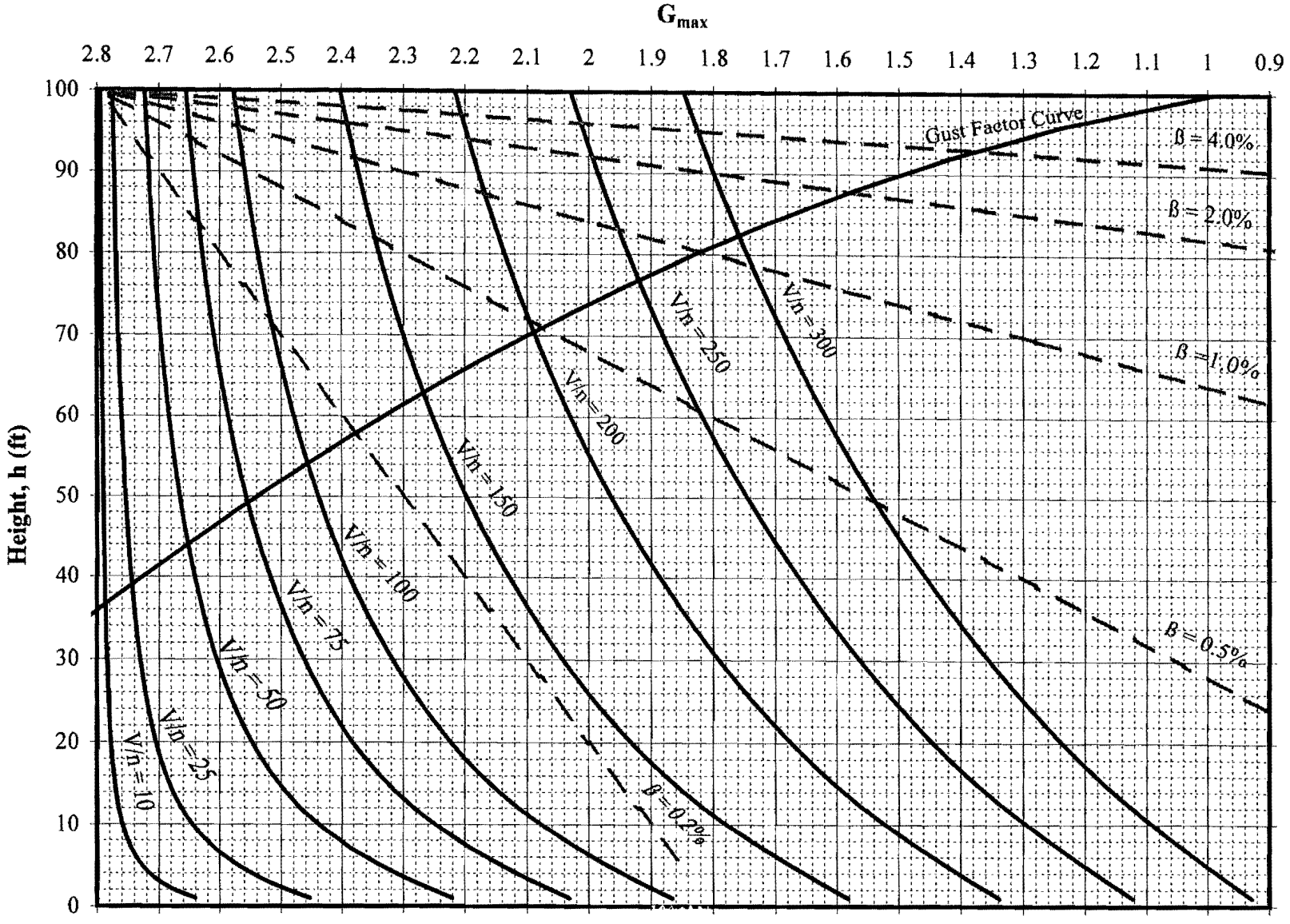

FIG. 51. Graphical Solution of G_{max} for Exposure D

4.3 DESIGN METHODOLOGY

The following steps outline a procedure for the design of flat plates constructed of recycled materials for use as highway sign blanks. This procedure limits the application of the design to "medium" size signs. For this section a medium size sign is defined as a sign which is at least 1.2 m in the least dimension and can be constructed out of one piece of material.

4.3.1 Material Properties

Knowledge of material properties listed in Table 18 is necessary for completion of the design procedure. The reader is also referred to Chapter 3 for information on how to determine these values.

TABLE 18. Material Properties

Property (1)	Symbol (2)
Unit weight	γ
Flexural modulus	E_s
Yield stress	σ_y
Ultimate shear stress	τ

4.3.2 Preliminary Design Procedure

Dead loads, ice loads, and wind loads can all act on a sign blank. For a preliminary design, only wind loads are taken into consideration. However, dead loads and ice loads should also be considered for a detailed analysis of the design by FEA.

To determine a preliminary sign thickness, a 50-year mean recurrence interval wind speed of 40 m/s is chosen. Static wind pressure on the sign face is specified by following the current ASCE 7-95 or equivalent standard (see section 4.2.4.3). K_z is determined by inspection of Table 12 and use of K_{zt}= (0.87). The geometry of the sign, including the size of windward face and the location and dimension of the supporting structure, also needs to be defined.

Procedures for two-pole and T-pole configurations follow.

4.3.2.1 Two-Pole Configuration

For a typical two-pole supporting structure, a preliminary estimate of the design thickness for the substrate may be determined by using standard mechanics of materials beam formulae. Based upon a simply supported strip of length (βW), width (b), and thickness (t) shown in Fig. 52, an approximation to the required thickness of the substrate is calculated according to the derivation that follows.

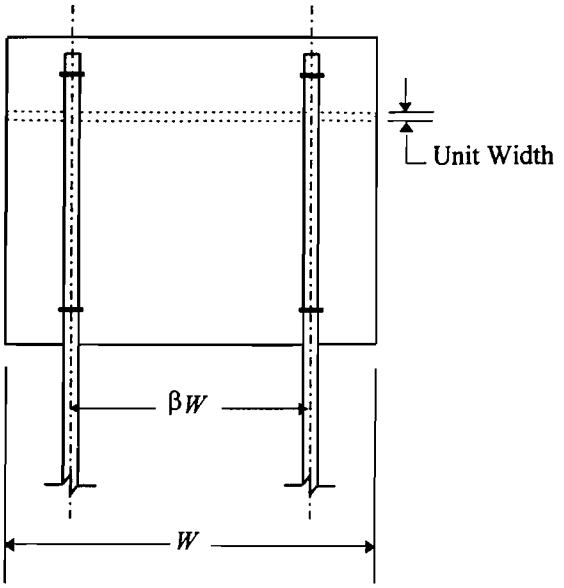

FIG. 52. Geometry of a Two-Pole Sign

For a simple two-pole supporting structure, transverse deflection at the centerline of a simply-supported strip of length L=βW, and taken in a direction orthogonal to the supporting structure is (Lindeburg 1992):

$$\Delta_c = \frac{5b(\beta W)^4 P}{384EI} \tag{42}$$

where P is the pressure on the substrate. A specification for the maximum allowable deflection (Δ_{cmax}) of the substrate is not currently available. However, some limit needs to be specified. For example, if the sign blank is made too flexible, a blinking effect may occur during a wind event. Alternatively, a substrate that is too stiff will not be economical. Here,

a maximum allowable deflection (Δ_{cmax}) of the sign blank is arbitrarily based on a serviceability limit of:

$$\Delta_{cmax} = \frac{\beta W}{50} \tag{43}$$

Other serviceability limits can also be used. For purposes of comparison, Table 19 gives design equations based upon other serviceability limits at the end of the derivation. Equating Eqs. 42 and 43 and solving the result for *I* gives:

$$I = \frac{250b(\beta W)^3 P}{384E} \tag{44}$$

For a beam of width (*b*) and thickness (*t*), the moment of inertia is:

$$I = \frac{bt^3}{12} \tag{45}$$

Substituting this equation into the left hand side of Eq. 44 and solving for *t* produces an expression for determining the design thickness of the material as a function of the sign geometry and material properties:

$$t = \beta W\left[\frac{125P}{16E}\right]^{\frac{1}{3}} \tag{46}$$

where *t* is the estimated thickness of the plate in meters, *w* is the width of the plate in meters, *P* is the applied pressure in kN/m^2, and *E* is the flexural modulus of the material in kPa. Table 19 lists formulae for determination of the required thickness.

TABLE 19. Design Equations for Two-Pole Supported Substrate

Deflection Criterion (1)	Design Equation (2)
$\Delta_{c\max} = \frac{\beta W}{10}$	$t = \beta W\left[\frac{75P}{48E}\right]^{\frac{1}{3}}$
$\Delta_{c\max} = \frac{\beta W}{20}$	$t = \beta W\left[\frac{75P}{24E}\right]^{\frac{1}{3}}$
$\Delta_{c\max} = \frac{\beta W}{30}$	$t = \beta W\left[\frac{75P}{16E}\right]^{\frac{1}{3}}$
$\Delta_{c\max} = \frac{\beta W}{40}$	$t = \beta W\left[\frac{75P}{12E}\right]^{\frac{1}{3}}$
$\Delta_{c\max} = \frac{\beta W}{50}$	$t = \beta W\left[\frac{125P}{16E}\right]^{\frac{1}{3}}$
$\Delta_{c\max} = \frac{\beta W}{60}$	$t = \beta W\left[\frac{75P}{8E}\right]^{\frac{1}{3}}$
$\Delta_{c\max} = \frac{\beta W}{70}$	$t = \beta W\left[\frac{175P}{16E}\right]^{\frac{1}{3}}$
$\Delta_{c\max} = \frac{\beta W}{80}$	$t = \beta W\left[\frac{75P}{6E}\right]^{\frac{1}{3}}$
$\Delta_{c\max} = \frac{\beta W}{90}$	$t = \beta W\left[\frac{225P}{16E}\right]^{\frac{1}{3}}$
$\Delta_{c\max} = \frac{\beta W}{100}$	$t = \beta W\left[\frac{375P}{24E}\right]^{\frac{1}{3}}$

4.3.2.2 T-Pole Configuration

For a typical T-pole supporting structure, a preliminary estimate of the design thickness for the substrate may be determined by a similar approach used for the two-pole supporting structure (see Fig. 53). Based upon a unit wide cantilevered strip of length *W*/2, an approximation to the required thickness of the substrate is calculated by the derivation that follows.

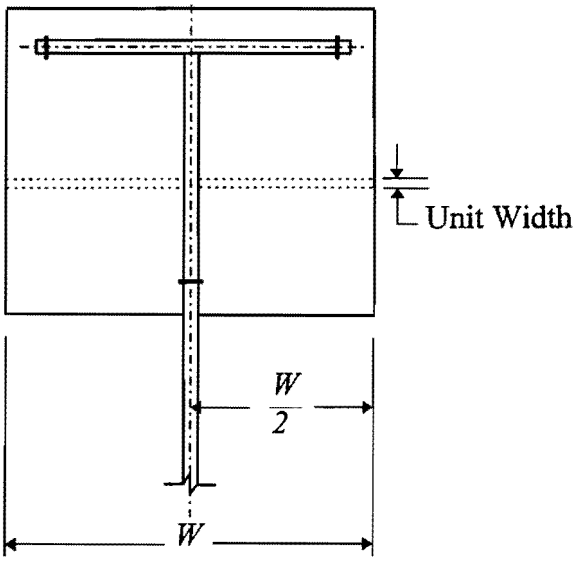

FIG. 53. Geometry of a T-Pole Sign

For a simple T-pole supporting structure, shown in Fig. 53, maximum deflection of a cantilevered strip of length (L=0.5W), thickness (t), and width (b), and taken in a direction orthogonal to the supporting structure is (Lindeburg 1992):

$$\Delta = \frac{0.75bP\left(\frac{W}{2}\right)^4}{6EI} \tag{47}$$

Similar to the two-pole design where a specification for the maximum permissible deflection is not available, a maximum allowable deflection (Δ_{max}) of the sign blank is arbitrarily based on a serviceability limit of:

$$\Delta_{max} = \frac{W}{50} \tag{48}$$

Table 20 gives design equations based upon other serviceability limits at the end of the derivation. Equating Eqs. 47 and 48 and solving for I gives:

$$I = \frac{75bP(W)^3}{48E} \tag{49}$$

Equating Eqs. 45 and 49 produces an expression for the design thickness of the material as a function of the sign geometry and material properties:

$$t = W\left[\frac{75P}{16E}\right]^{\frac{1}{3}} \tag{50}$$

where t is the required thickness of the plate in meters, w is the width of the plate in meters, P is the applied pressure in kN/m^2, and E is the flexural modulus of the material in kPa.

TABLE 20. Design Equations for T-Pole Supported Substrate

Deflection Criterion (1)	Design Equation (2)
$\Delta_{cmax} = \frac{\beta W}{10}$	$t = W\left[\frac{15P}{16E}\right]^{\frac{1}{3}}$
$\Delta_{cmax} = \frac{\beta W}{20}$	$t = W\left[\frac{15P}{8E}\right]^{\frac{1}{3}}$
$\Delta_{cmax} = \frac{\beta W}{30}$	$t = W\left[\frac{45P}{16E}\right]^{\frac{1}{3}}$
$\Delta_{cmax} = \frac{\beta W}{40}$	$t = W\left[\frac{15P}{4E}\right]^{\frac{1}{3}}$
$\Delta_{cmax} = \frac{\beta W}{50}$	$t = W\left[\frac{75P}{16E}\right]^{\frac{1}{3}}$
$\Delta_{cmax} = \frac{\beta W}{60}$	$t = W\left[\frac{45P}{8E}\right]^{\frac{1}{3}}$
$\Delta_{cmax} = \frac{\beta W}{70}$	$t = W\left[\frac{105P}{16E}\right]^{\frac{1}{3}}$
$\Delta_{cmax} = \frac{\beta W}{80}$	$t = W\left[\frac{15P}{2E}\right]^{\frac{1}{3}}$
$\Delta_{cmax} = \frac{\beta W}{90}$	$t = W\left[\frac{675P}{16E}\right]^{\frac{1}{3}}$
$\Delta_{cmax} = \frac{\beta W}{100}$	$t = W\left[\frac{75P}{8E}\right]^{\frac{1}{3}}$

4.4 EXAMPLE: DESIGN OF TWO-POLE SUBSTRATE USING ASCE 7-95

4.4.1 General

The following detailed example illustrates the determination of the design thickness of a sign substrate using the wind pressure design procedures outlined in this chapter and in ASCE 7-95. A two-pole sign is placed in Bryan, Texas. Dimensions of the substrate are 1.52 m wide by 1.22 m high (see Fig. 54). The selected recycled plastic material has mechanical and dynamic properties listed in Table 21.

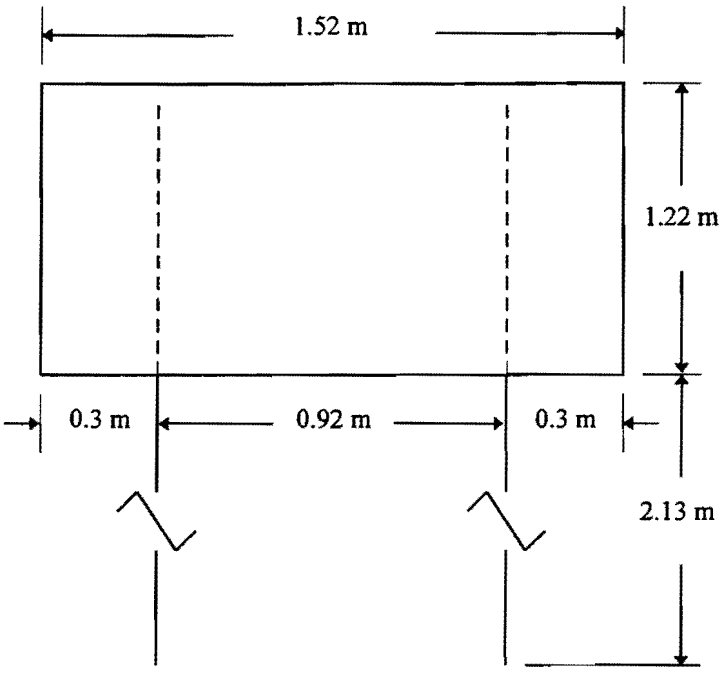

FIG. 54. Sign Geometry for Example

TABLE 21. Material and System Properties for Example Design

Material Property (1)	Value (2)
Damping (β)	3.81%
Flexural modulus (E_b)	1.37×10^6 kN/m^2
Unit weight (γ)	5.83 kN/m^3
*Natural frequency (n_1)	2.875 Hz
Height of sign centroid	2.74 m
Sign width	1.52 m

*Natural frequency obtained from FEA

The sign is located in flat open terrain that is classified as Exposure C in ASCE 7-95.

4.4.2 Design Wind Pressure

The governing wind pressure equation is given by (see Eq. 17):

$$P = q_z G_f C_f \tag{51}$$

and q_z is the wind velocity pressure in Pa given by:

$$q_z = 0.613 K_z K_{zt} V^2 I \tag{52}$$

From Fig. 6-1 in ASCE 7-95, $V_{ref} = 40$ m/s. Table 6-3 in ASCE 7-95 gives K_z to be 0.85. K_{zt} is unity since the sign is not located on a hill or escarpment. The importance factor I is 0.87 for a Category I structure. The velocity pressure is:

$$\begin{aligned} q_z &= 0.613(0.85)(1)(40)^2(0.87) \\ q_z &= 725.30 \frac{N}{m^2} \end{aligned} \tag{53}$$

The force coefficient (C_f) in Eq. 51 is given in Table 6-8 in ASCE 7-95. In this example the ratio of the height of the sign to the width of the sign is 1.4:1; therefore, C_f is 1.2.

The only remaining variable to be determined in Eq. 51 is G_f. The ASCE 7-95 procedure for determining the gust factor is presented in section 4.2.4.2. Note that although G_f is non-dimensional, the procedure outlined in ASCE 7-95 is in English units which necessitates their use here also. Table 22 gives a summary of the necessary variables.

Preliminary calculations are performed with the exposure category constants listed in Table 22 as follows:

TABLE 22. Gust Factor Variables for Design Example

Variable (1)	Given Value (2)
Exposure category	C
$\hat{V}_{ref}$	90 mph
$\bar{\alpha}$	$^1/_{6.5}$
$\bar{b}$	0.65
c	6 ft
ε	$^1/_{5.0}$
z_{min}	15 ft

$$I_{\bar{z}} = 0.20\left(\frac{33}{15}\right)^{\frac{1}{6}} = 0.2281 \tag{54}$$

$$L_{\bar{z}} = 500\left(\frac{15}{33}\right)^{\frac{1}{5.0}} = 427.06 \tag{55}$$

$$\bar{V}_{\bar{z}} = 0.65\left(\frac{15}{33}\right)^{\frac{1}{9.5}}(90) = 53.84 \tag{56}$$

The secondary computations may now be performed:

$$N_1 = \frac{2.3(427.06)}{53.84} = 18.24 \tag{57}$$

$$\eta_b = 4.6\frac{2.875(5)}{53.84} = 1.228 \tag{58}$$

$$\eta_h = 4.6\frac{2.875(9.0)}{53.84} = 2.211 \tag{59}$$

In preparation for calculation of the resonant response factor, the following quantities are determined:

$$R_b = \frac{1}{1.228} - \frac{1}{2(1.228)^2}\left(1 - e^{-2(1.228)}\right) = 0.511 \tag{60}$$

$$R_h = \frac{1}{2.221} - \frac{1}{2(2.221)^2}\left(1 - e^{-2(2.221)}\right) = 0.350 \tag{61}$$

and:

$$R_n = \frac{7.465(18.24)}{\left(1+10.302(18.24)\right)^{\frac{5}{3}}} = 2.189 \times 10^{-2} \tag{62}$$

The square of the resonant response factor is:

$$R^2 = \frac{1}{.0381}\left(2.189 \times 10^{-2}\right)(0.511)(0.350) = 0.103 \tag{63}$$

The square of the background response is:

$$Q^2 = \frac{1}{1+0.63\left(\frac{5+9.0}{427.06}\right)^{0.63}} = 0.932 \tag{64}$$

All of the necessary parameters for determining G_f have now been calculated. The gust factor from Eq. 29 is:

$$G = \frac{1+7(0.2281)\sqrt{(0.932)^2+(0.103)^2}}{1+7(0.2281)} = 0.96 \tag{65}$$

Finally, the design pressure is calculated from Eq. 51:

$$\begin{aligned} P &= (725.3)(0.96)(1.2) \\ P &= 835.55\frac{N}{m^2} \end{aligned} \tag{66}$$

4.4.3 Design Thickness

The design thickness of the material may now be determined based upon given deflection criteria. In this example the maximum permissible deflection is taken to be $^{\beta w}/_{70}$. The modulus of the material may be found in Table 21, and the design thickness of the material is:

$$\begin{aligned} t &= 0.91\left[\frac{175(835.55)}{16\left(1.37 \times 10^6\right)}\frac{1\ kN}{1000\ N}\right]^{\frac{1}{3}} \\ t &= 0.0171\ \text{m} \end{aligned} \tag{67}$$

Although the design thickness is an ideal value, a sign substrate of this thickness may not be commercially available. Therefore, it may be necessary to round the thickness up to the nearest available dimension. For this example the ordered thickness is 0.019 m.

4.4.4 Stress Prediction by FEA

The finite element model later described in section 5.6.1 is used to evaluate maximum stresses from the preliminary design. A static pressure of 835.55 is applied uniformly to the face of the substrate in the numerical model (see Fig. 55). The extreme tensile and compressive stresses are 3.343×10^6 Pa and -3.477×10^6 Pa, respectively (see Table 23). The yield stress for GTHW is 1.24×10^7 Pa. The maximum and minimum stresses in the material correspond to only 27% and 28% of the yield stress in the material.

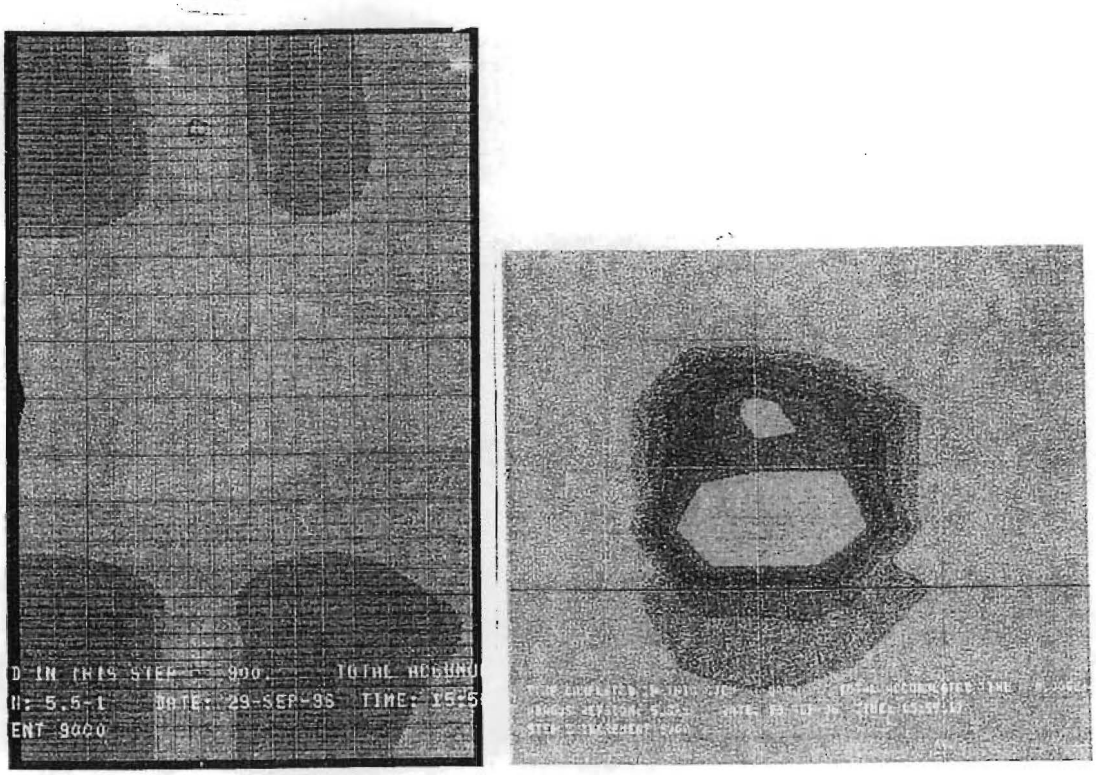

(a) (b)

FIG. 55. FEM Prediction of Stress Field: (a) One-Half of Sign Substrate; (b) Substrate at Hardware Connection

TABLE 23. Extreme Stress Predicted by FEA in Substrate

(1)	Stress (Pa) (2)	Percent of Yield (%) (3)
Maximum	3.343×10^6	27
Minimum	-3.477×10^6	28

5. EXPERIMENTAL SIMULATION

5.1 GENERAL

Due to a lack of understanding of the behavior of sign substrates that have a moderate size and are subjected to oscillatory wind loads, complementary experimental procedures need to be carried out. One of the most commonly used approaches is to place a scale model of a sign panel in a variable speed wind tunnel. However, the study of sign substrates in wind tunnels presents several difficulties. First, large wind tunnels that produce variable speed winds are rare. In order to vary the speed in a wind tunnel, the pitch of the blades of the wind source must be altered. Moreover, in most tunnels the wind must travel around the entire circumference of the tunnel before it reaches the specimen. The length of travel reduces the intensity of the gust, thereby reducing or eliminating the effectiveness of the experiment.

Similitude represents a second obstacle to overcome when performing wind tunnel experiments. As a general rule, the projected area of the specimen is not allowed to exceed one-third of the cross-sectional area of the tunnel so that boundary effects are minimized. If the specimen is too large relative to the aperture of the tunnel, the testing fluid is accelerated as it passes between the specimen and the wall of the tunnel. In order for the test specimen not to exceed these limits, similitude must be used. Ideally, similitude should be maintained with respect to specimen geometry, stiffness, fluid velocity, and density. For these and other reasons, wind tunnel testing is complicated and expensive. These deterrents motivate the development of a technique where reasonably approximate dynamic structural responses in a sign substrate may be produced using actuators in a laboratory testing facility.

When a roadside sign is subjected to oscillatory wind loading, two primary forces are transmitted by the substrate to the supporting structure. First, the wind load, which acts as a pressure force distributed over the projected area of the sign, is carried through the connections to the supporting poles. Second, the dynamic nature of the wind and the mass of the sign substrate create an inertia force throughout the continuum of the sign that is also transmitted to the supporting structure. In contrast, a sign substrate that is loaded by mechanical excitation of the supporting structure experiences only inertia forces generated

from the acceleration of its own mass. In order to develop an approximately equivalent response between a laboratory specimen loaded by a forcing function at the supports and a substrate that is loaded by a strong wind event, a series of response functions must be determined in order to develop a time history of force that can be applied by an electro-mechanical actuator to produce the desired response.

5.2 THEORY

For a linear system the structure may be thought of as a function that transfers an excitation $f(t)$ to a response $x(t)$ (Lutes and Sarkani 1997). This same approach can also be used to determine the acceleration response $\ddot{x}(t)$ to a wind time history $f(t)$ (see Fig. 56).

The linear system that represents the sign substrate may be denoted in the time domain by $h_x(t)$, where $h_x(t)$ is the unit-impulse response function. The impulse response function is defined as $x(t)$ when $f(t)=\delta(t)$, where $\delta(t)$ is an impulse of unit magnitude (Clough and Penzien 1993). If an excitation is considered to be composed of an infinite series of Dirac-delta inputs, the response may be found in closed-form by performing the following integration, known as Duhamel integral or convolution integral (Lutes and Sarkani 1997):

$$x(t) = \int_{-\infty}^{+\infty} f(s)h_x(t-s)ds \tag{68}$$

Similarly, the acceleration response is found by:

$$\ddot{x}(t) = \int_{-\infty}^{+\infty} f(s)h_{\ddot{x}}(t-s)ds \tag{69}$$

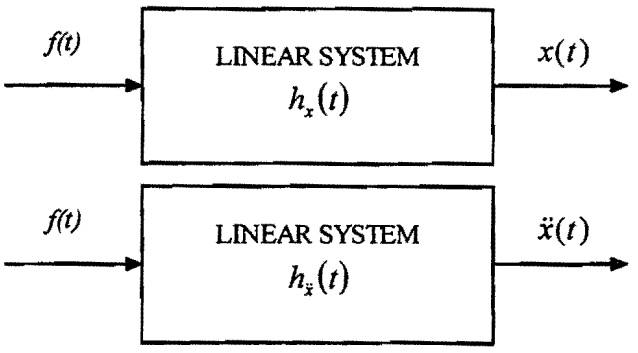

FIG. 56. Schematic of General Linear System (Lutes and Sarkani 1997)

The frequency-domain method of dynamic analysis may be implemented through use of the Fourier transform (Chopra 1995). The Fourier transform is defined as (Lutes and Sarkani 1997):

$$\tilde{f}(\omega) = \frac{1}{2\pi} \int_{-\infty}^{+\infty} f(t) e^{-i\omega t} dt \tag{70}$$

where $\tilde{f}(\omega)$ represents the transformed function. This operation is performed on a set of numerical data using the fast Fourier transform (FFT) by:

$$X(k) = \sum_{j=1}^{N} x(j) \omega_N^{(j-1)(k-1)} \tag{71}$$

where *X=fft(x)* are the transformed vectors of length *N* and:

$$\omega_N = e^{\frac{-2\pi i}{N}} \tag{72}$$

is an N^{th} root of unity (MATLAB®). If the data set of *N* data points does not contain a number of data points that is a power of 2, the prime factors of *N* and the mixed-radix discrete Fourier transforms of the shorter sequences can be calculated. That is, Fourier analysis holds for data sets that are not a power of 2 in length.

Impulse response functions $h_x(t)$ and $h_{\ddot{x}}(t)$ may be converted into the frequency domain by use of Eq. 70 in order to determine the complex frequency response function, $H(i\omega)$ and $\ddot{H}(i\omega)$:

$$H(i\omega) = \frac{1}{2\pi} \int_{0}^{+\infty} h(t) e^{i\omega t} dt \tag{73}$$

and,

$$\ddot{H}(i\omega) = \frac{1}{2\pi} \int_{0}^{+\infty} \ddot{h}(t) e^{i\omega t} dt \tag{74}$$

$H(i\omega)$ and $\ddot{H}(i\omega)$ may be used to determine the frequency response to any particular dynamic loading (see Fig. 57).

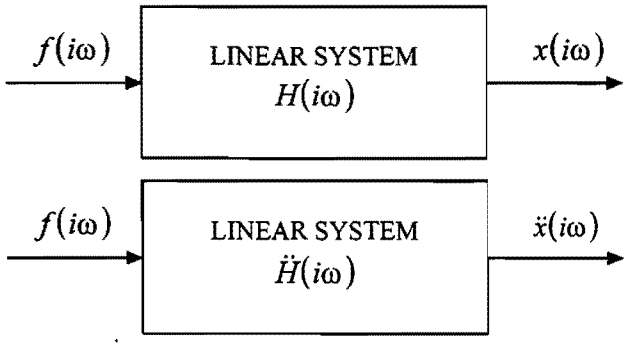

FIG. 57. Schematic of General Linear System in Frequency Domain (Lutes and Sarkani 1997)

The harmonic transfer function, $\ddot{H}(i\omega)$, is the ratio of the Fourier transform of the acceleration response to the Fourier transform of the excitation:

$$\ddot{H}(i\omega) = \frac{\ddot{x}(i\omega)}{f(i\omega)} \tag{75}$$

where $\ddot{x}(i\omega)$ is the Fourier transform of the acceleration response, and $f(i\omega)$ is the Fourier transform of the excitation. Numerically, this operation may be performed by using the fast Fourier transform (FFT). The FFT is a direct method by which the frequency content of a numerical set of data is determined. One benefit of using the FFT is that many software packages contain the ability to perform this operation. However, the FFT amplitude has both a real and an imaginary part. To avoid the use of complex arithmetic in a software package, the FFT is converted from a real and imaginary amplitude to a real amplitude and phase angle.

The real amplitude is merely the square root of the sum of the squares of the real and imaginary parts:

$$A(\omega) = \sqrt{R(\omega)^2 + I(\omega)^2} \tag{76}$$

where $A(\omega)$ is the real amplitude, $R(\omega)$ is the real part, and $I(\omega)$ is the imaginary part. The phase angle is the inverse tangent of the ratio of the imaginary part to the real part:

$$\theta(\omega) = tan^{-1}\left(\frac{I(\omega)}{R(\omega)}\right) \tag{77}$$

The use of amplitude and phase allows Eq. 75 to become:

$$\ddot{H}(i\omega) = \frac{A_{\ddot{x}_H}(\omega)e^{i\theta_{\ddot{x}_H}(\omega)}}{A_{f_H}(\omega)e^{i\theta_{f_H}(\omega)}} = \frac{A_{\ddot{x}_H}(\omega)}{A_{f_H}(\omega)}e^{i\left[\theta_{\ddot{x}_H}(\omega)-\theta_{f_H}(\omega)\right]} \tag{78}$$

where $A_{\ddot{x}_H}(\omega)$ is the amplitude of the Fourier transform of the acceleration response, $A_{f_H}(\omega)$ is the amplitude of the Fourier transform of the excitation, $\theta_{\ddot{x}_H}(\omega)$ is the phase of the Fourier transform of the acceleration response, and $\theta_{f_H}(\omega)$ is the phase of the Fourier transform of the excitation.

5.3 EXPERIMENTAL SETUP

An analytical closed-form approach to the representation of a transfer function for a sign substrate and its support structure would be very difficult to formulate because the structure and its boundary conditions are complicated. Moreover, a simplified, single degree of freedom system can not adequately represent the dynamic response of the sign support and substrate. Therefore, a frequency-based experimental approach is developed in what follows.

First, a two-pole supported sign was erected at an outdoor field location. The sign was constructed so that it is representative of a typical two-pole supported sign. A finite element model (FEM) was developed using a commercial code (ABAQUS). Finite element analysis (FEA) was validated with the response of the outdoor structure so that simulations could be carried out for wind events acquired from Texas Technological University in order to determine the predicted response to a dynamic wind load. This response was converted into the frequency domain by use of a FFT. Next, a full scale model of a roadside sign with a two-pole supporting structure was erected in a laboratory. The laboratory model was characterized by the frequency response to an impact load produced by an electro-mechanical actuator. Frequency output from the FEM was used in conjunction with the laboratory model frequency response function in order to determine the required frequency content of the actuator used to excite the supporting structure. This spectrum of frequency input for the load was then converted back to the time domain by use of the inverse fast Fourier transform (IFFT). The time history was applied to the sign structure by an electro-mechanical actuator. The actuator was used to excite the laboratory structure and response characteristics were compared with those obtained from FEA (see Fig. 58).

Once the procedure has been verified, any number of wind time histories can be applied to the laboratory structure. Actuators can be used to produce very nearly the same response as a sign substrate would undergo in a strong wind event. Of course, limitations of the approach include neglect of localized effects, vortex shedding, unsymmetric boundary conditions, and so on. Details of this procedure are described in the following subsections.

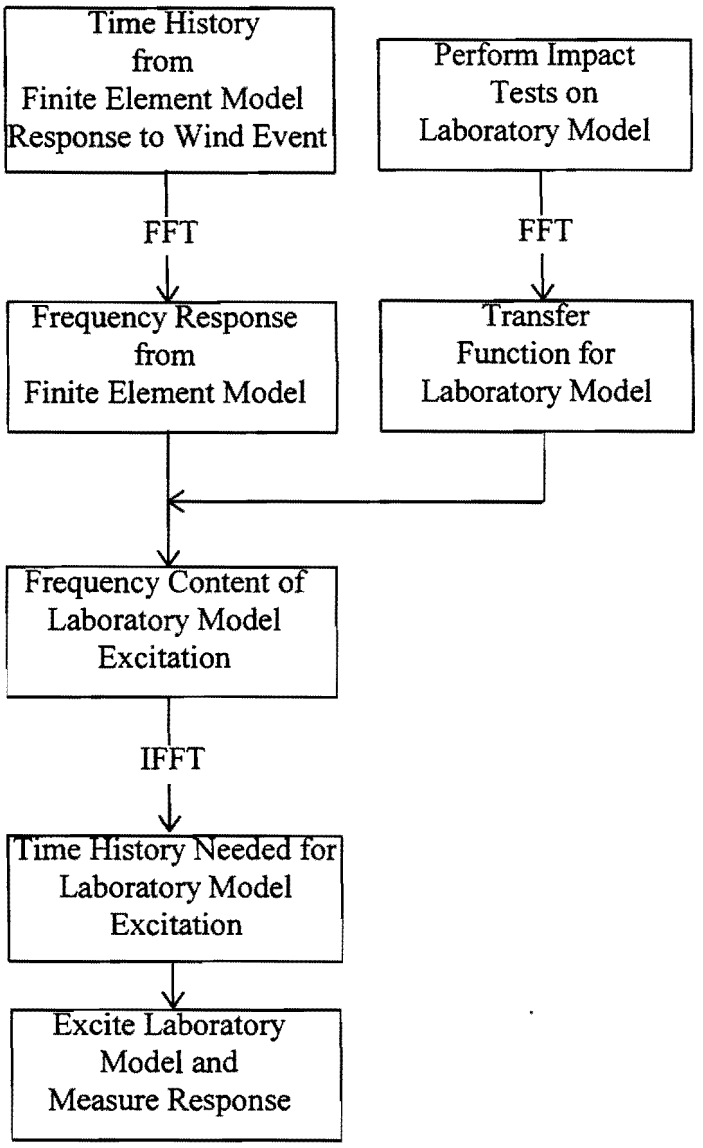

FIG. 58. Experimental Procedure

5.3.1 Construction of Full-Scale Model

A full-scale sign was erected in the Structures Laboratory at Texas A&M University (see Figs. 59 and 60). The sign was mounted on two galvanized steel poles that were obtained from the Texas Department of Transportation (TxDOT) office in Bryan, Texas. Each pole has a diameter of 6.10 cm. The poles were attached to the thick strong floor of the laboratory by insertion into a steel pipe whose inner diameter was in tolerance with the outer diameter of the pole. The poles and pipes were inserted into the concrete slab along with galvanized steel sheeting to closely approximate conditions of wedged supports currently used in field installations by TxDOT (see Fig. 61). Although this connection technique did not produce perfect fixity at the base of the sign poles, it was very nearly rigid. After inspection of similar roadside sign structures, researchers determined that the laboratory model is reasonably representative of a typical field installation.

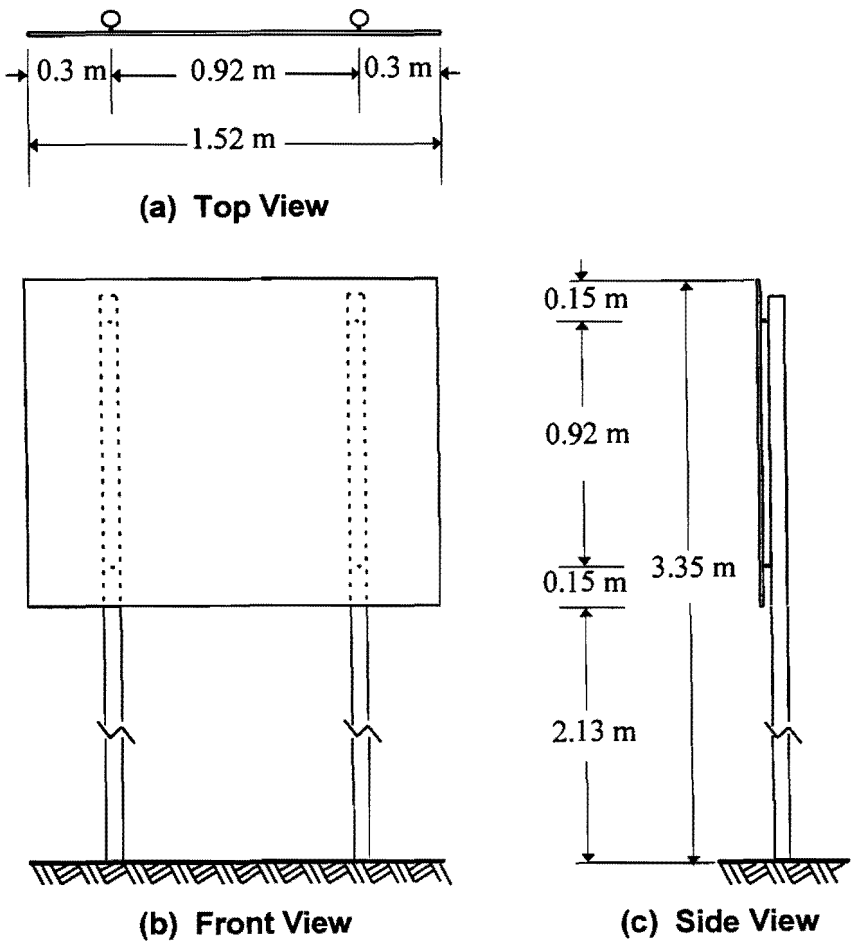

FIG. 59. Full Scale Laboratory Sign: (a) Top View; (b) Front View; and (c) Side View

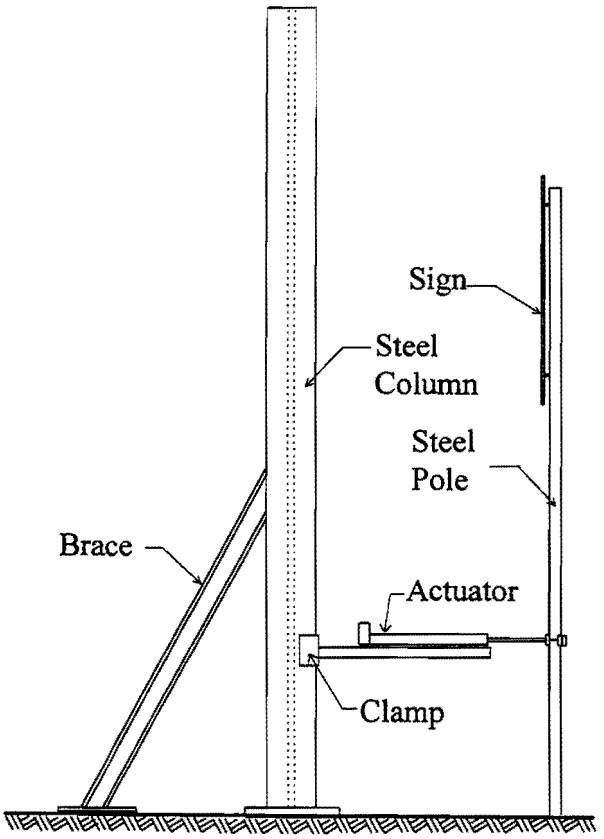

FIG. 60. Laboratory Setup

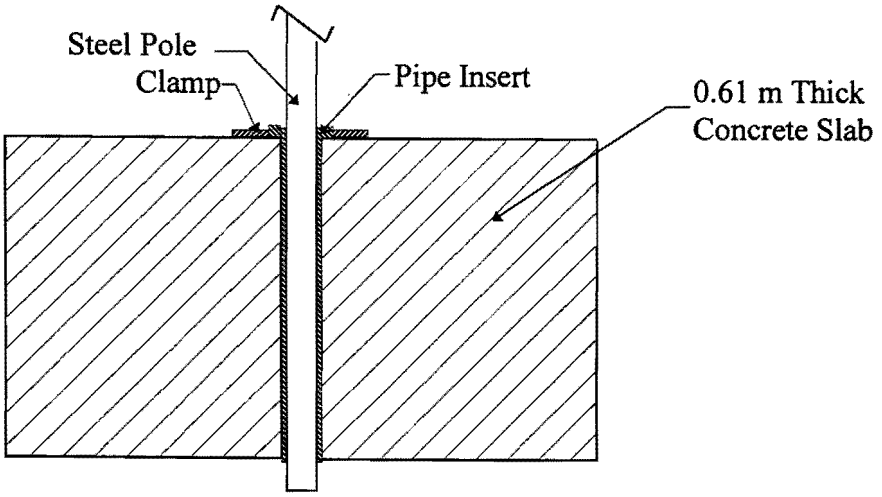

FIG. 61. Insertion of Sign Pole into Concrete Strong Floor

An indirect method was used to load the sign substrate so that it responded with dynamic motion. Here, the substrate was excited by means of an electro-mechanical actuator attached to a load bar that was rigidly connected to each post. The load bar (see Fig. 62) was a 3.81 cm square steel tube with a wall thickness of 1.59 mm. The actuator applied load to the bar through a stiffened connection at the center of the load bar (see Fig. 63). A bolt that passed through the ball joint at the end of the cylinder minimized side moments and lateral forces from being transmitted to the cylinder. Load was transferred equally from the load bar by clamping channel sections that were clamped to each pole (see Fig. 64).

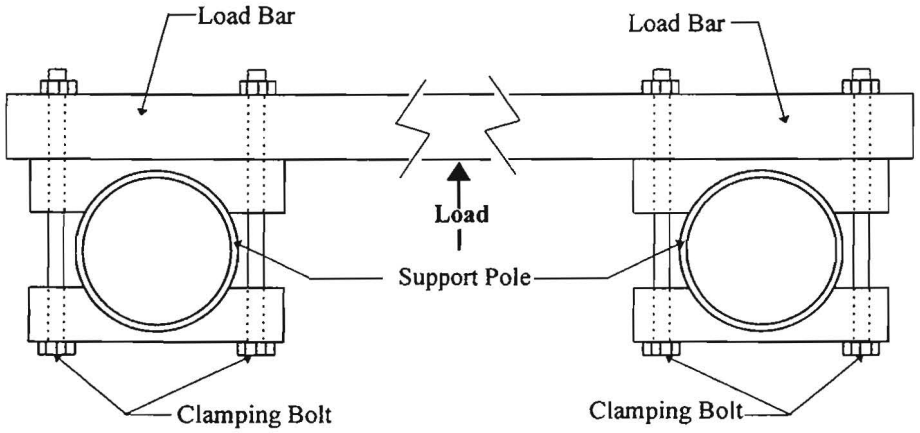

FIG. 62. Load Distribution Mechanism

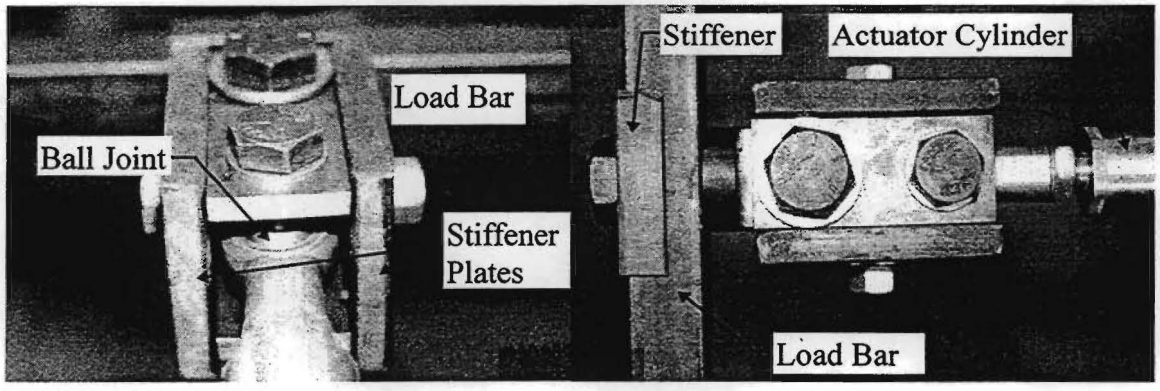

(a) **(b)**

FIG. 63. Actuator Connection Detail: (a) View Normal to Bar; and (b) View Normal to Actuator

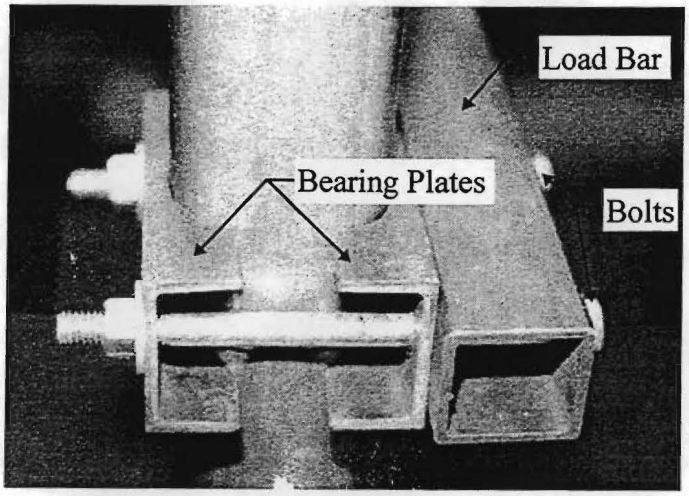

FIG. 64. Load Bar-to-Supporting Structure Connection

The substrate tested in the laboratory was a recycled plastic material that was designated GTHW by Pelletech, Inc. Properties of this material are given in Chapters 3 and 4. The sign substrate was attached to the supporting structure by clamping hardware at four points. The connection was fixed to the pole by U-bolts and a single bolt that penetrated the substrate (see Fig. 65).

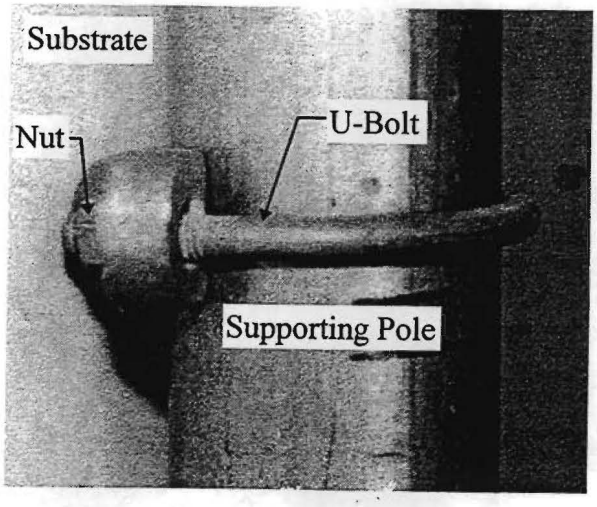

FIG. 65. Supporting Pole-to-Substrate Connection

5.3.2 Transducers and Data Acquisition

In order to measure response of the structure to excitation, the sign and supporting structure were instrumented with 5 ENDEVCO model 7290A-10 MICROTRON accelerometers (see Fig. 66). The accelerometers were located on the left edge, center, and right edge of the sign substrate and on both the left and right poles. All accelerometers were placed on a horizontal axis that intersected the geometric center of the substrate (see Fig. 67). These transducers measured acceleration on an axis orthogonal to the plane of the substrate; however, they were limited to a maximum acceleration of 10 times the acceleration of gravity and were sensitive to electronic noise.

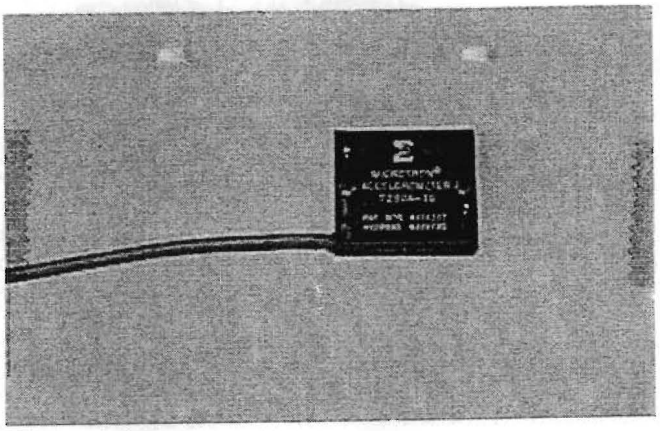

FIG. 66. Typical Accelerometer

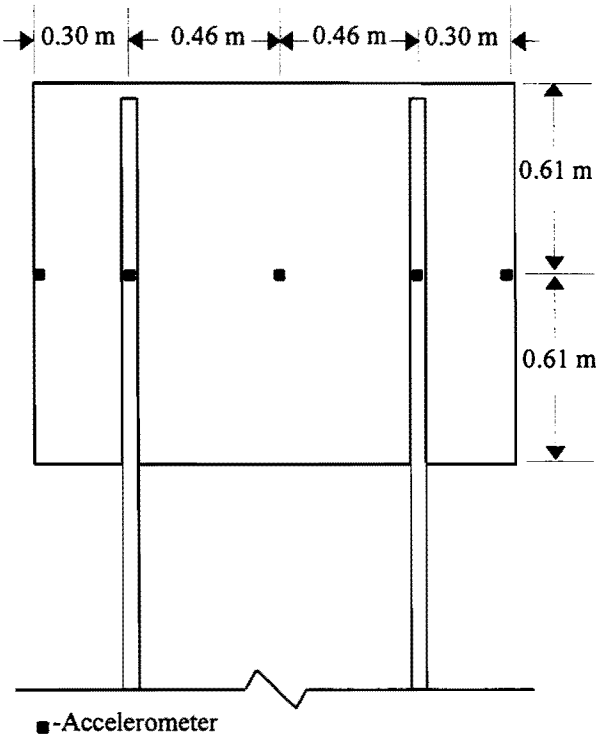

FIG. 67. Instrumentation of Laboratory Model

Data acquisition (DAQ) was performed with hardware obtained from National Instruments and its companion LABVIEW virtual instrument software (see Fig. 68). The hardware consisted of a high performance, software-configurable, 16-bit data acquisition board (AT-MIO-16X) containing a 16-bit, 10 μsec sampling analog-to-digital converter. The DAQ board was connected to a SCXI-1001 chassis that holds up to 12 conditioning units, typically a SCXI-1121 4-channel isolation amplifier with excitation. Four channels of data were collected for the conditioning unit by a SCXI-1321 terminal block.

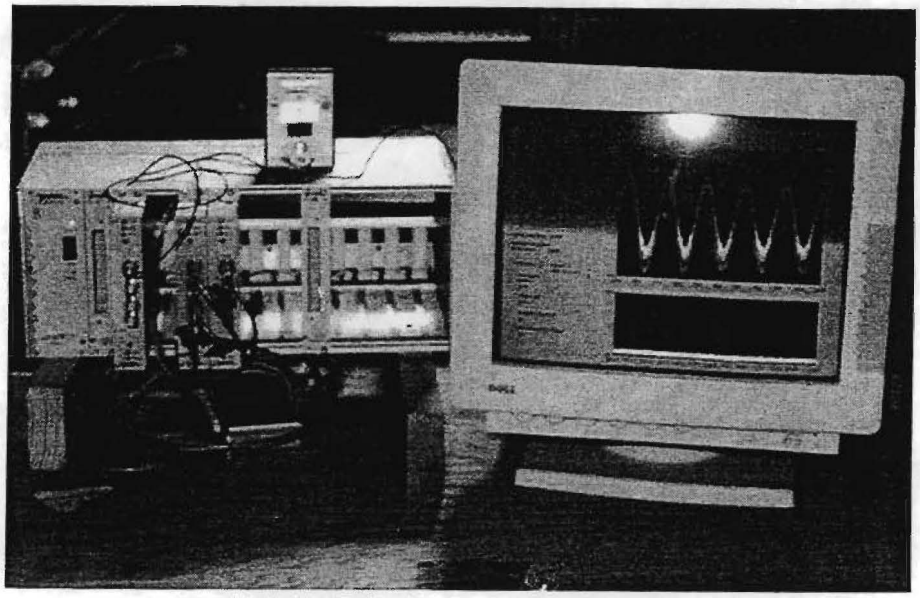

FIG. 68. SCXI Data Acquisition Hardware

5.3.3 T-Series Electric Cylinders

The laboratory model was excited by an Industrial Devices Corporation (IDC) T-series electro-mechanical actuator, model number TB3201B-24-MS2-FS2-DB-C25. The device is capable of producing a full stroke of 61.0 cm and a maximum axial force of approximately 3.07 kN. The actuator provides axial force through the use of gears and an applied torque. Analog control of the applied torque was achieved by sending a ± 10v signal to a B8001 brushless servo drive (see Fig. 69). The B8001 is a 5 amp continuous, 10 amp peak, digital brushless servo drive capable of driving the T-series electric cylinder. The B8001 was configured using tuning software provided by Industrial Devices Corporation.

The torque applied varied linearly with the analog command signal received by the B8001 servo drive. In order to apply a force time history, an equivalent input voltage history had to be determined. To accomplish this the actuator was calibrated by placing a 8.9 kN MTS load cell in line between the actuator and load bar (see Fig. 70) and supplying the B8001 with sinusoidal voltage signals of differing amplitudes and frequencies. The command signal and load cell signal were recorded for approximately two periods, and a linear relationship between the command voltage and applied force was determined using

linear interpolation. The command signal calibration factor was 307.12 N/volt and the monitor signal calibration was 2,520.7 N/volt centered at 2.5 volts.

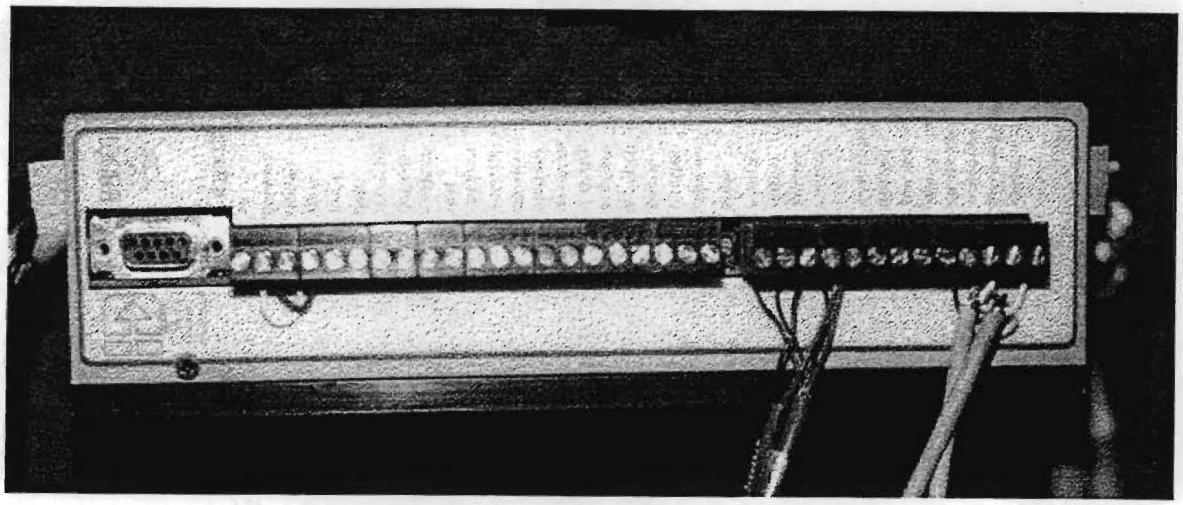

FIG. 69. B8001 Brushless Servo Drive

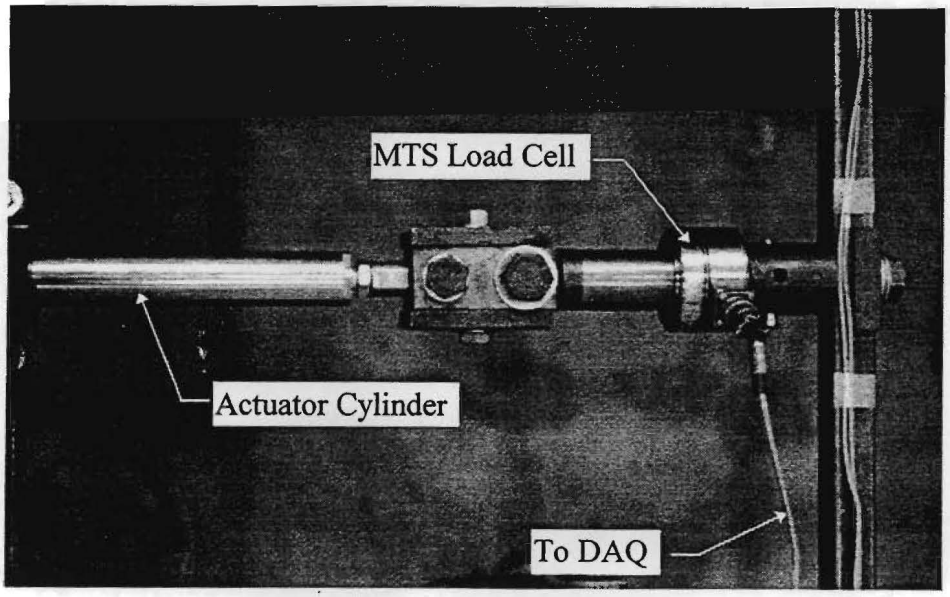

FIG. 70. Calibration of T-Series Electric Cylinder

5.4 ANALYSIS OF LABORATORY MODEL

In order to characterize response of the laboratory model, impact tests were performed. A Lixie hammer with a piezo conditioner, SN 9314, and load cell, SN 3304, was used (see Fig. 71) to develop an impact time history for the actuator to apply to the structure. The actuator and servo-controller provided a closed-loop system such that the applied load

was always being monitored and adjusted. The servo-controller monitored the applied torque in the gears at the rear of the actuator assembly. Since this system can not be monitored at the load bar and fed back to the controller, the actuator cylinder had to be included in the system when determining $\ddot{H}(i\omega)$. To achieve this, the actuator applied an impact force developed by recording the impact history of the piezoelectric impact hammer (see Fig. 72).

The impact hammer has a variety of impact heads that may be used to deliver the impact. The different heads vary in stiffness. A relatively soft head was selected. The soft head delivers a rounded impulse function that allows many data points to define the impact in time domain, but still delivers a sufficiently broad range of frequency content (see Fig. 73). The impact acquired from the impact hammer was doubled in duration and amplitude to allow the actuator to more accurately apply the load. Impact tests were performed with a high-speed data acquisition system collecting data at 500 Hz in conjunction with LABVIEW software. The acquired signal contained data for approximately 0.10 sec (100 points) prior to impact and 7.9 sec (7,900 points) after impact for a total test duration of 20.0 sec (10,000 points).

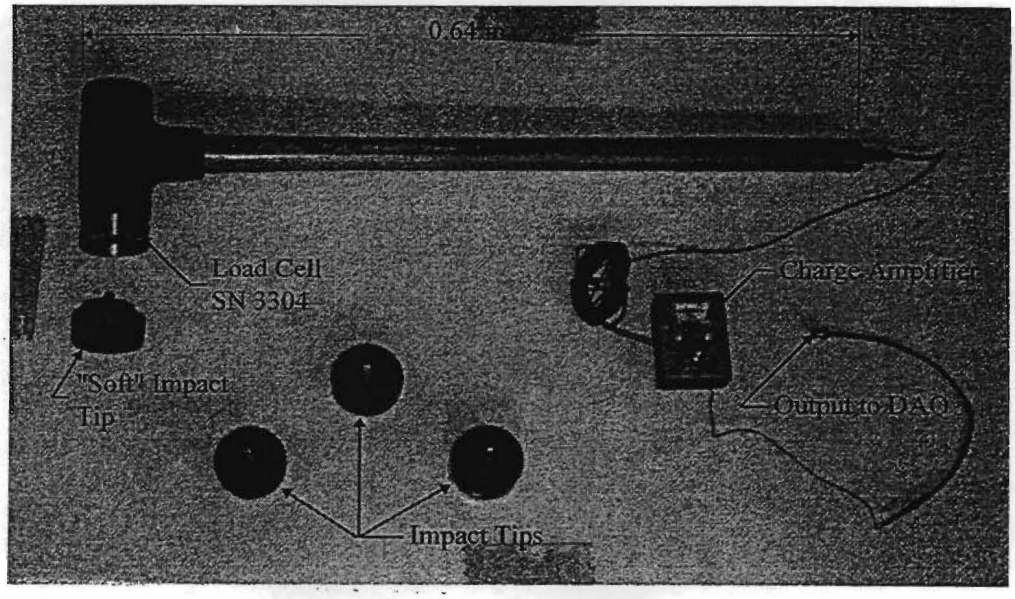

FIG. 71. Lixie Impact Hammer

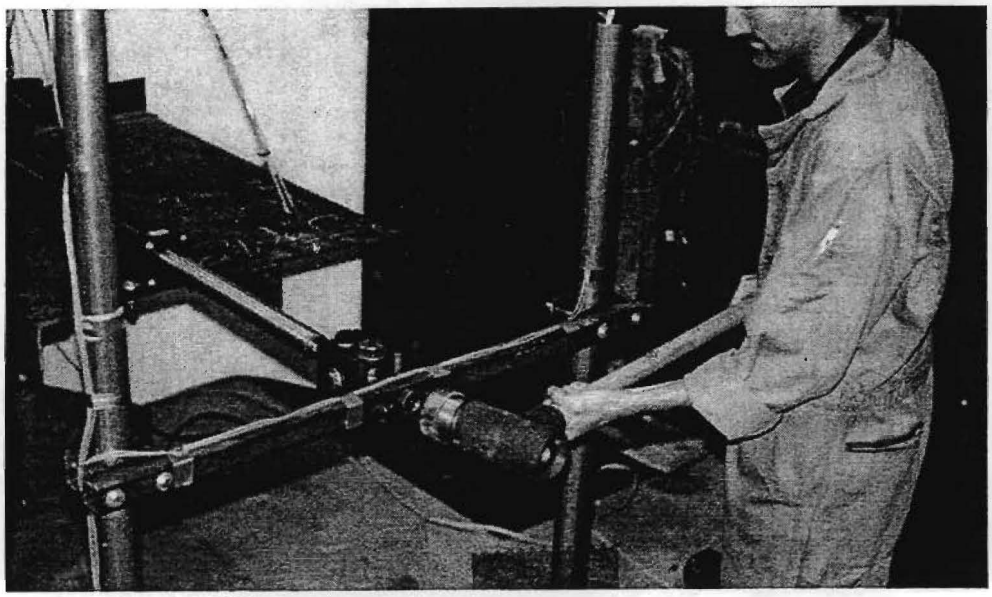

FIG. 72. Development of Impact Time History

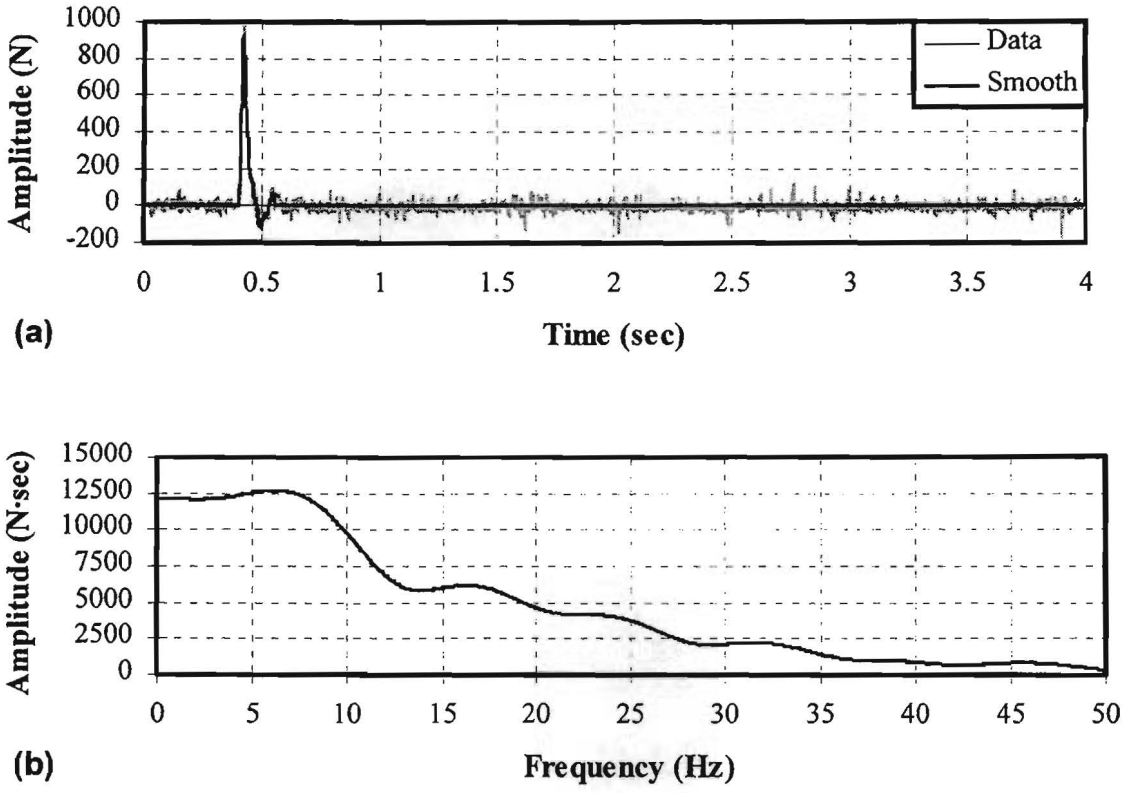

FIG. 73. Typical Impact Excitation as Applied by the Actuator: (a) Time Domain; and (b) Frequency Domain

Having the actuator apply the impact ensured that interaction effects between the actuator and the structure of the sign were included in the determination of the transfer function. Five acceleration response time histories were recorded for each impact and converted into the frequency domain. Typical edge, pole, and center frequency responses to the impact are presented in Figs. 74-76. Peak amplitudes in the frequency domain occurred at 3.8, 5.7, 25.5, and 29.0 Hz. As can be seen, the lowest frequency, or fundamental frequency, of the laboratory structure was significantly higher that the fundamental frequency of the FEM, 2.8 Hz (see Fig. 94). The shift in frequency of the first mode was due to the stiffening of the structure that resulted from attaching the actuator to the supporting structure. When the actuator was attached and excited the sign, the structure did not respond as it did when the actuator was unattached. Therefore, in order to develop the proper force time history, the actuator had to be left intact when determining $\ddot{H}(i\omega)$.

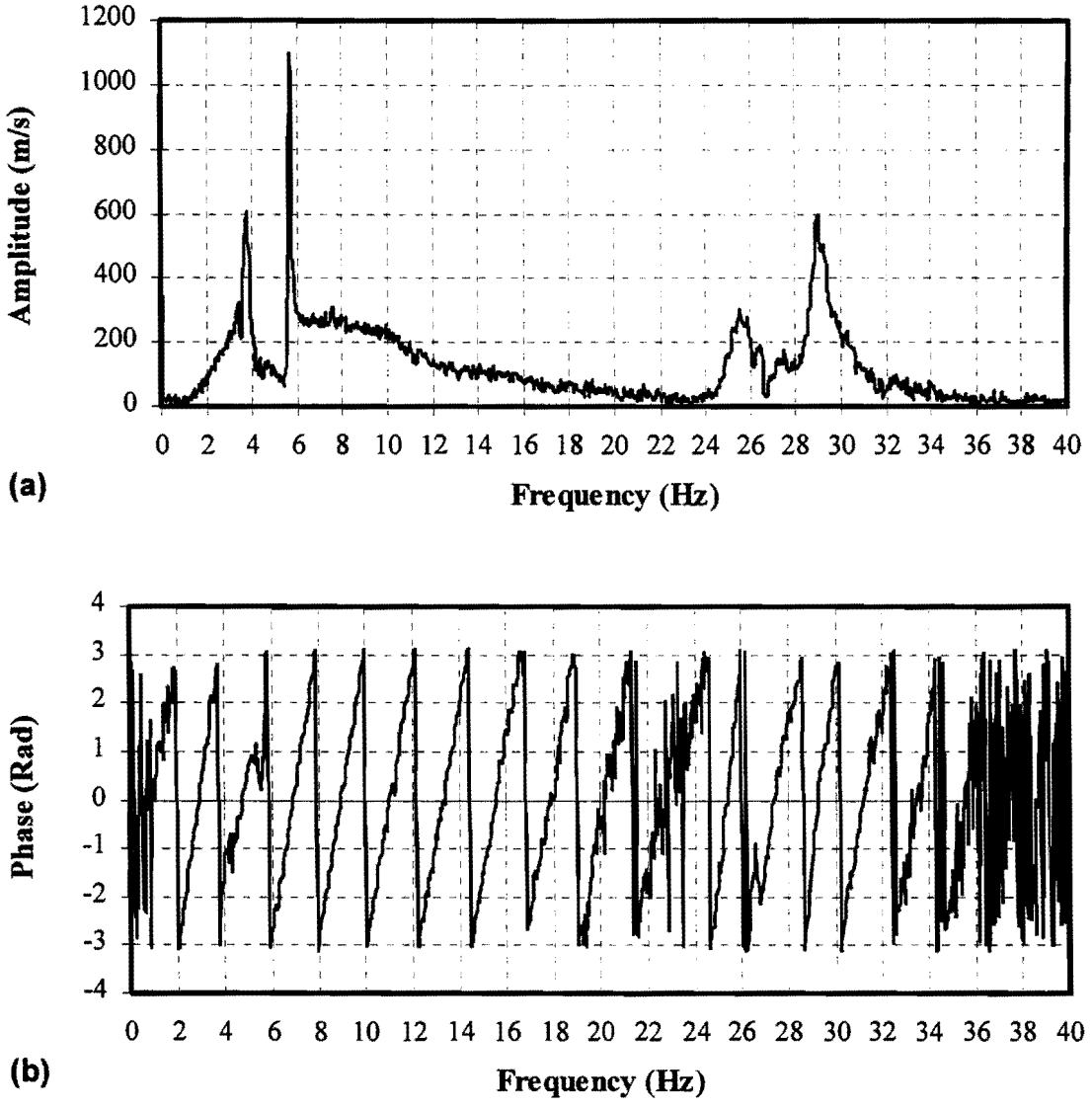

FIG. 74. Typical Edge Frequency Response to Impact: (a) Amplitude; and (b) Phase

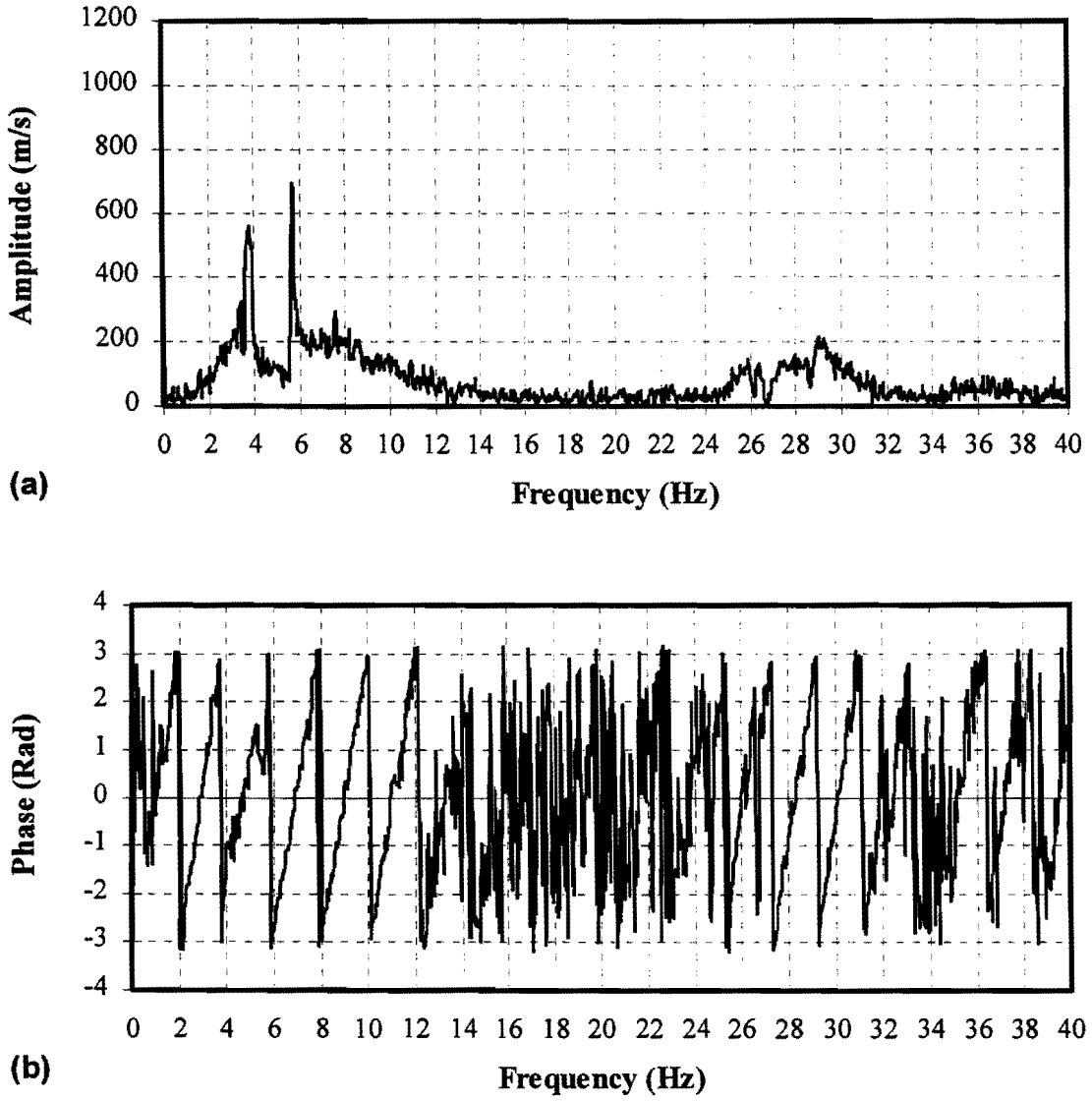

FIG. 75. Typical Pole Frequency Response to Impact: (a) Amplitude; and (b) Phase

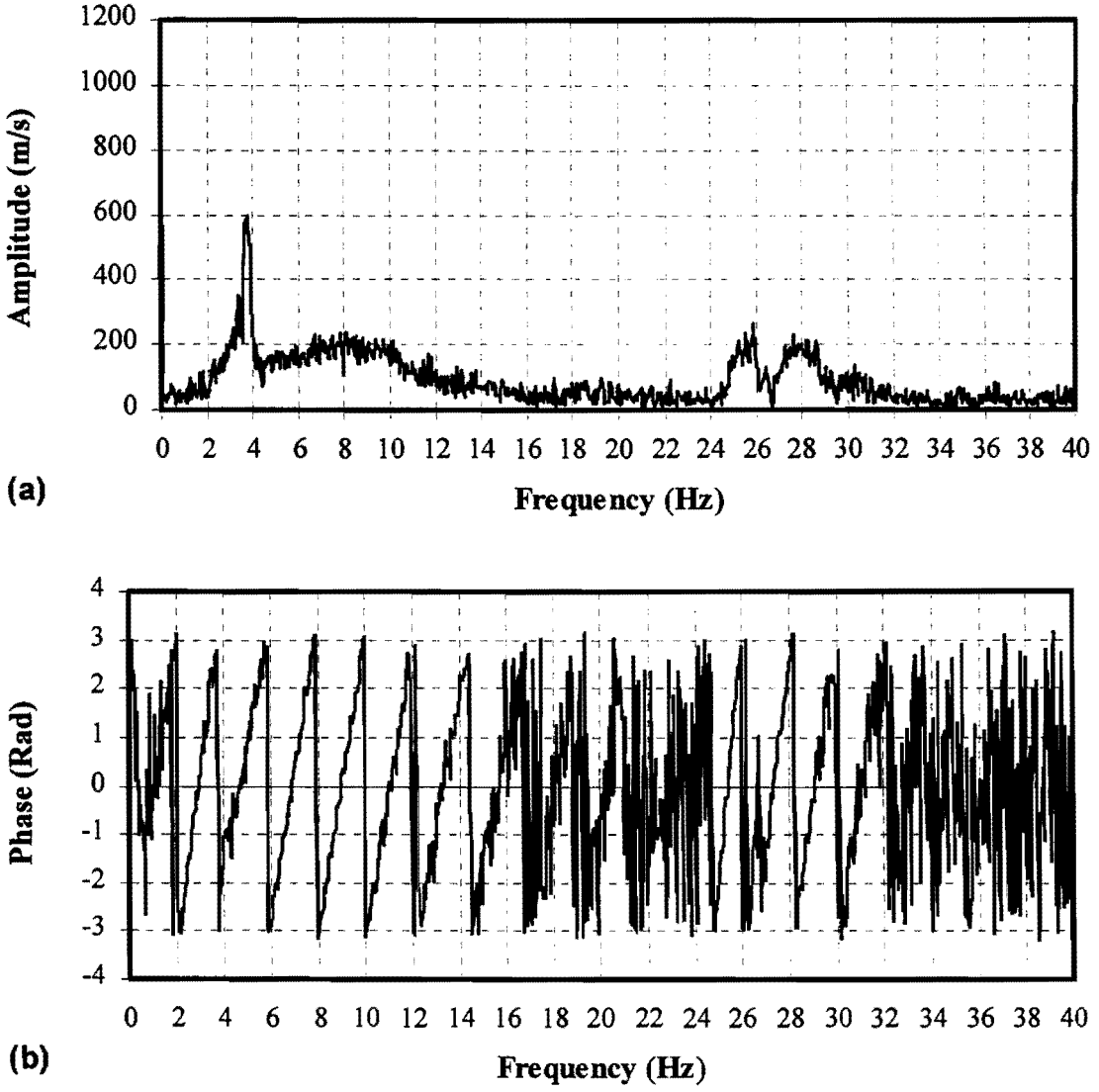

FIG. 76. Typical Center Frequency Response to Impact: (a) Amplitude; and (b) Phase

As defined by Eq. 78, the experimental transfer functions are merely the ratio of the response to the excitation for all frequencies. Results are presented in Figs. 77-81, where (a) is the amplitude, and (b) is the phase of the transfer function. The phase has the form of a step function, and the modes pertaining to the substrate show higher amplitudes on the edges and center.

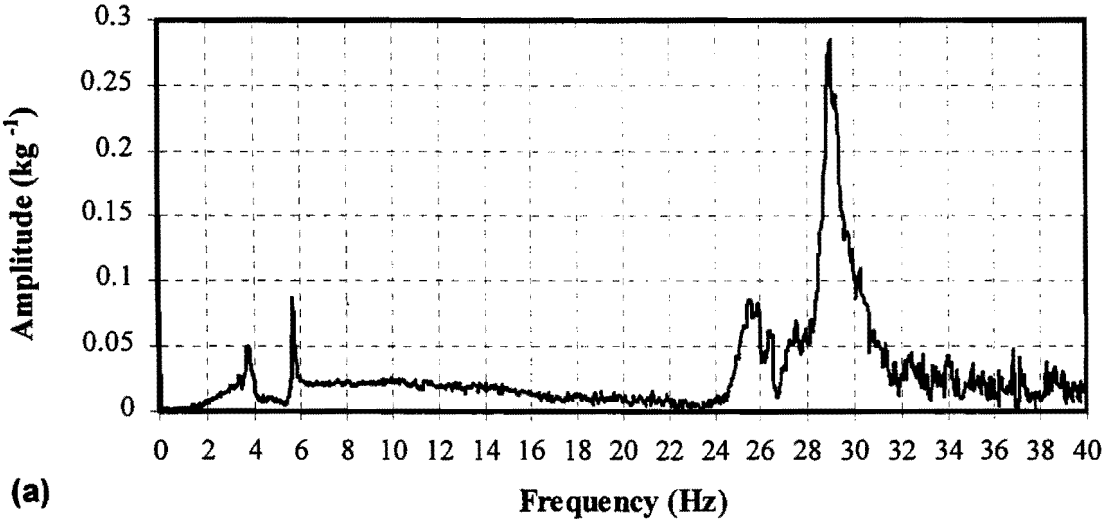

(a)

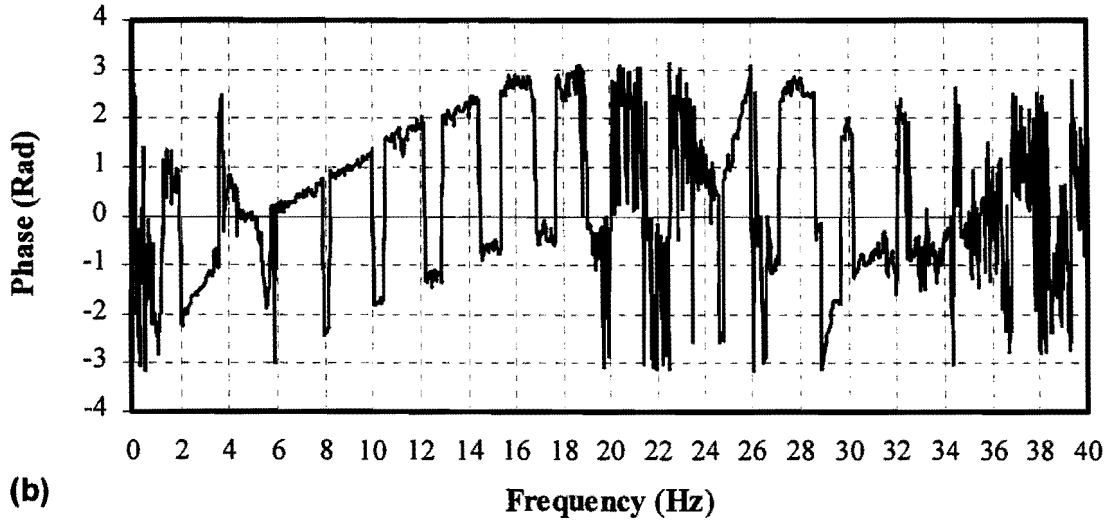

(b)

FIG. 77. Transfer Function for Left-Edge: (a) Amplitude; and (b) Phase

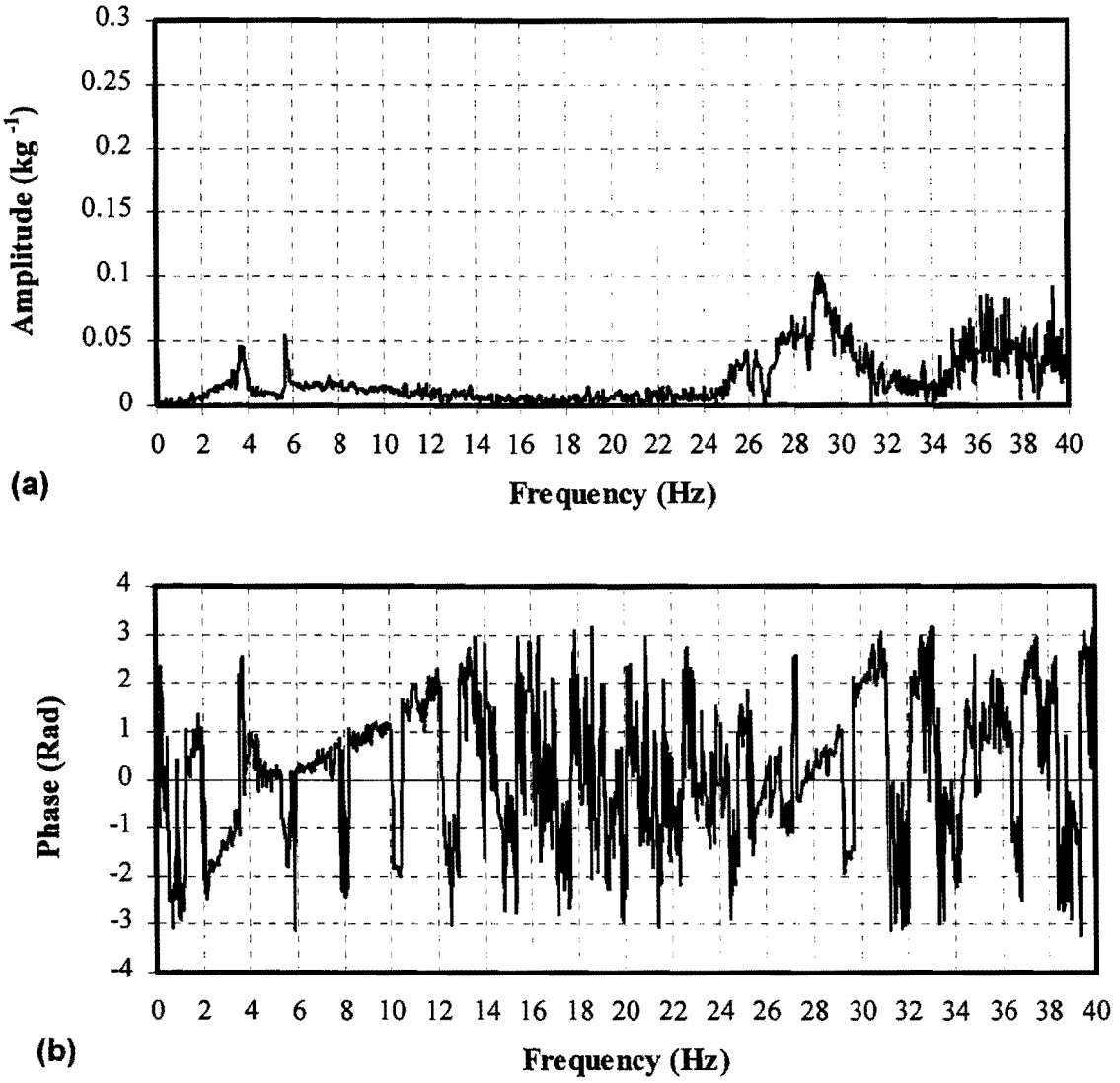

FIG. 78. Transfer Function for Left-Pole: (a) Amplitude; and (b) Phase

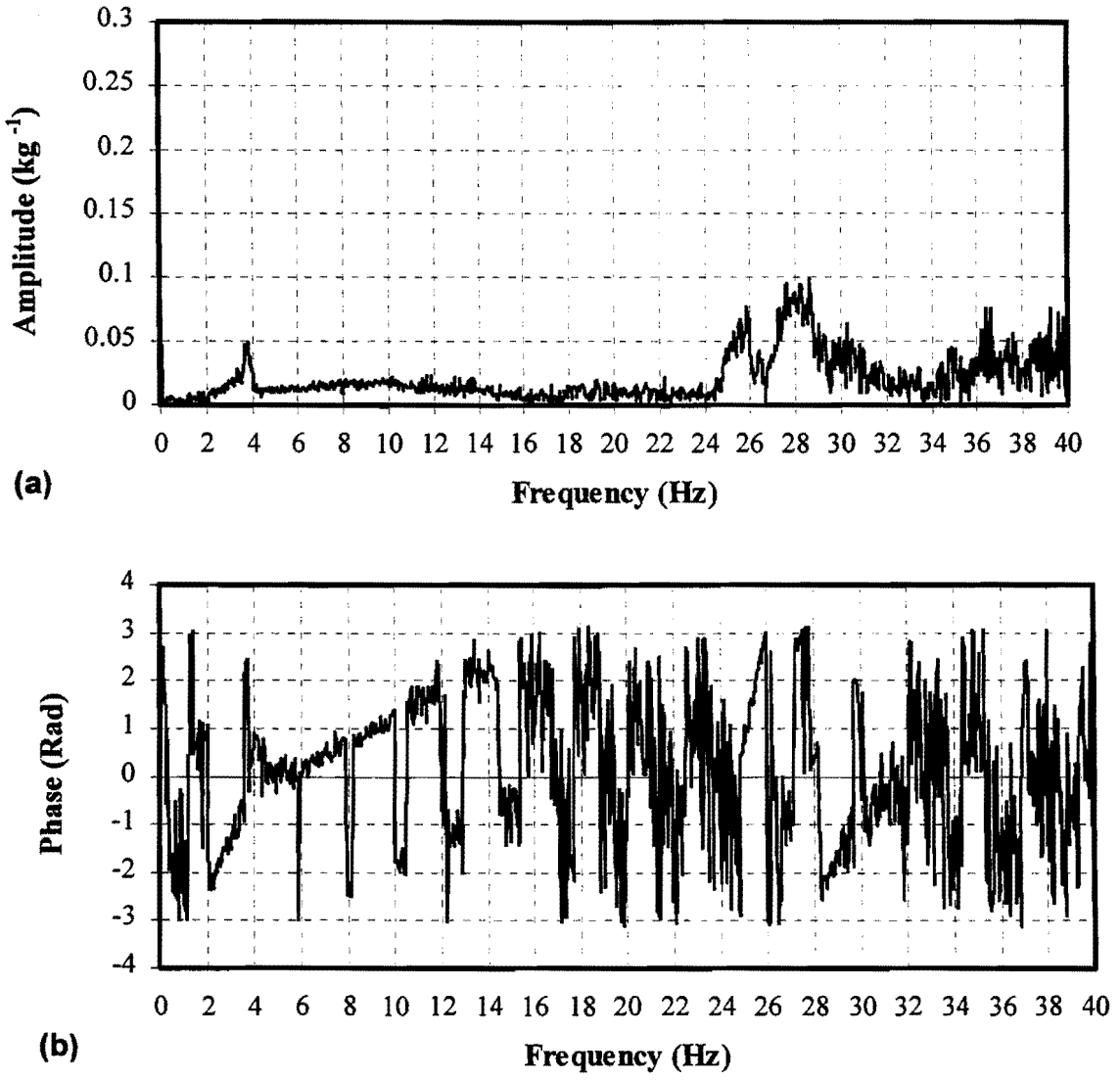

FIG. 79. Transfer Function for Center: (a) Amplitude; and (b) Phase

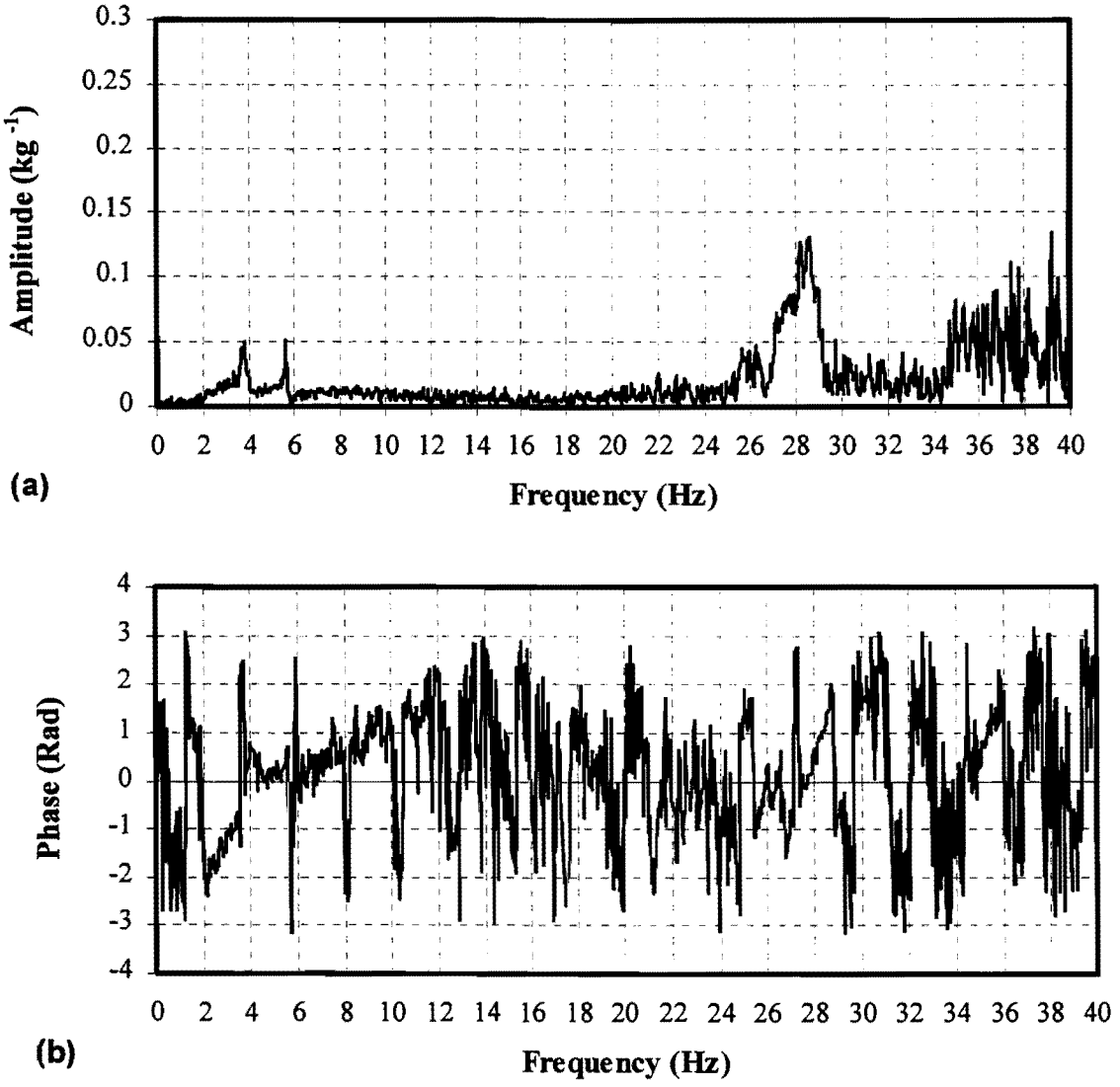

FIG. 80. Transfer Function for Right-Pole: (a) Amplitude; and (b) Phase

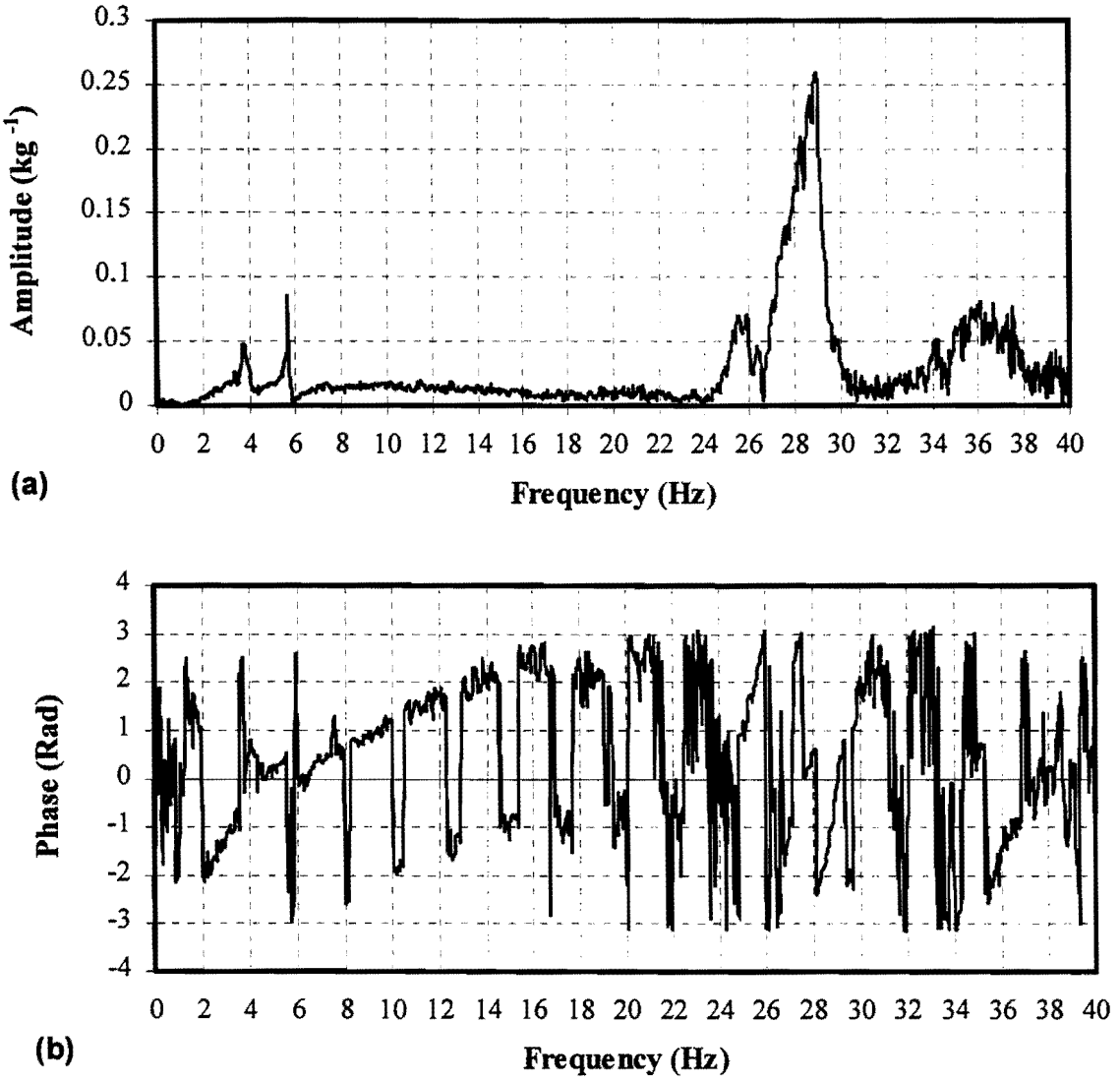

FIG. 81. Transfer Function for Right-Edge: (a) Amplitude; and (b) Phase

Figs. 77-81 reveal that the left and right sides of the laboratory structure are relatively symmetric in their response. Therefore, in what follows, results of the left and right pole, and the left and right edge are presented simply as pole and edge to eliminate redundancy.

5.5 WIND EVENT

Wind speed time histories were obtained from the Wind Engineering Research Center (WERC) at Texas Technological University as part of the Texas Tech Field Experiment Data Package. Two wind events, M15N541 and M15N571, are included in the package. Each

time history includes wind speed data at elevations of 4, 10, 21, and 49 m above ground. The data were recorded using 3-cup anemometers on a 49 m meteorological tower at a data acquisition rate of 10 Hz for 900 seconds and low-pass filtered at 8 Hz. The terrain surrounding the tower is both flat and open which is consistent with ASCE 7-95 exposure category C.

5.5.1 Characterization of Wind Events

Wind speed data recorded from the 4 m anemometer were used for this study (see Figs. 82 and 83) due to the relative proximity in above-ground elevation of the anemometer to the height of a roadside sign. In order to produce a substantial level of response in the laboratory sign the mean wind speeds of the data sets taken in the field needed to be increased. Higher accelerations increased the amplitude of excitation that needed to be applied by the electro-mechanical actuator during laboratory simulation. As shown later, if the actuator command forces are too low the actuator can not overcome internal friction and does not excite the structure. Therefore, the data sets, M15N541 and M15N571, obtained from WERC were amplified to a mean wind speed of 26.82 m/s. To achieve this, the same coefficient of variation was maintained between the original time histories and the amplified time histories. Table 24 gives statistical characteristics of the complete wind speed time histories. Notations M15H541 and M15H571 designate amplified time histories M15N541 and M15N571, respectively.

TABLE 24. Wind Speed Characteristics

Parameter	Recorded Time History		Amplified Time History	
	M15N541	M15N571	M15H541	M15H571
(1)	(2)	(3)	(4)	(5)
Mean wind speed	9.06 m/s	7.22 m/s	26.82 m/s	26.82 m/s
Standard deviation	1.73 m/s	1.29 m/s	5.11 m/s	4.78 m/s
Coefficient of variation	19.0%	17.8%	19.0%	17.8%

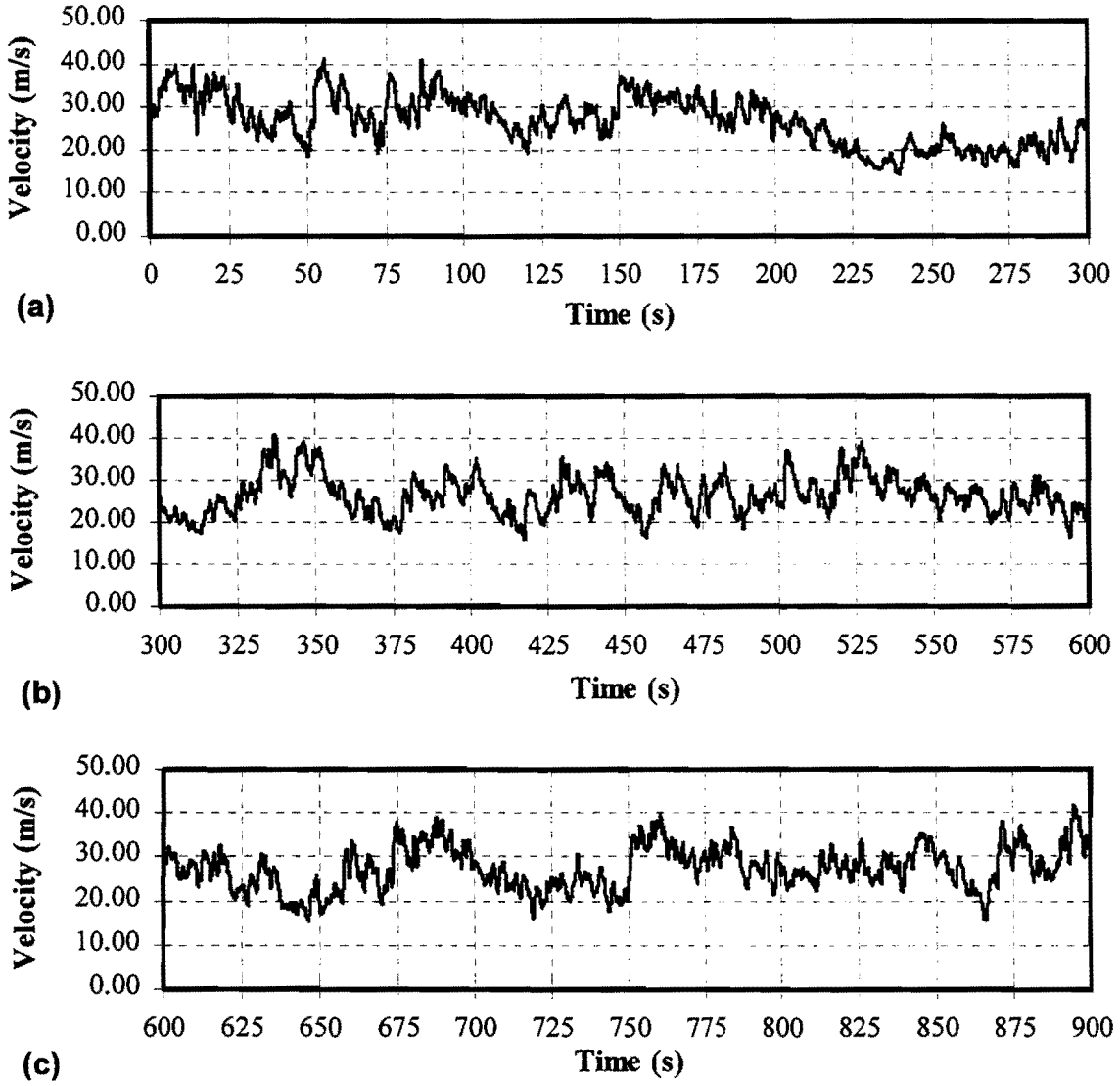

FIG. 82. M15H541 Wind Speed Time History: (a) 0-300 sec.; (b) 300-600 sec.; and (c) 600-900 sec.

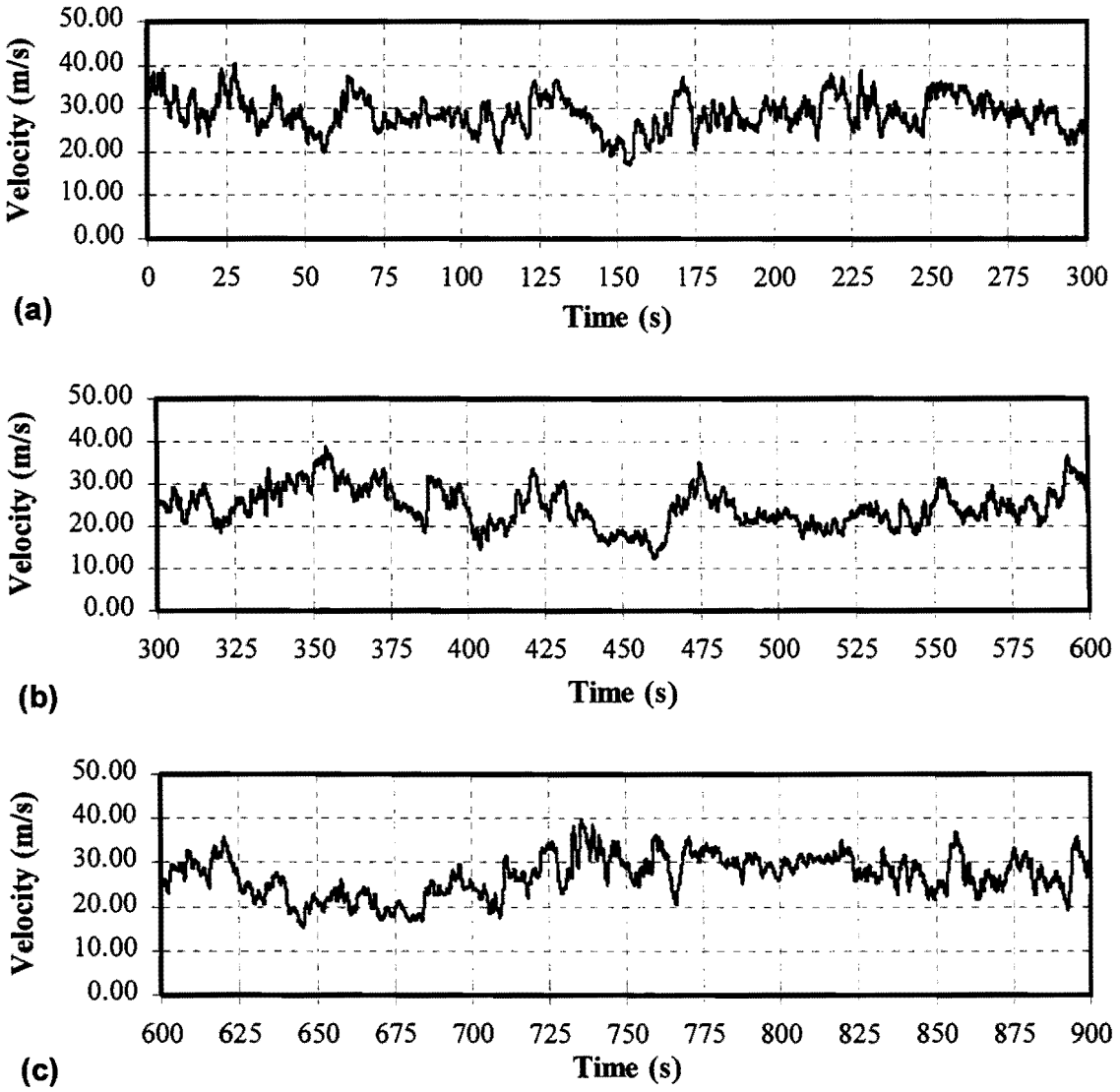

FIG. 83. M15H571 Wind Speed Time History: (a) 0-300 sec.; (b) 300-600 sec.; and (c) 600-900 sec.

5.5.2 Pressure

The sign is excited by means of a pressure force applied to the surface of the substrate. If the flow of air is assumed to be uniform, the drag force applied to the structure may be expressed as:

$$F_D = \frac{1}{2}\rho U^2 A C_D \tag{79}$$

where ρ is the fluid density, U is the velocity of the fluid, A is the area of the surface on which the fluid acts, and C_D is a dimensionless drag coefficient (Blevins 1984). If the pressure is assumed to act uniformly over the surface of the sign substrate, then the pressure may be determined by dividing both sides of Eq. 79 by the area. The pressure force is:

$$P = \frac{1}{2}\rho U^2 C_D \tag{80}$$

where P is the force per unit area acting normal to the surface of the substrate. The drag coefficient, C_D, is defined as:

$$C_D = \frac{\mathcal{D}}{\frac{1}{2}\rho U^2 A} \tag{81}$$

where $\mathcal{D}$ is the drag force acting on the plate parallel to the streamlines (Munson et al. 1994). The drag coefficient for a thin rectangular plate perpendicular to flow (see Fig. 84) is a function of the aspect ratio (L/D) of the plate (Blevins 1984). The drag coefficient for a thin rectangular plate (see Fig. 85) may be approximated by:

$$C_D = 3.507\times10^{-4}\left(\frac{L}{D}\right) - 6.318\times10^{-3}\left(\frac{L}{D}\right) + 5.161\times10^{-2}\left(\frac{L}{D}\right) + 1.008 \tag{82}$$

The aspect ratio (L/D) of the 1.52 m × 1.22 m laboratory sign is 1.25. Therefore, C_D is given by Eq. 82 to be 1.065, and the equation relating wind speed to pressure becomes:

$$P = \frac{1.065}{2}\rho U^2 \tag{83}$$

where ρ is 1.23 kg/m^3 for air at 15° C.

The pressure acting on the face of the substrate is assumed to act uniformly across the entire face of the sign. Wind speed time histories M15N41 and M15N71 are used in conjunction with Eq. 83 to produce wind pressure time histories M15N41 and M15N71 (see Figs. 86 and 87). Frequency content of the two wind events is presented in Fig. 88.

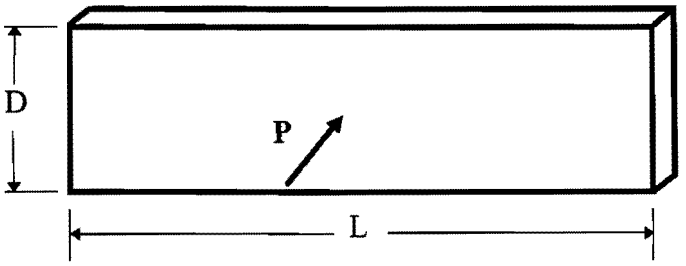

FIG. 84. Thin Rectangular Plate Perpendicular to Flow

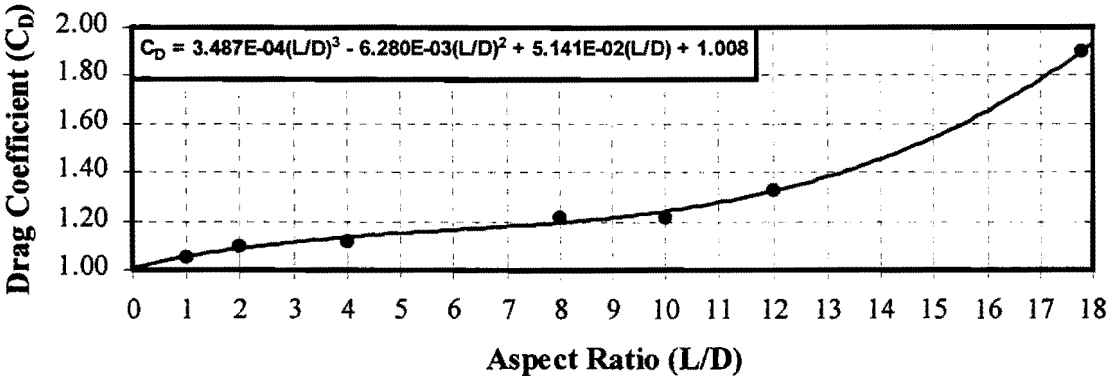

FIG. 85. C_D for a Thin Rectangular Plate Perpendicular to Flow (Blevins 1984)

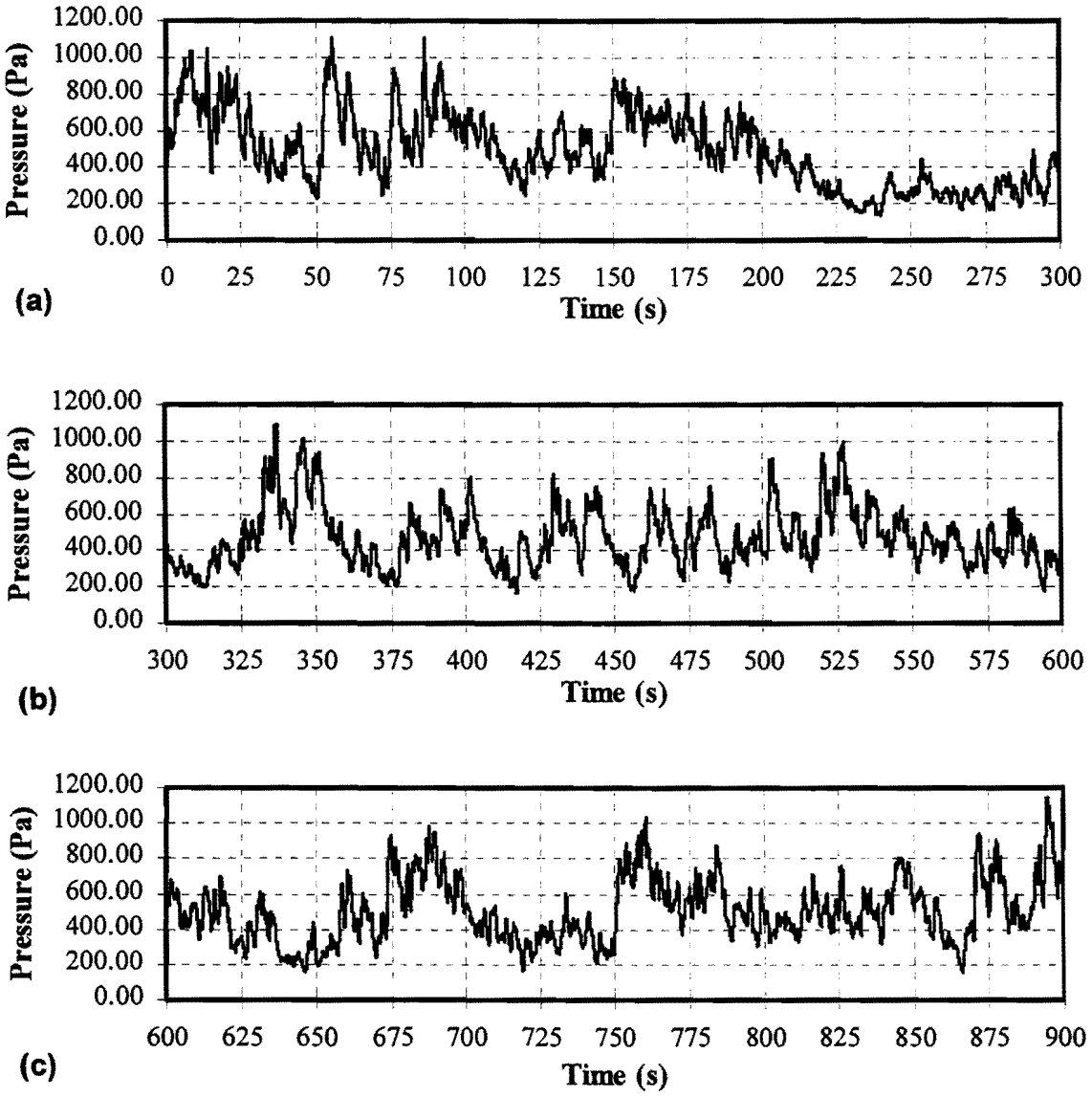

FIG. 86. M15H541 Wind Pressure Time History: (a) 0-300 sec.; (b) 300-600 sec.; and (c) 600-900 sec.

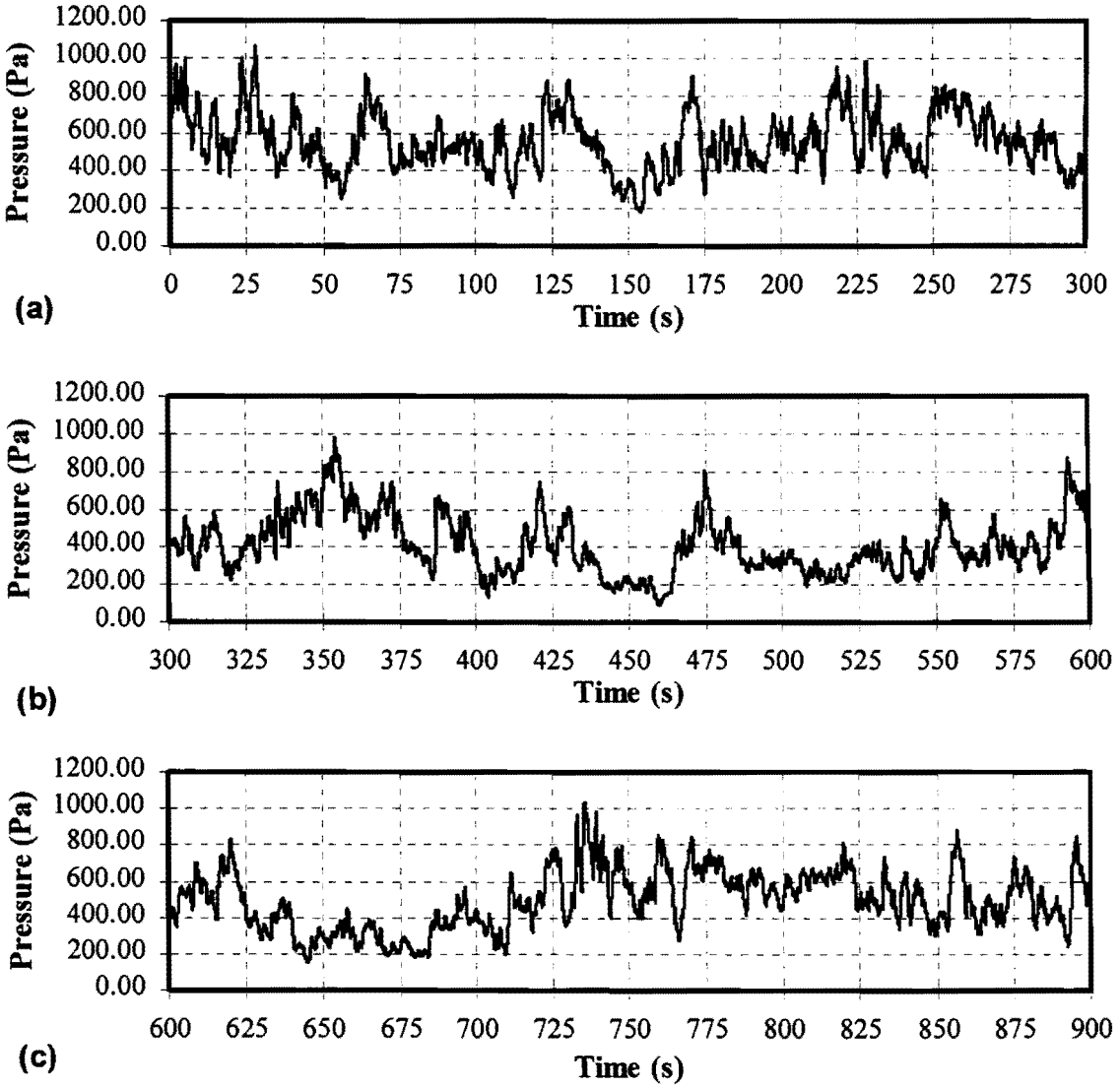

FIG. 87. M15H571 Wind Pressure Time History: (a) 0-300 sec.; (b) 300-600 sec.; and (c) 600-900 sec.

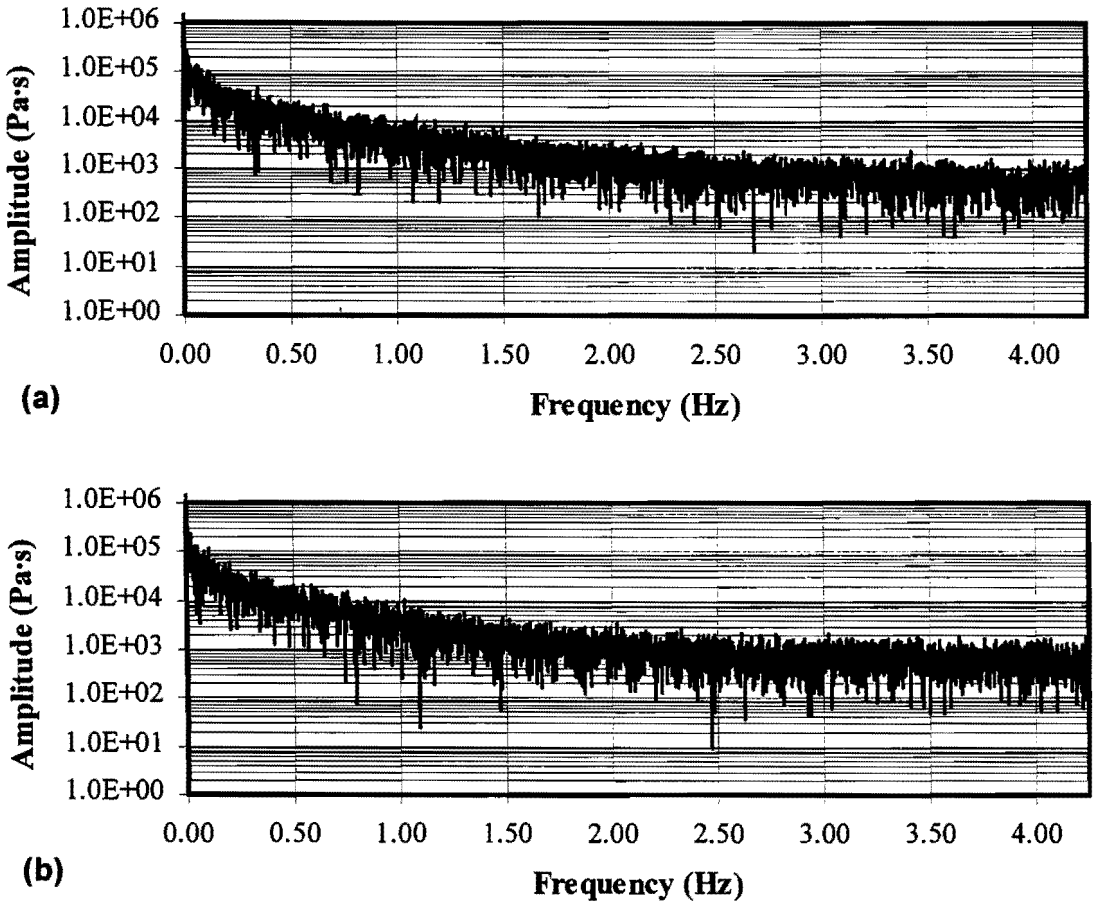

FIG. 88. Frequency Content of Pressure Events: (a) M15H541; and (b) M15H571

5.6 FINITE ELEMENT ANALYSIS

Numerical simulation of the dynamic response of an actual sign structure to an impact load was carried out using a commercial finite element code. This simulation served to calibrate the finite element modeling of the fixity at the base of the sign poles and its ability to predict acceleration response at specific locations on the sign substrate. A sign that is similar to the one erected in the laboratory was embedded in the ground at the Texas A&M University Riverside Campus (see Fig. 89). Fig. 59 shows the spacing of the poles. Height of the bottom of the sign substrate above the ground was 2.08 m. The sign substrate was made from recycled material GTHW (see sec. 3.1) and had the properties listed in Table 21.

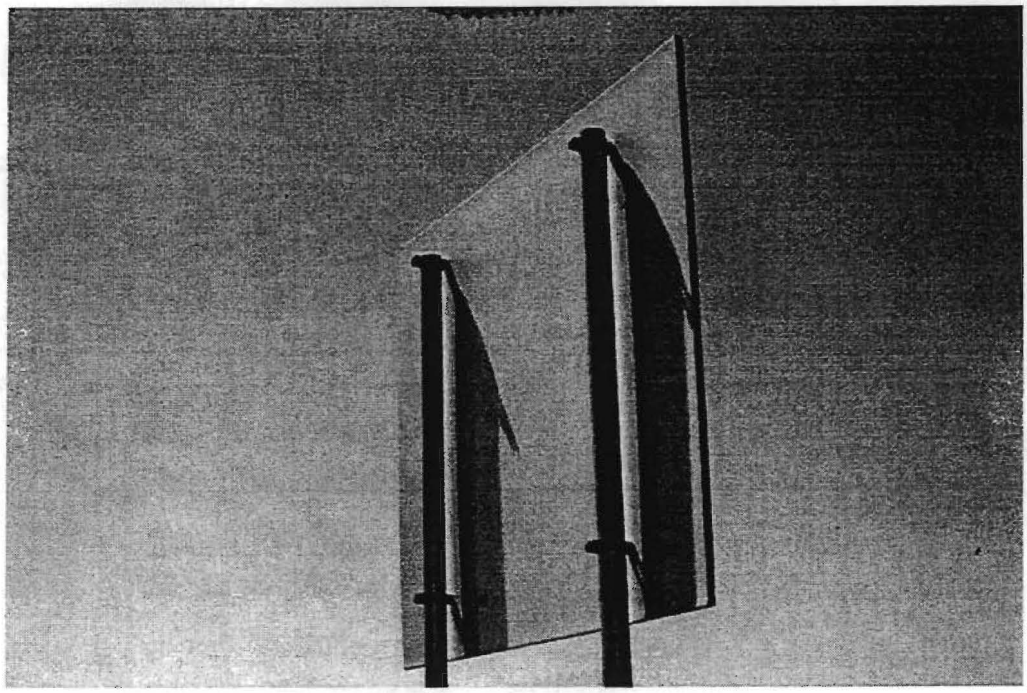

FIG. 89. Modeled Recycled Content Sign

5.6.1 Description of FEM

A finite element model was developed using the commercial code ABAQUS (see Fig. 90). The supporting poles were modeled using beam bending elements that had a moment of inertia equivalent to the cylindrical steel poles used in the field prototype. Connections between the substrate and poles were modeled with very stiff beam elements that separated the shell elements used for the substrate and the pole elements. The sign substrate was modeled with S8R5 shear deformable shell elements. Discretization of the element mesh was fine in the vicinity of the hardware connection where the stress gradient was expected to be high. The base of the poles was fixed against translation in three directions, fixed rotationally about the vertical axis and the horizontal axis orthogonal to the plane of the substrate. Restraint about a horizontal axis that passes through the base of both poles was modeled using rotational springs. The rotational spring stiffness was adjusted until the fundamental frequency of the numerical model corresponded to the fundamental frequency of the field model that was obtained using an experimental system identification technique (see section 5.6.2).

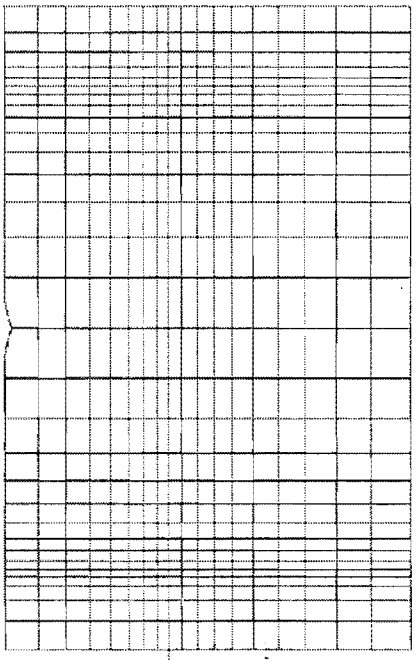

FIG. 90. Finite Element Model Mesh

5.6.2 FEM Calibration and Validation

The FEM was calibrated and validated by striking the lowest center portion of the substrate with the impact hammer (see Figs. 71 and 91), and the acceleration response of the pole and the substrate center was recorded with the data acquisition system described in section 5.3.2 (see Fig. 68). Accelerometers identical to those described in section 5.3.2 were used (see Fig. 66). A time-history of the force (see Fig. 92) obtained from the impact hammer was applied to the corresponding node in the FEM mesh. The FEM response to the load was then compared with response of the field structure in both the frequency and time domains. Stiffness of the rotational springs at the base of the supporting poles was adjusted so that the fundamental period of the numerical model was identical to the first period of the field model. Modal damping values of the experimental structure were determined through the use of the half-power bandwidth method. In this approach, the modal damping value is determined from frequencies at which the response amplitude is reduced by $1/\sqrt{2}$:

$$\xi_k = \frac{\omega_2 - \omega_1}{2\omega_k} \tag{84}$$

where ω_1 and ω_2 are the upper and lower frequencies whose amplitudes are $\rho_k/\sqrt{2}$, ρ_k is the modal amplitude, and ω_k is the frequency.

FIG. 91. Impact Hammer Test on Modeled Sign

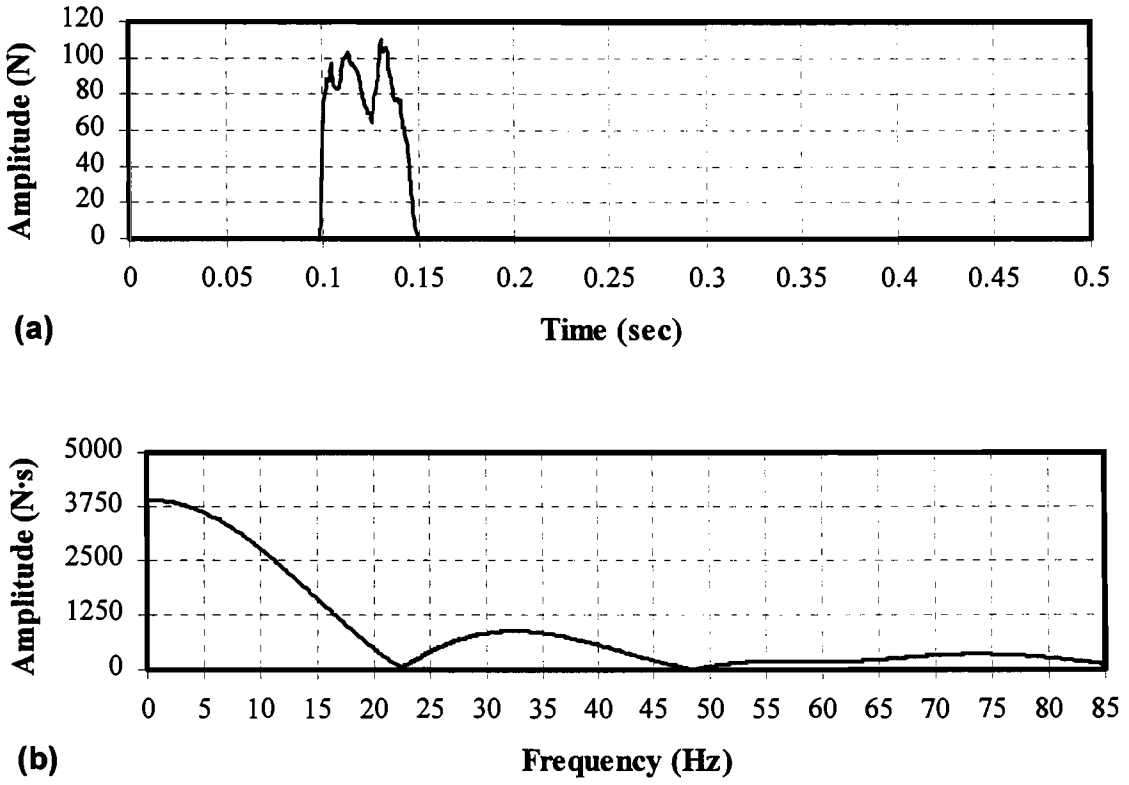

FIG. 92. Typical Impact Excitation of Field-Model: (a) Time Domain; and (b) Frequency Domain

Fig. 93 compares the response of the numerical simulation and the field structure to an impact excitation. The response of the FEM compares favorably to the response of the field model. The FEM and field structure oscillate in an approximately identical fashion. Inspection of the frequency domain plots in Fig. 94 reveals that the first mode of the FEM is very similar to the first mode of the field model with respect to frequency, amplitude, and bandwidth. Higher modes of the structure are also reasonably well represented by the FEM.

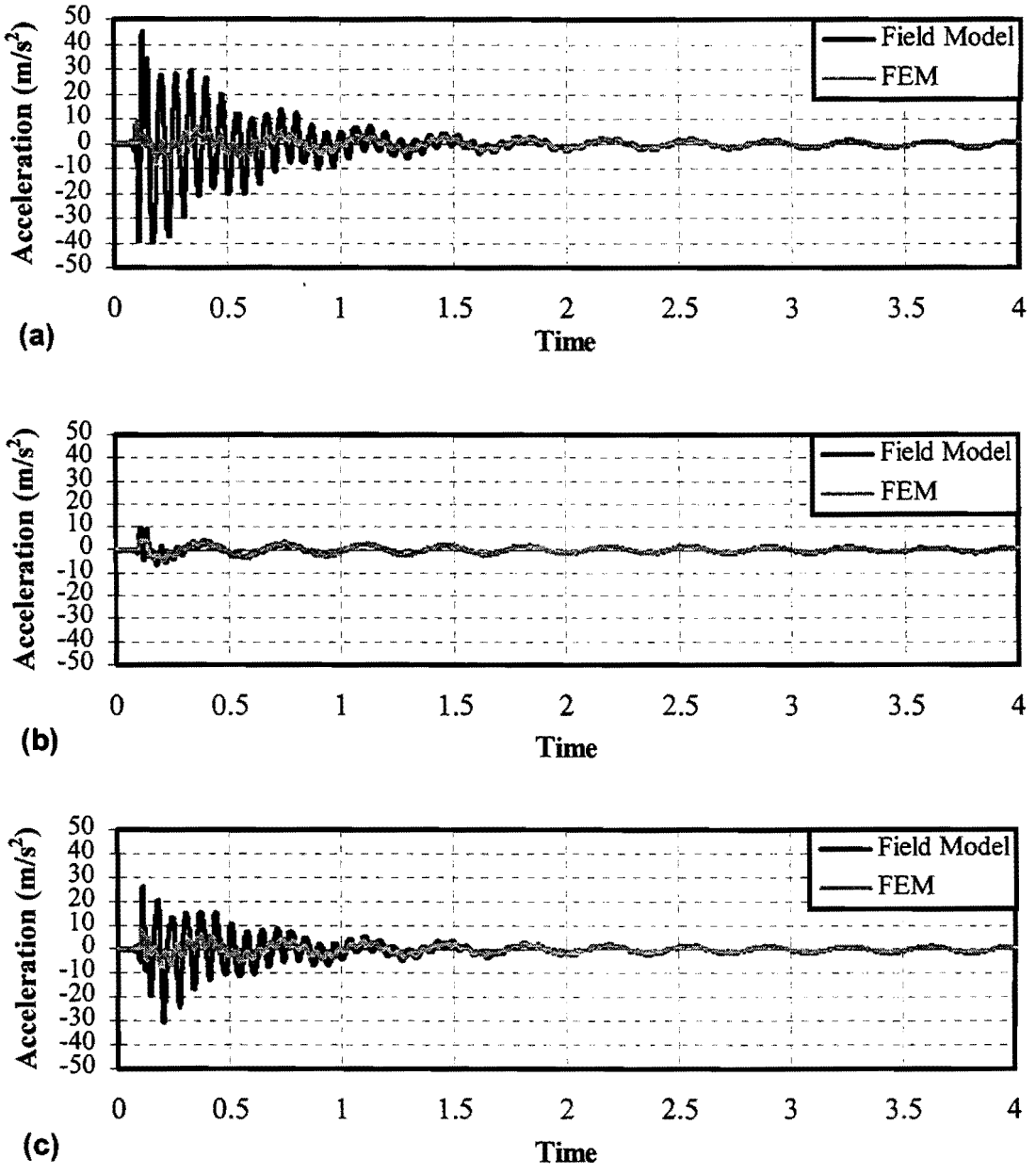

FIG. 93. Comparison of FEM and Model Time Domain Response: (a) Edge; (b) Pole; and (c) Center

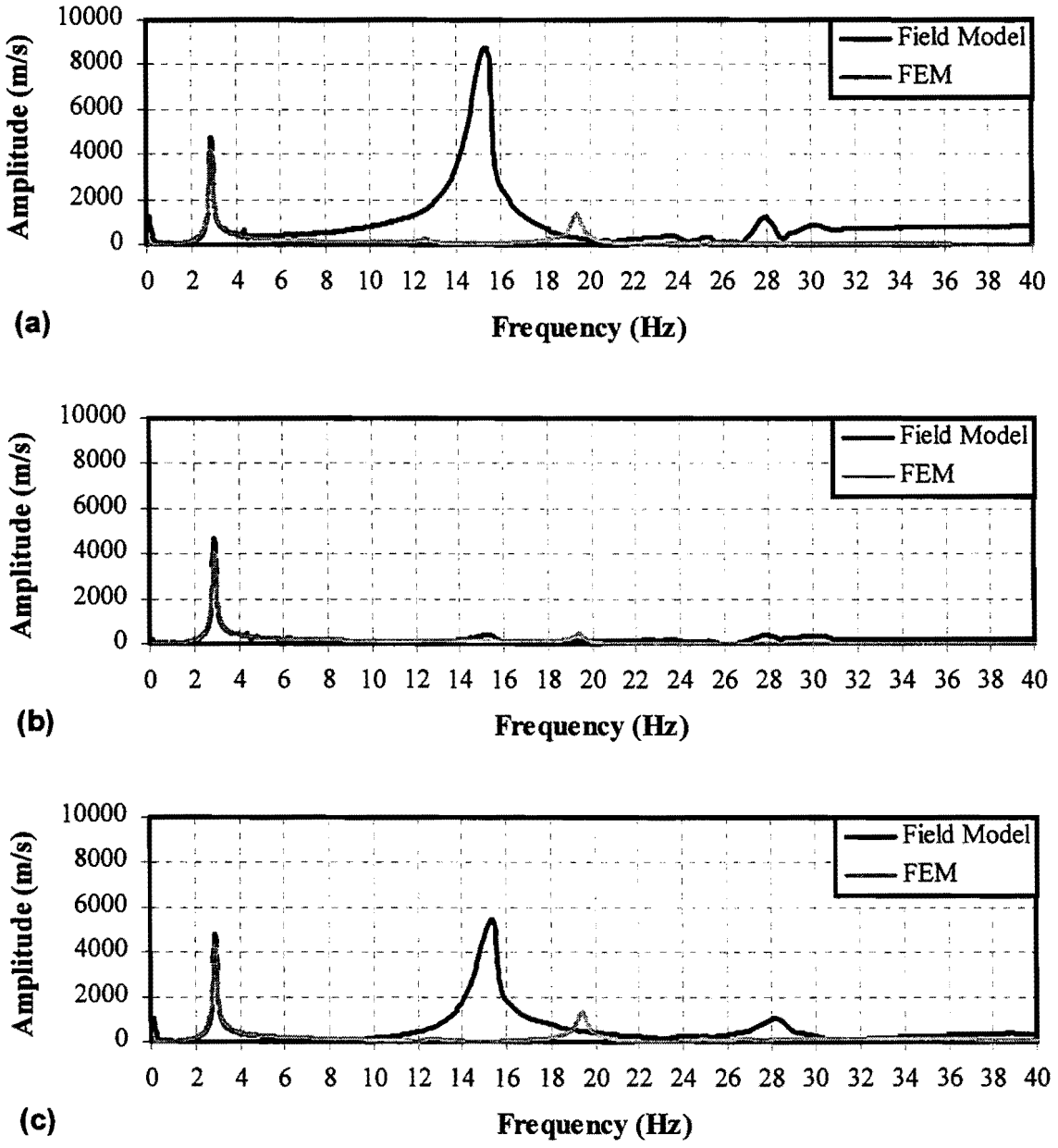

FIG. 94. Comparison of FEM and Model Frequency Response: (a) Edge; (b) Pole; and (c) Center

5.7 ACCELERATION RESULTS FROM FEM

Finite element analysis was performed to develop numerically predicted responses to the M15H541 and M15H571 time histories. The predicted acceleration of the edge, pole, and center of structure (see Fig. 67) for each wind event is presented in Figs. 95-100. To help reduce the effects of an artificial impact at the beginning of the wind event, the initial wind speed was developed linearly over a period of one second.

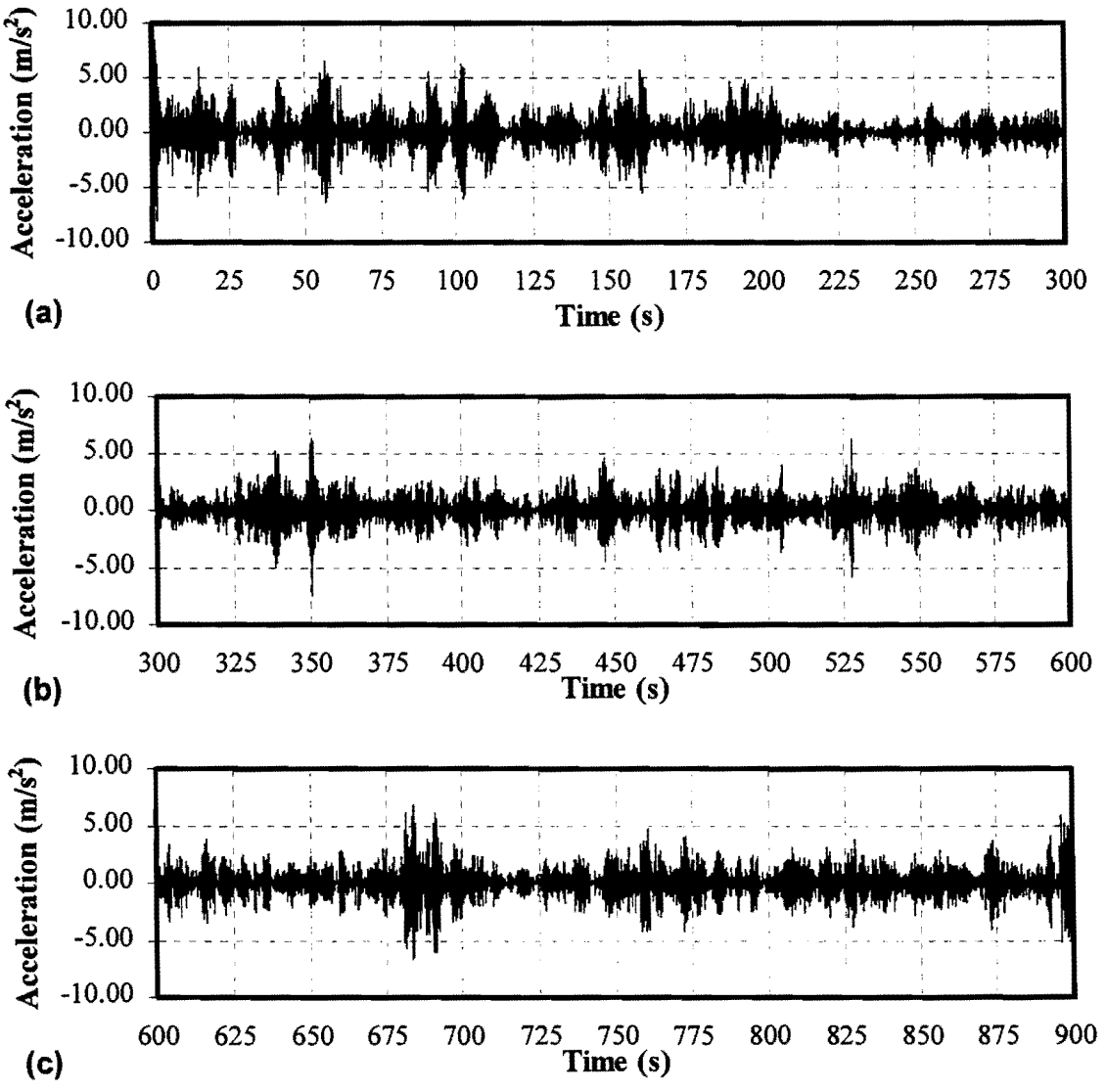

FIG. 95. FEM Response of Substrate Edge to M15H541: (a) 0-300 sec.; (b) 300-600 sec.; and (c) 600-900 sec.

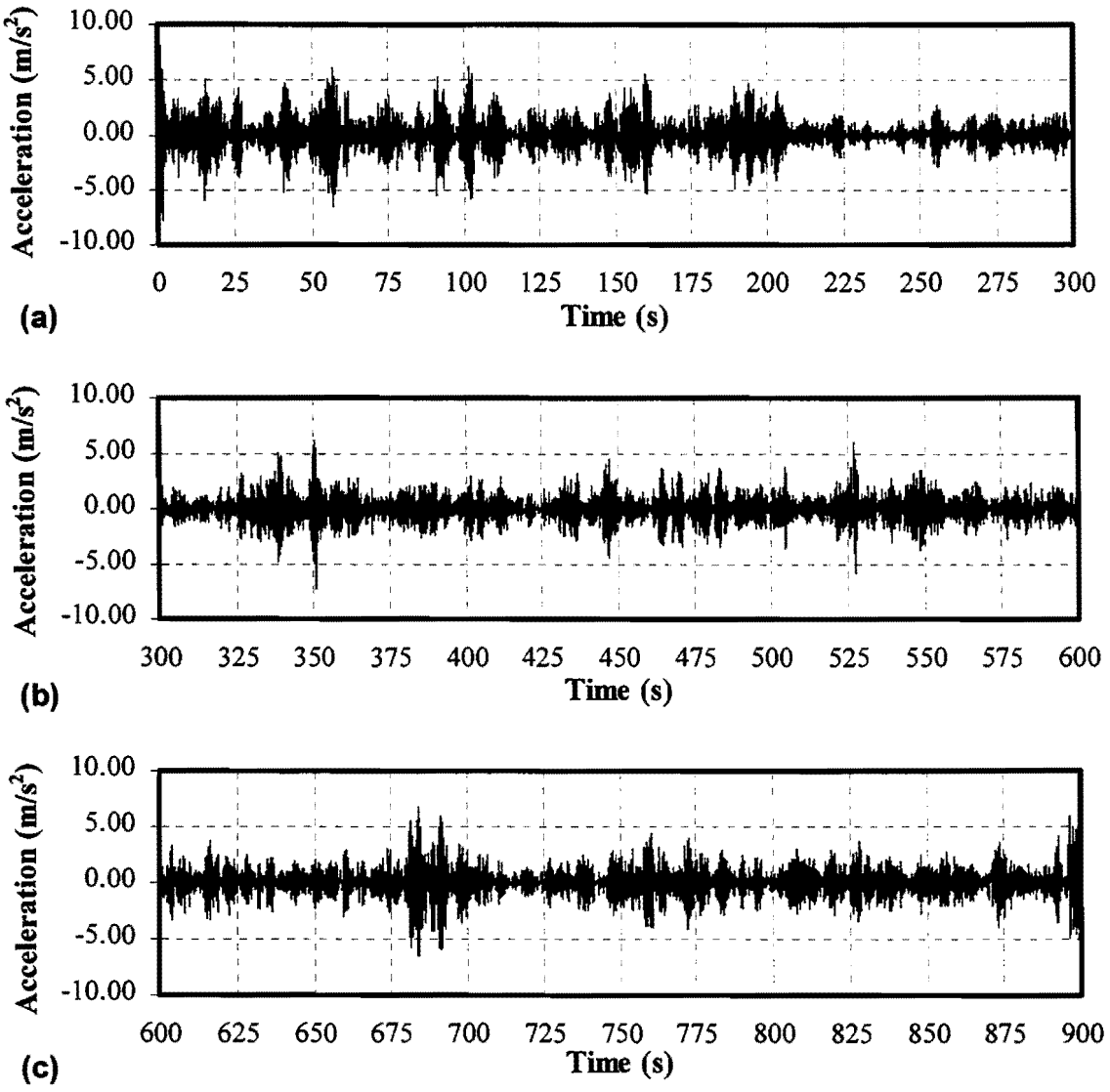

FIG. 96. FEM Response of Sign Pole to M15H541: (a) 0-300 sec.; (b) 300-600 sec.; and (c) 600-900 sec.

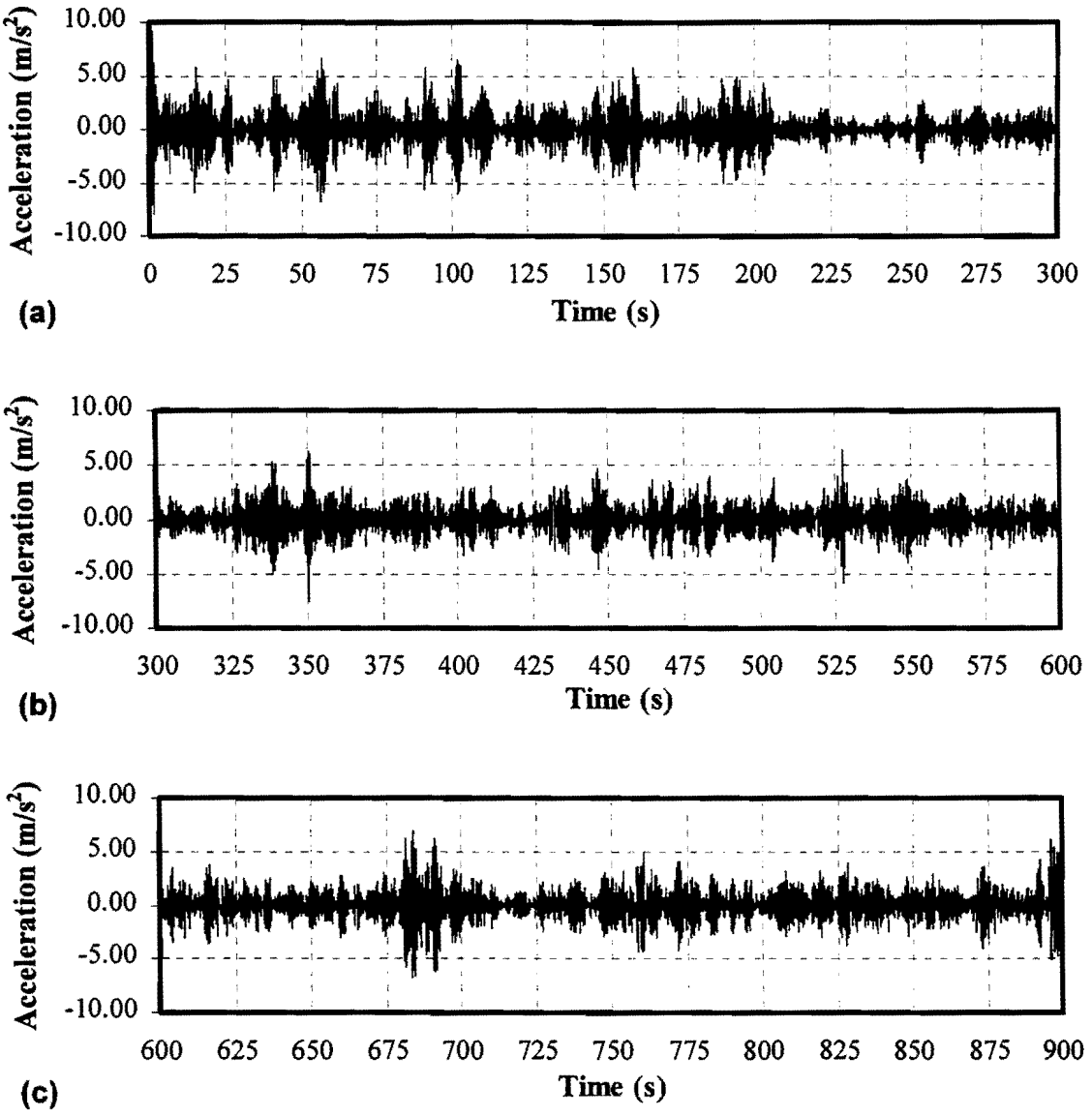

FIG. 97. FEM Response of Substrate Center to M15H541: (a) 0-300 sec.; (b) 300-600 sec.; and (c) 600-900 sec.

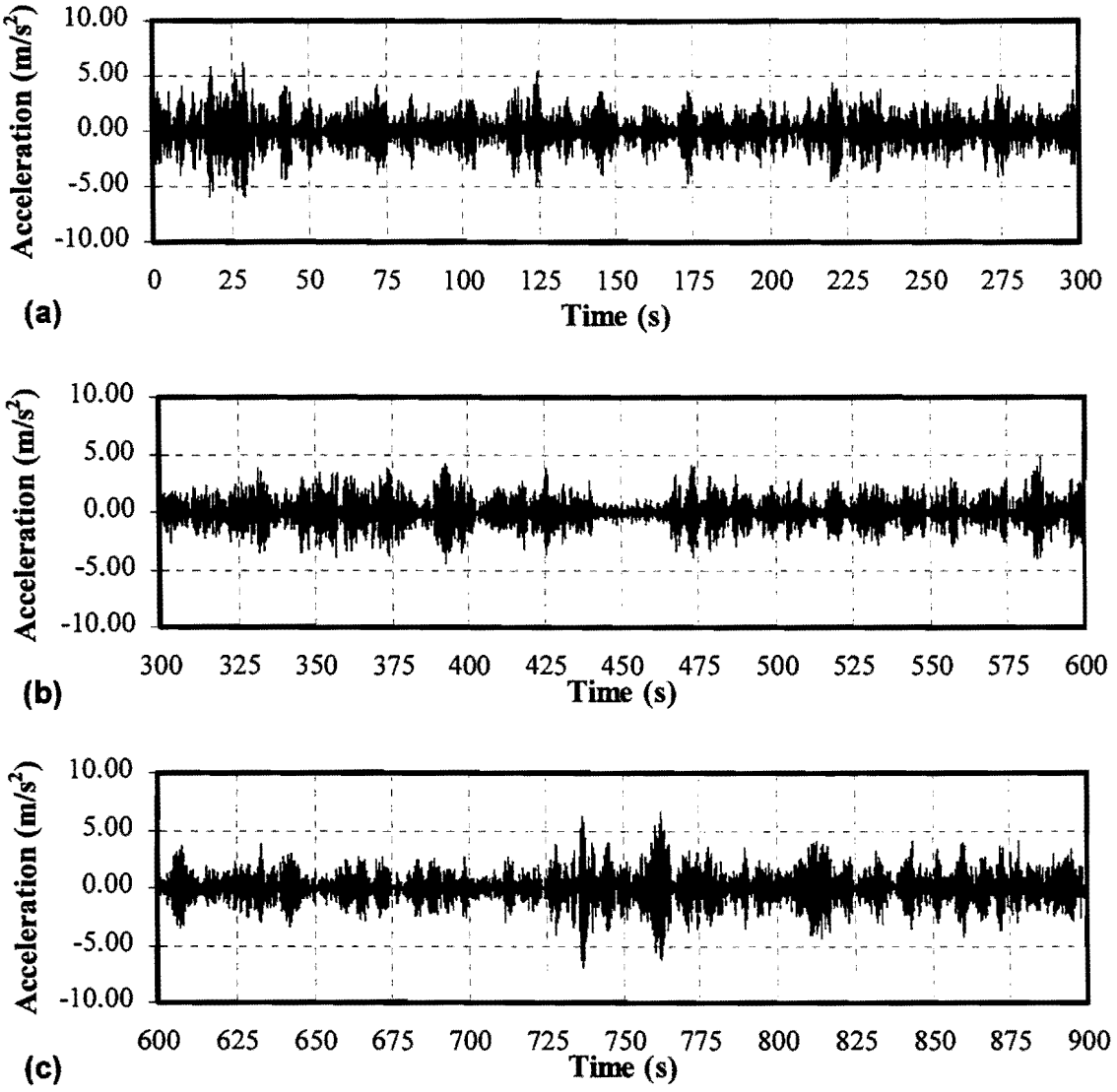

FIG. 98. FEM Response of Substrate Edge to M15H571: (a) 0-300 sec.; (b) 300-600 sec.; and (c) 600-900 sec.

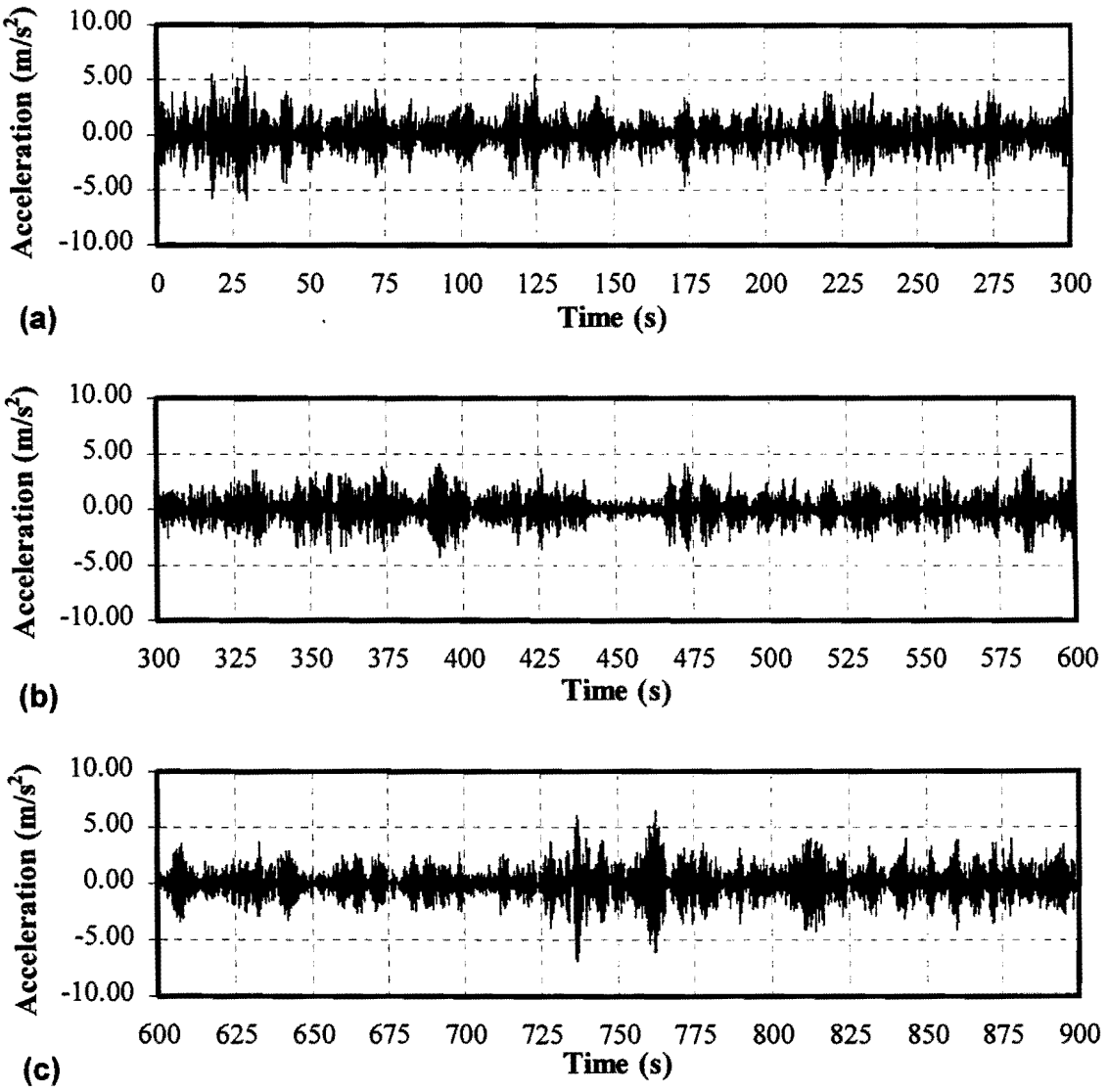

FIG. 99. FEM Response of Sign Pole to M15H571: (a) 0-300 sec.; (b) 300-600 sec.; and (c) 600-900 sec.

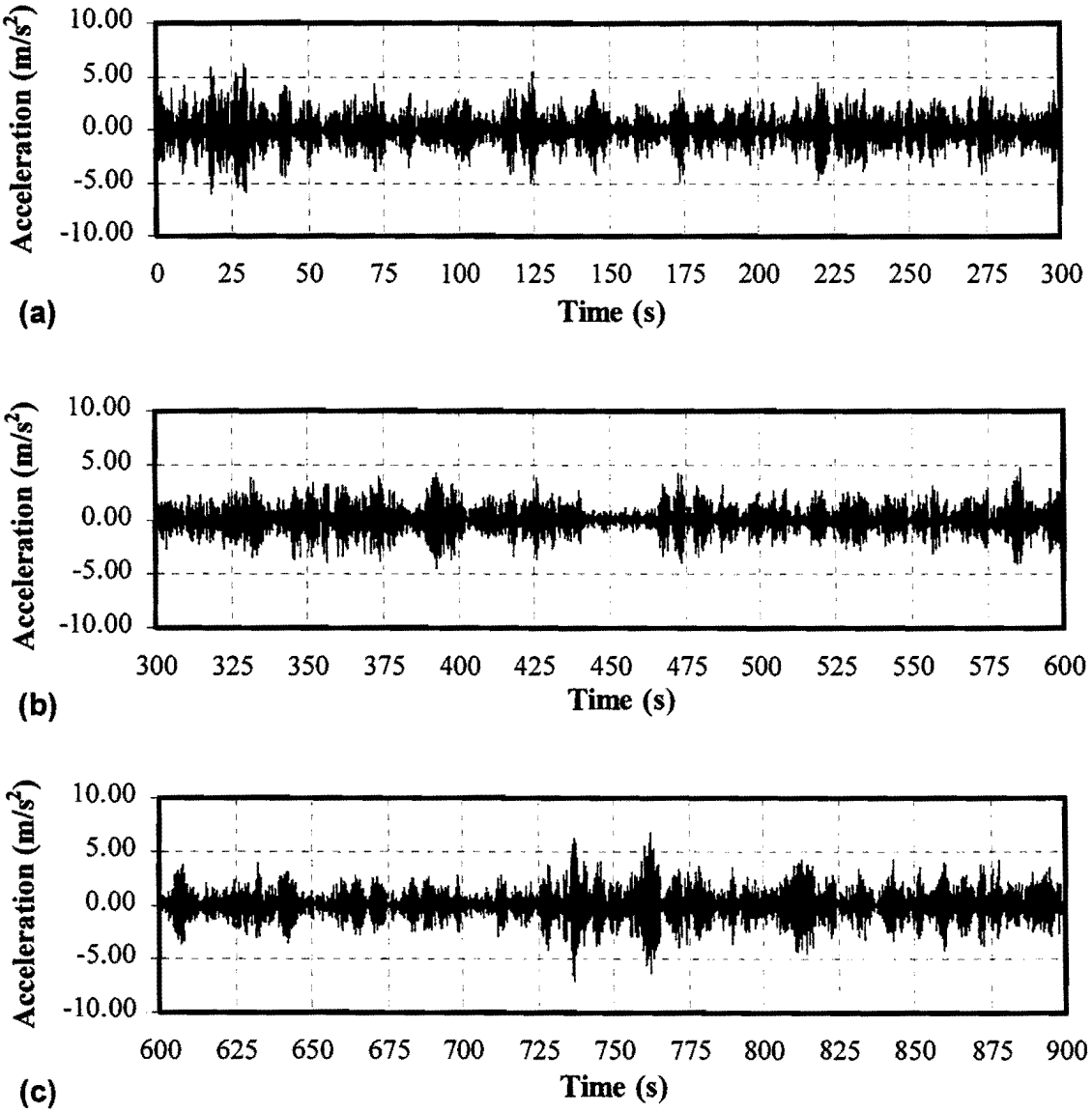

FIG. 100. FEM Response of Substrate Center to M15H571: (a) 0-300 sec.; (b) 300-600 sec.; and (c) 600-900 sec.

Each simulated response was converted to the frequency domain by use of FFT. Figs. 101-106 illustrate amplitude and phase at three of the accelerometer locations shown in Fig. 66 from the M15N541 and M15N571 wind events. The frequency content of the acceleration responses shows that the wind events used in this study can only significantly excite the first mode of the response that occurs at a frequency of 2.875 Hz. This behavior is a result of the

wind events having very small significant frequency content at frequencies over 5 Hz (see Fig. 88).

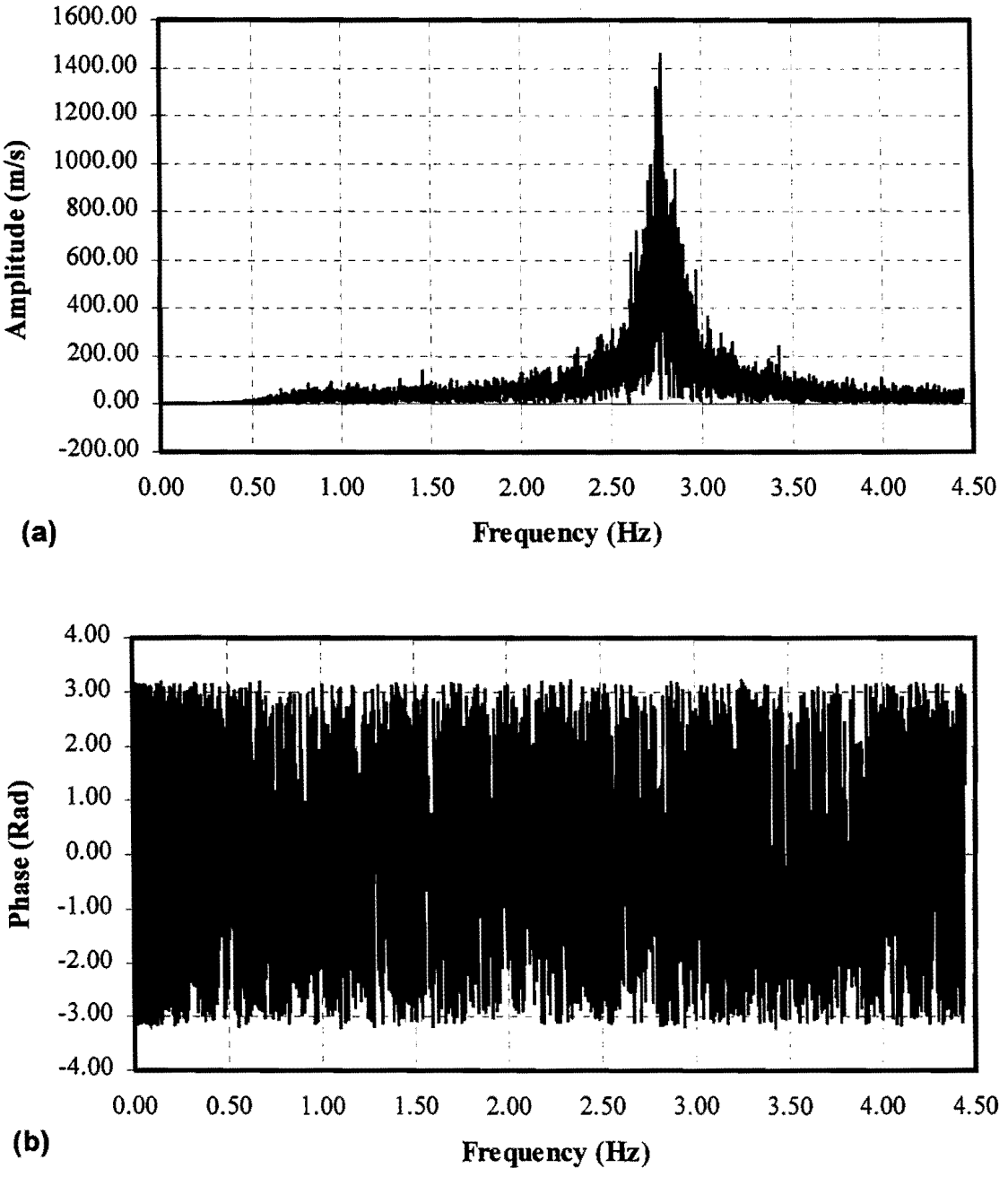

FIG. 101. FEM Frequency Response of Substrate Edge to M15H541: (a) Amplitude; and (b) Phase

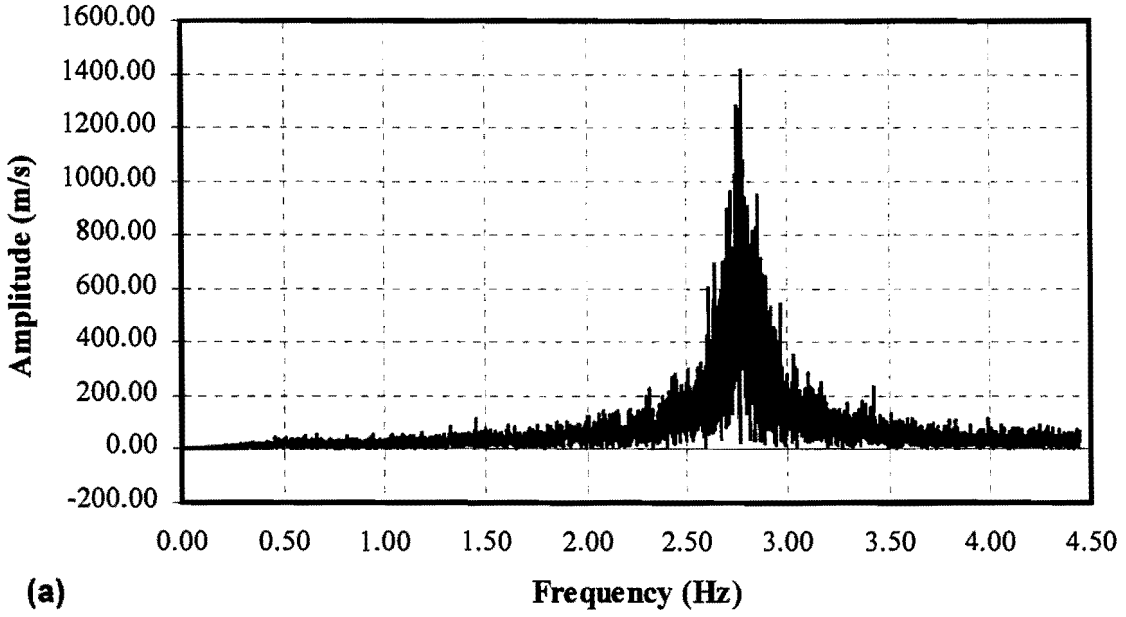

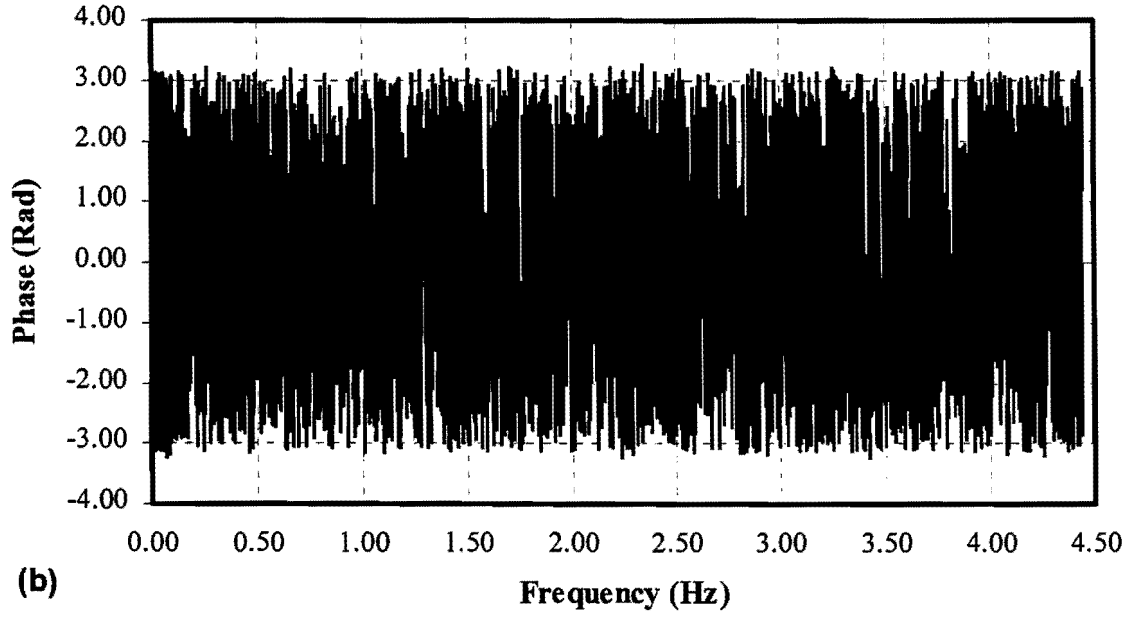

FIG. 102. FEM Frequency Response of Sign Pole to M15H541: (a) Amplitude; and (b) Phase

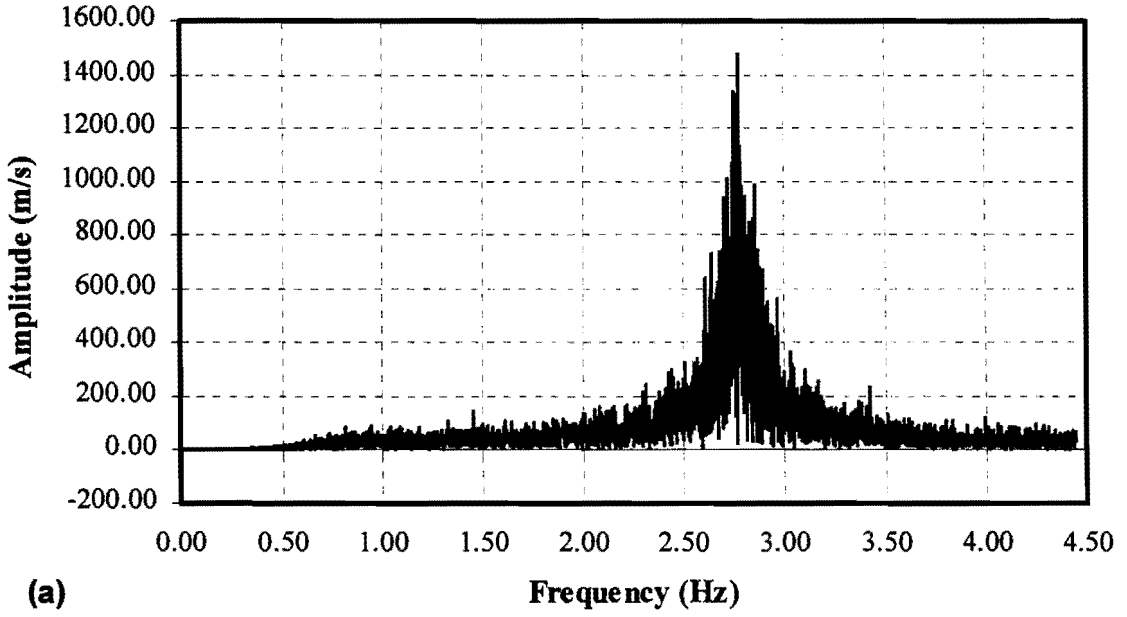

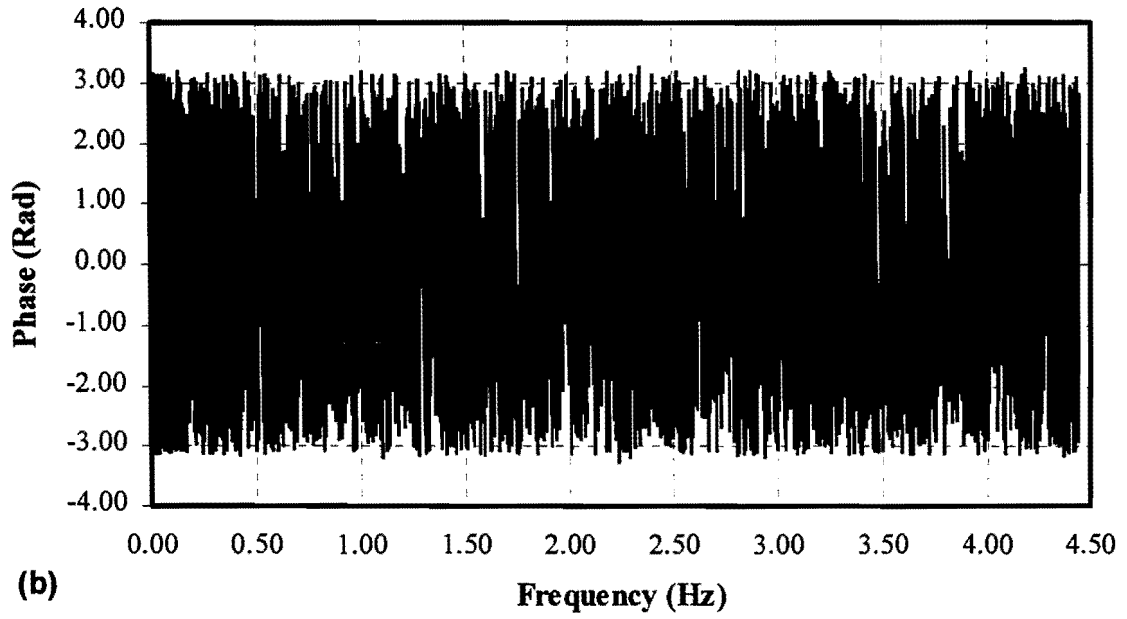

FIG. 103. FEM Frequency Response of Substrate Center to M15H541: (a) Amplitude; and (b) Phase

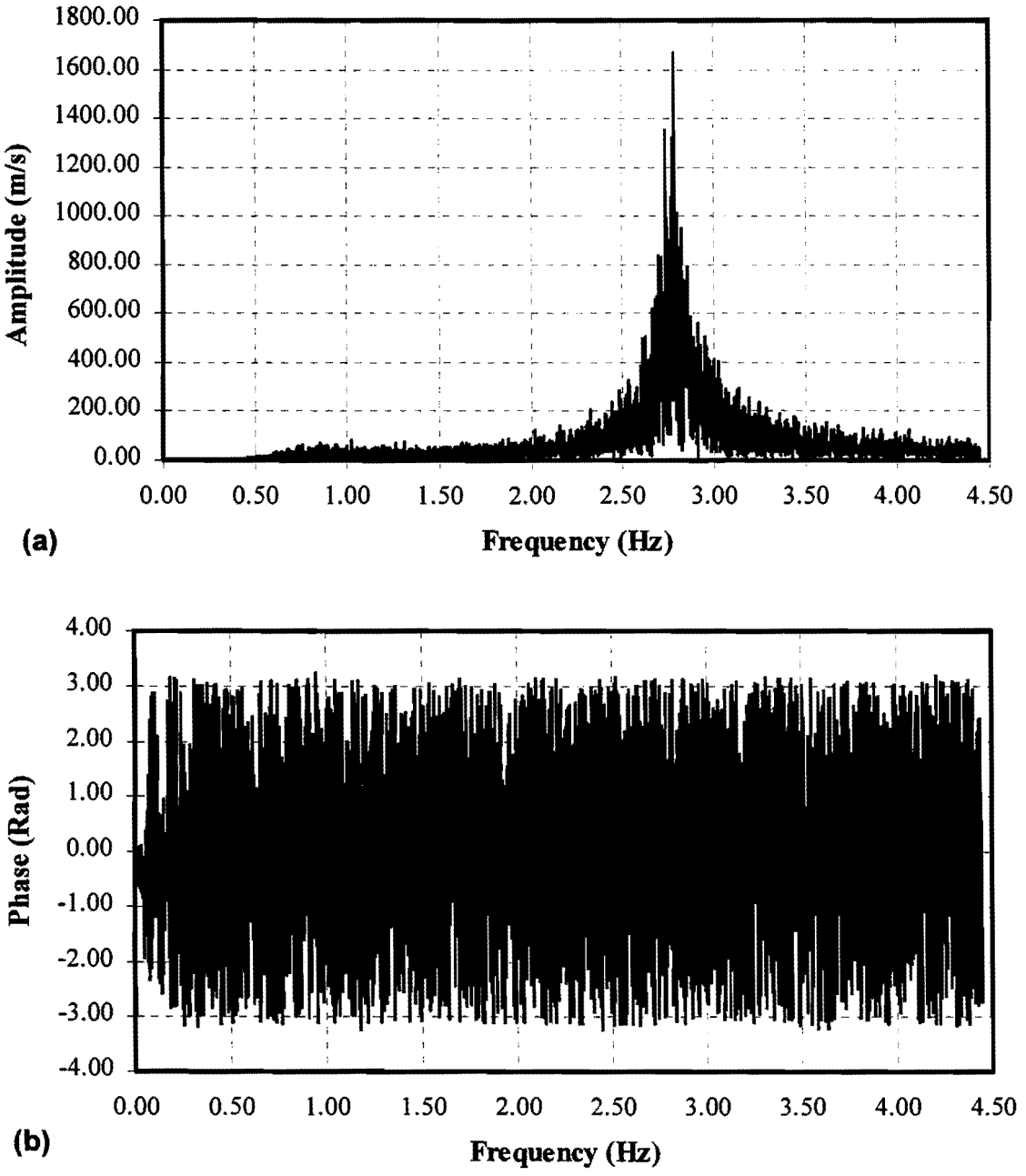

FIG. 104. FEM Frequency Response of Substrate Edge to M15H571: (a) Amplitude; and (b) Phase

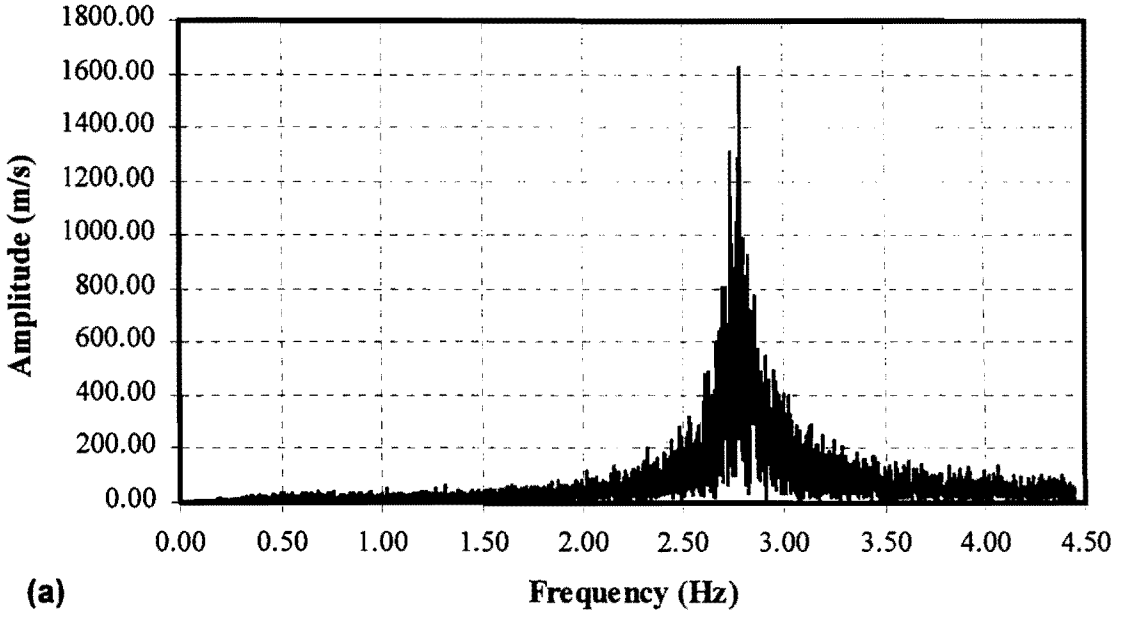

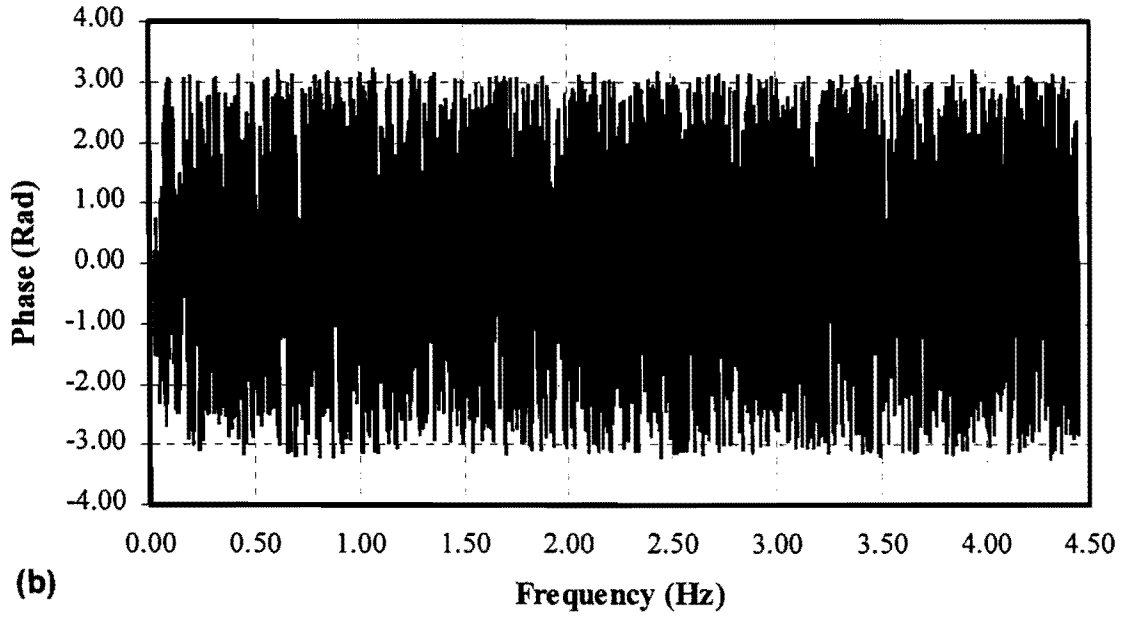

FIG. 105. FEM Frequency Response of Sign Pole to M15H571: (a) Amplitude; and (b) Phase

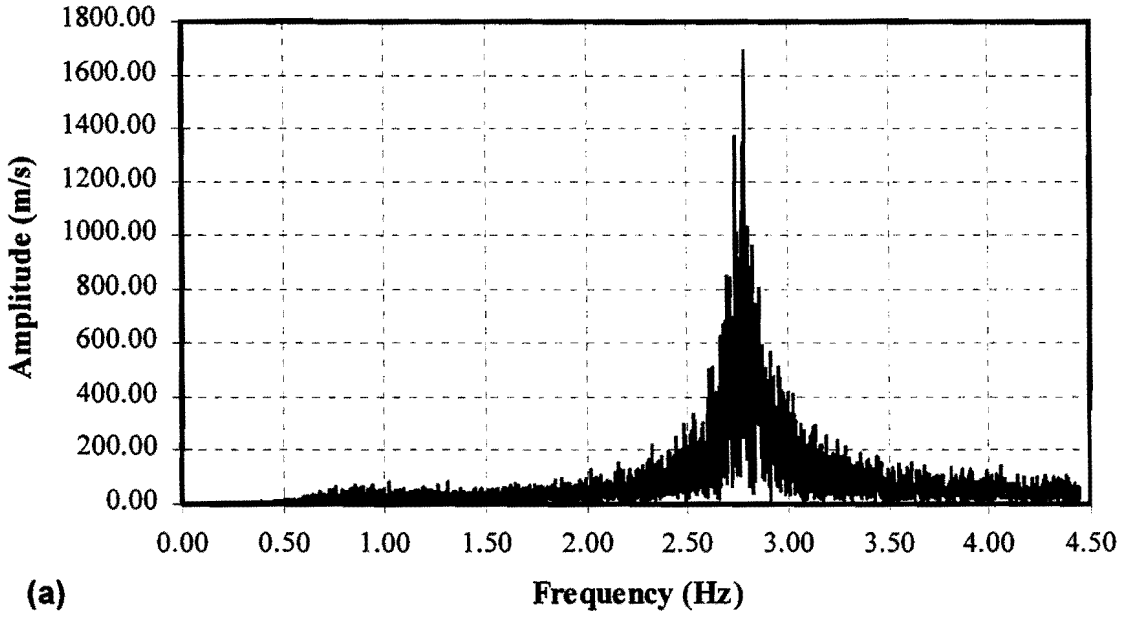

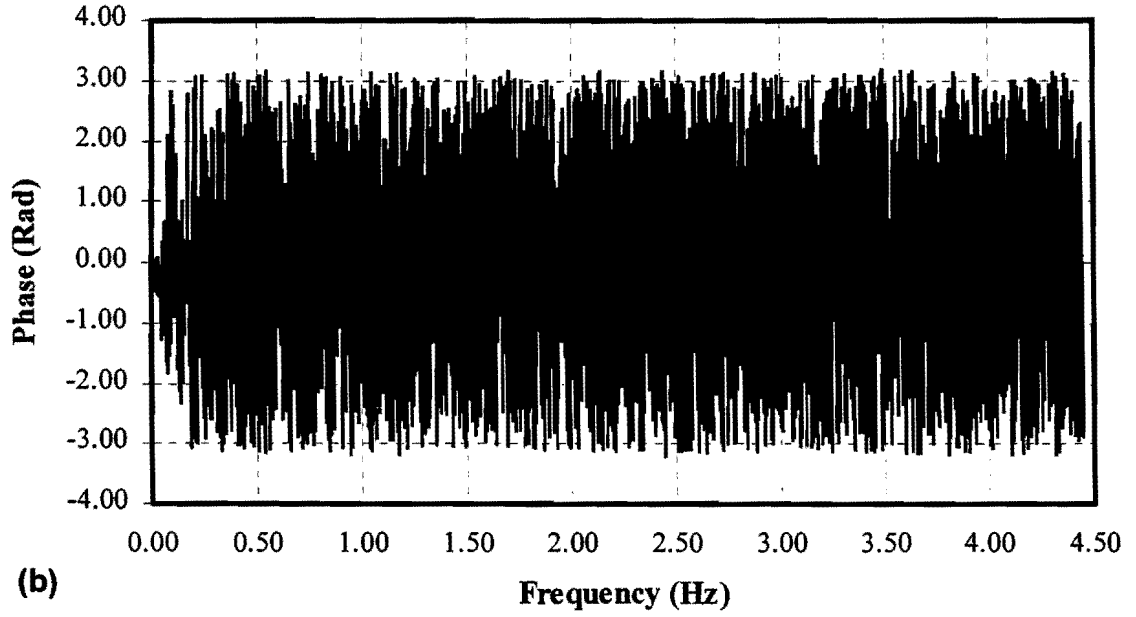

FIG. 106. FEM Frequency Response of Substrate Center to M15H571: (a) Amplitude; and (b) Phase

5.8 CALCULATION OF TIME HISTORY OF ACTUATOR FORCE

Since the transfer function, $\ddot{H}(i\omega)$, is defined as the ratio of the acceleration response to the excitation in the frequency domain, the product of the transfer function and the frequency content of the actuator force produces the frequency response predicted by FEM. Therefore, the frequency content of the actuator is determined by dividing the FEM frequency response by the transfer function:

$$f_A(\omega) = \frac{A_{\ddot{x}_{FEM}}(\omega) e^{i\theta_{\ddot{x}_{FEM}}(\omega)}}{\ddot{H}(i\omega)} \tag{85}$$

where $f_A(\omega)$ is the theoretical or target frequency content for the electric actuator in amplitude and phase, $A_{\ddot{x}_{FEM}}(\omega)$ represents the Fourier amplitude of an acceleration in the FEM, and $\theta_{\ddot{x}_{FEM}}$ represents the phase of an acceleration response in the FEM. Substituting Eq. 78 into Eq. 85 gives:

$$f_A(\omega) = \frac{A_{\ddot{x}_{FEM}}(\omega) e^{i\theta_{\ddot{x}_{FEM}}(\omega)}}{\frac{A_{\ddot{x}_H}(\omega)}{A_{f_H}(\omega)} e^{i\left[\theta_{\ddot{x}_H}(\omega) - \theta_{f_H}(\omega)\right]}} \tag{86}$$

and simplifying leads to:

$$F_A(\omega) = \frac{A_{\ddot{x}_{FEM}}(\omega) A_{F_H}(\omega)}{A_{\ddot{x}_H}(\omega)} e^{i\left[\theta_{\ddot{x}_{FEM}} - \theta_{\ddot{x}_H}(\omega) + \theta_{F_H}(\omega)\right]} \tag{87}$$

Application of Eq. 87 provides the frequency content for the laboratory actuator in amplitude and phase (see Figs. 107-109). If the frequency content of the actuator is to produce a response in the structure that closely approximates the response of the sign to an actual wind event, the amplitude will increase at the natural frequency of the modeled structure. Although wind does not have a dominant frequency, when significant frequency content of the wind matches the fundamental frequency of the excited structure, an amplified response is produced from resonance. However, by attaching the actuator to the structure in the laboratory, the fundamental frequency of the system is increased due to interaction between the actuator and sign. Therefore, the resonant frequency of the combined system does not match the fundamental frequency predicted by FEM. In order for the actuator to produce the level of response in the substrate predicted by FEM, the force required of the

actuator at this frequency must be amplified. The frequency content of the actuator signal fits this expectation. For example, Fig. 107 shows a dominant frequency of the actuator signal to be identical to the fundamental frequency of the FEM given in Fig. 101. Presentation of intermediate results is limited to M15H571 to prevent redundancy.

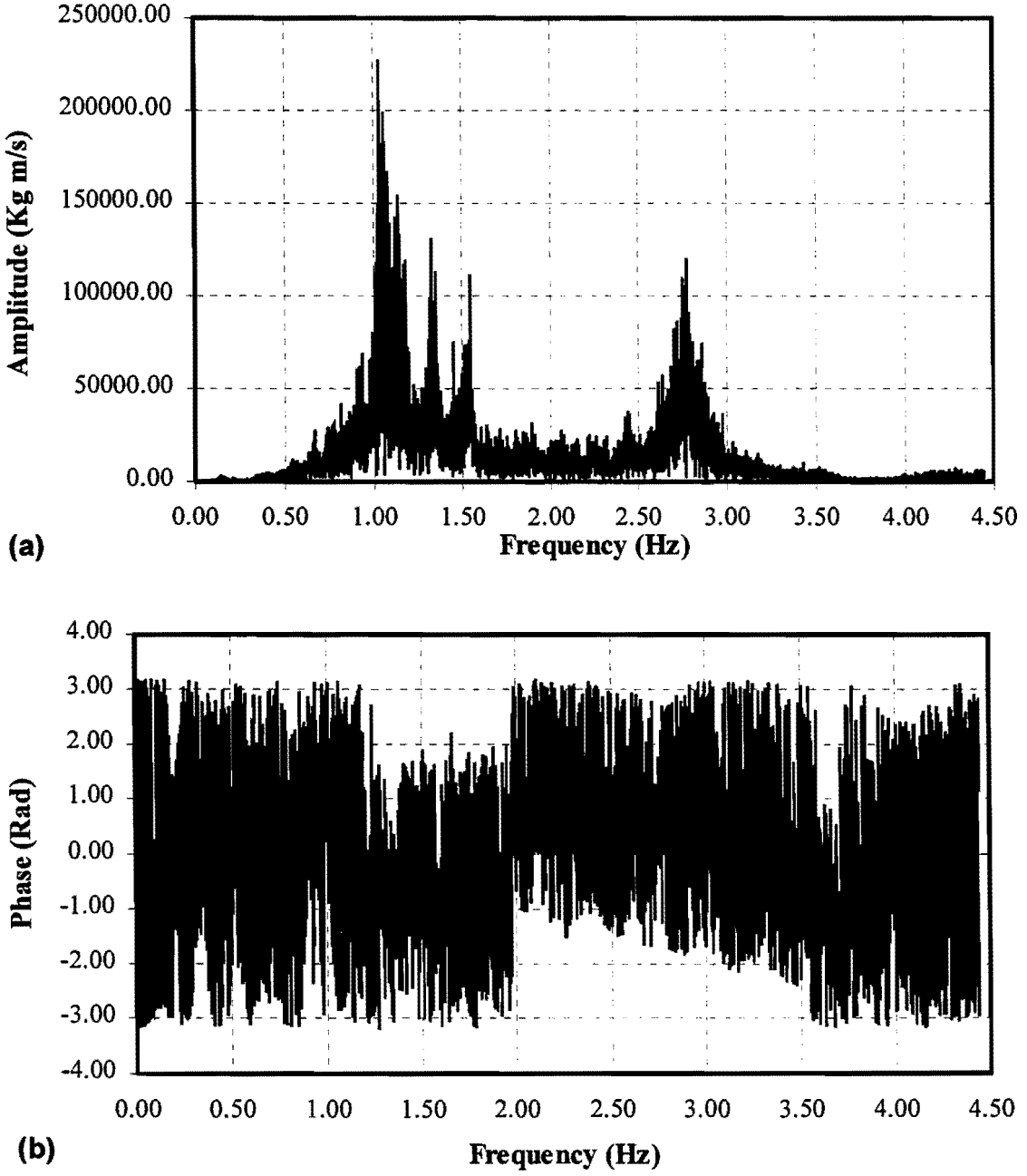

FIG. 107. Actuator Frequency Content for Duplicating Edge Response to M15H541: (a) Amplitude; and (b) Phase

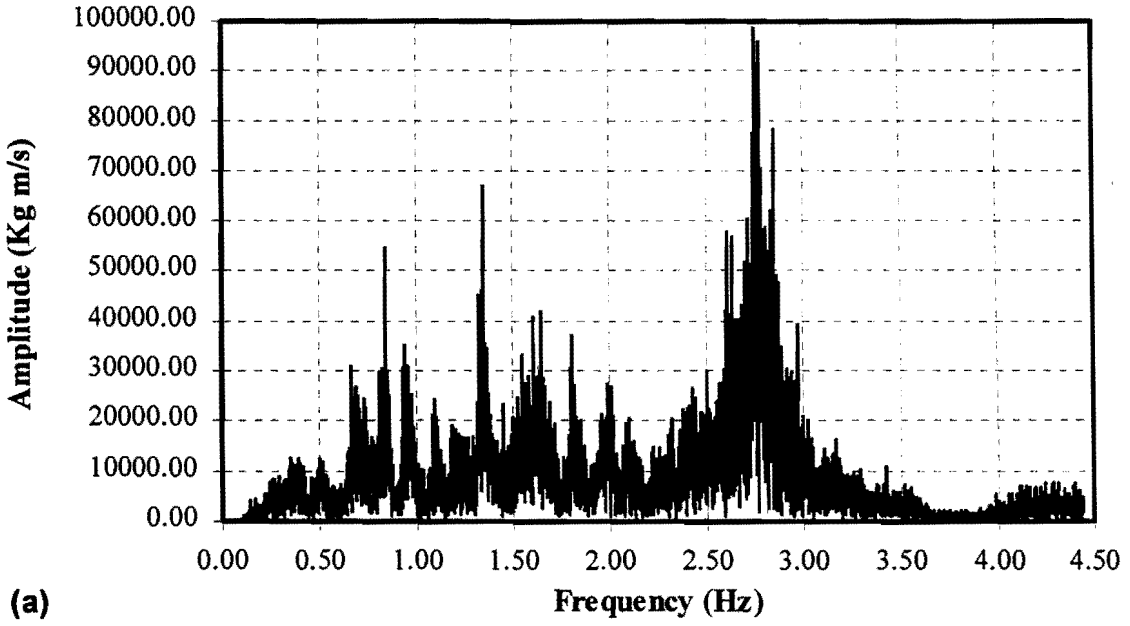

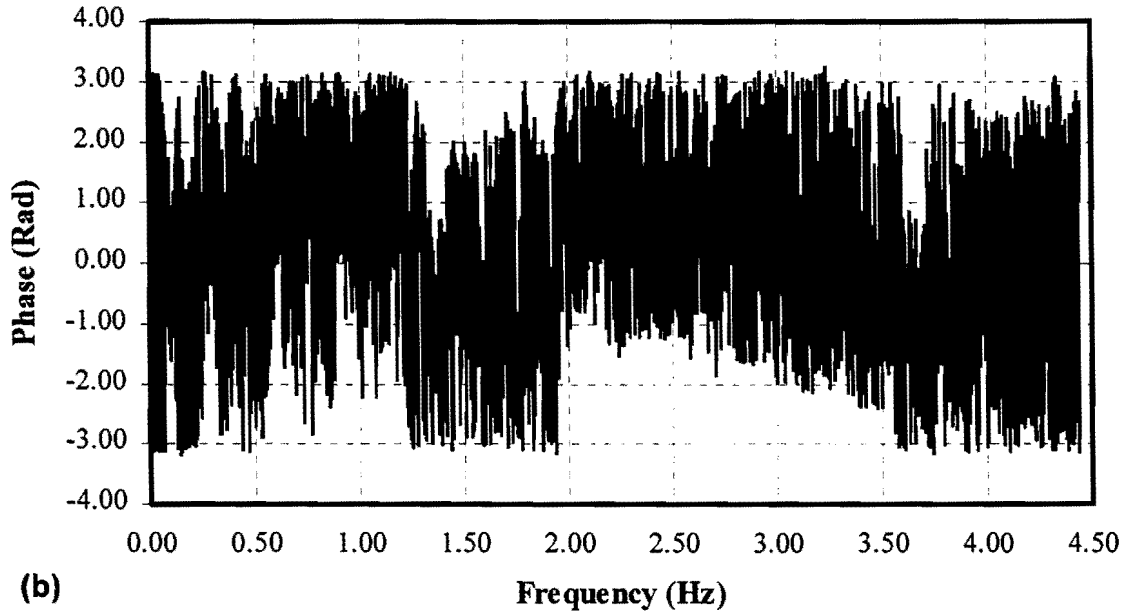

FIG. 108. Actuator Frequency Content for Duplicating Pole Response to M15H541: (a) Amplitude; and (b) Phase

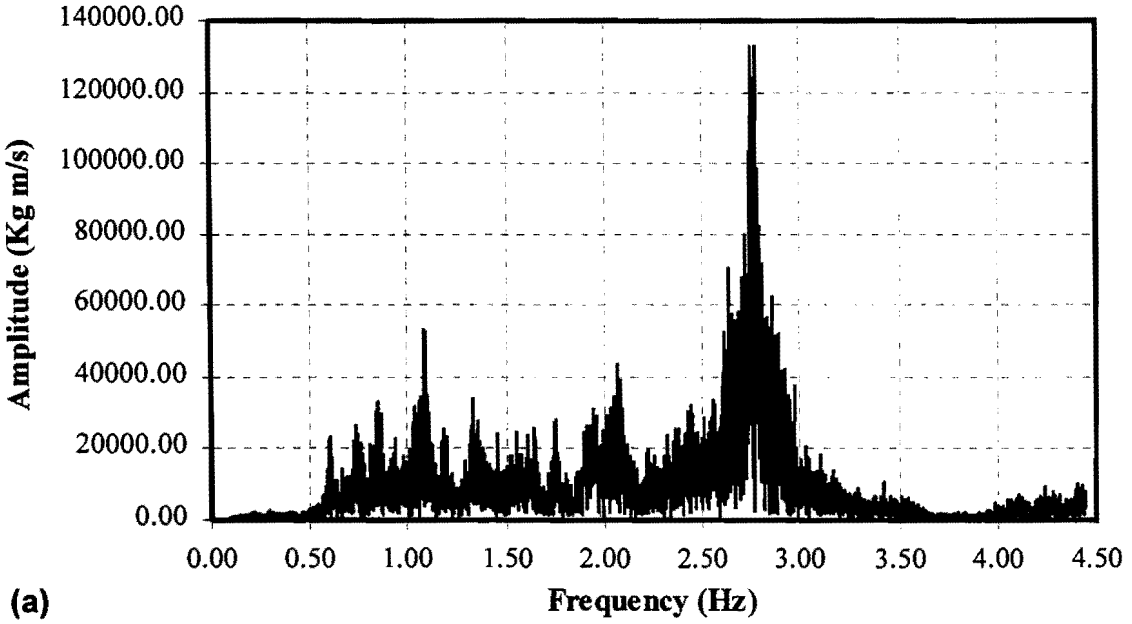

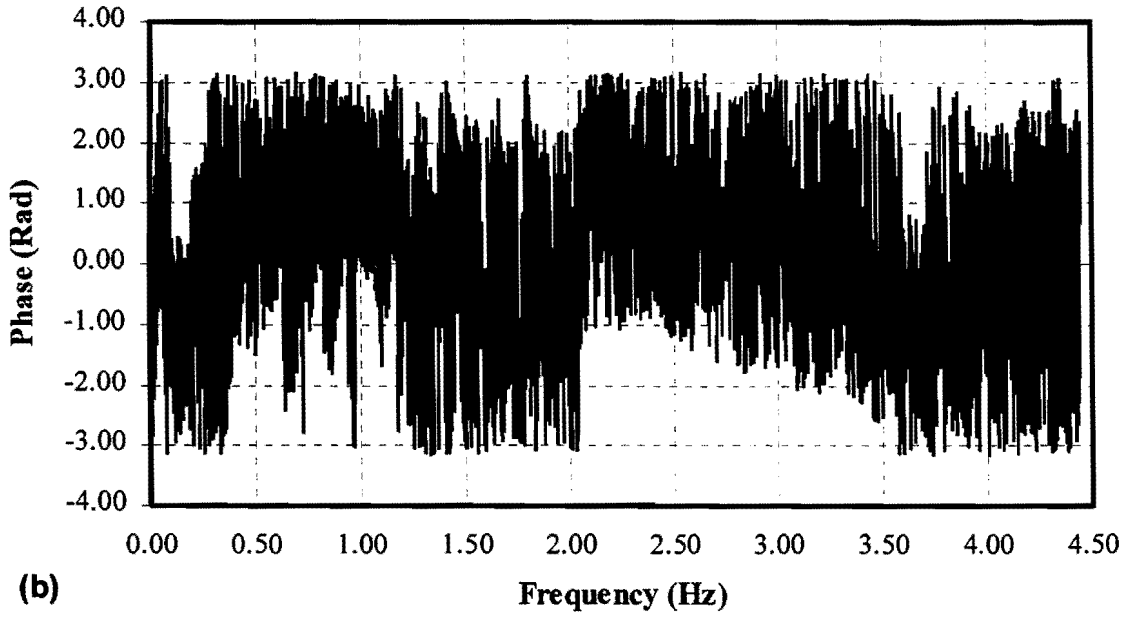

FIG. 109. Actuator Frequency Content for Duplicating Center Response to M15H541: (a) Amplitude; and (b) Phase

In order to apply an actual time history of force to the load bar attached to the poles, the frequency content of the actuator signal was converted back to the time domain by use of inverse Fourier transform (IFT). IFT is an analytical method for performing the inverse Fourier transform that is defined as follows (Lutes and Sarkani 1997):

$$f(t) = \int_{-\infty}^{\infty} \tilde{f}(\omega) e^{i\omega t} d\omega \tag{88}$$

where the numerical equivalent of the analytical IFT is the inverse fast Fourier transform (IFFT):

$$x(j) = \left(\frac{1}{N}\right) \sum_{k=1}^{N} X(k) \omega_N^{-(j-1)(k-1)} \tag{89}$$

x=IFFT(X), and ω_N is as in Eq. 72 (MATLAB®). The final actuator time histories were produced using MATLAB (see Figs. 110-112). Results are only presented for M15N541 since it produces the largest response in the FEM (see Figs. 95-100). The MATLAB session file, or M-file, for calculating the IFFT is presented in Appendix C. There is a unique time history from the IFFT process since both the amplitude and phase were defined.

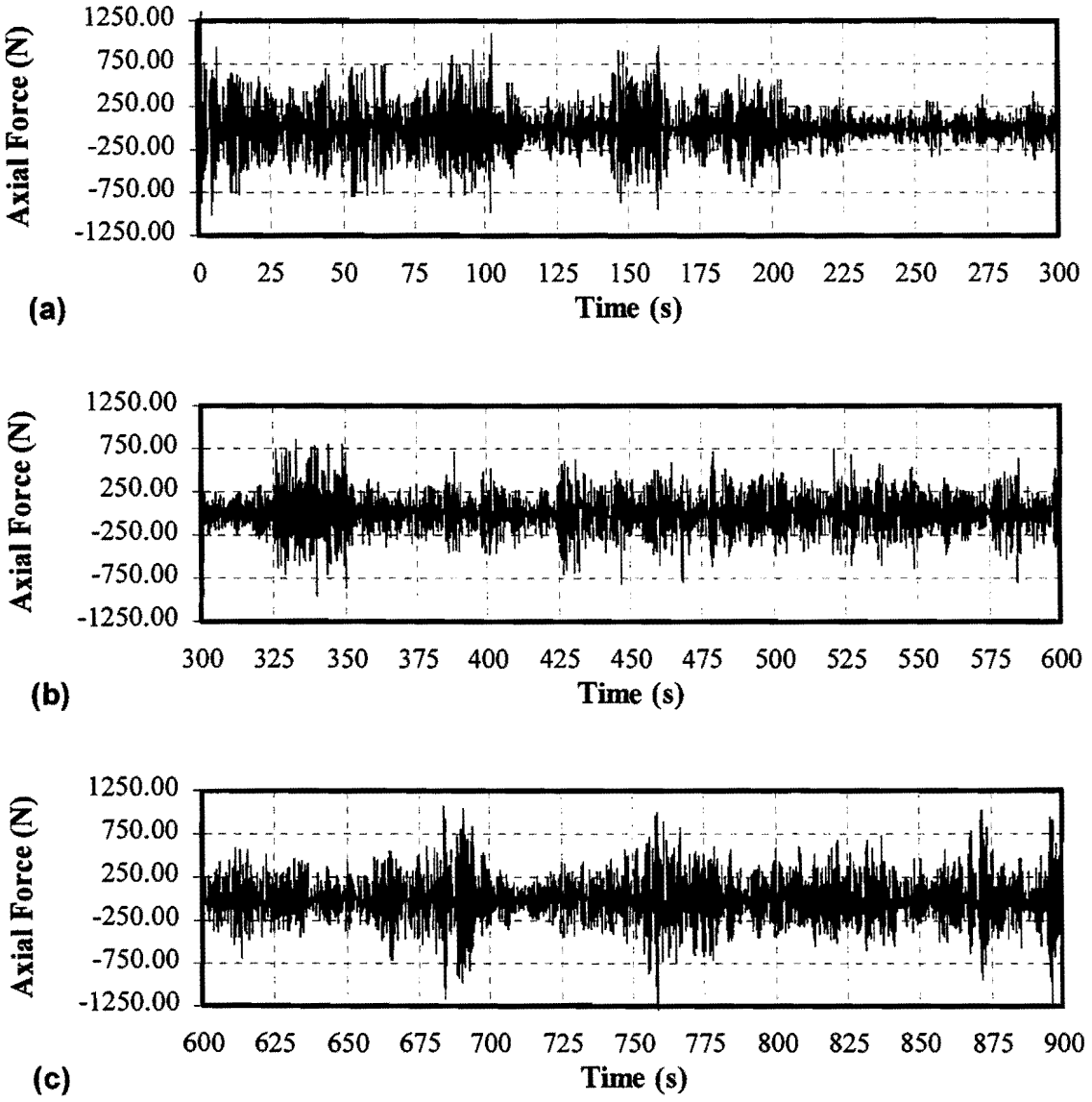

FIG. 110. Actuator Time History for Edge Response to M15H541: (a) 0-300 sec.; (b) 300-600 sec.; and (c) 600-900 sec.

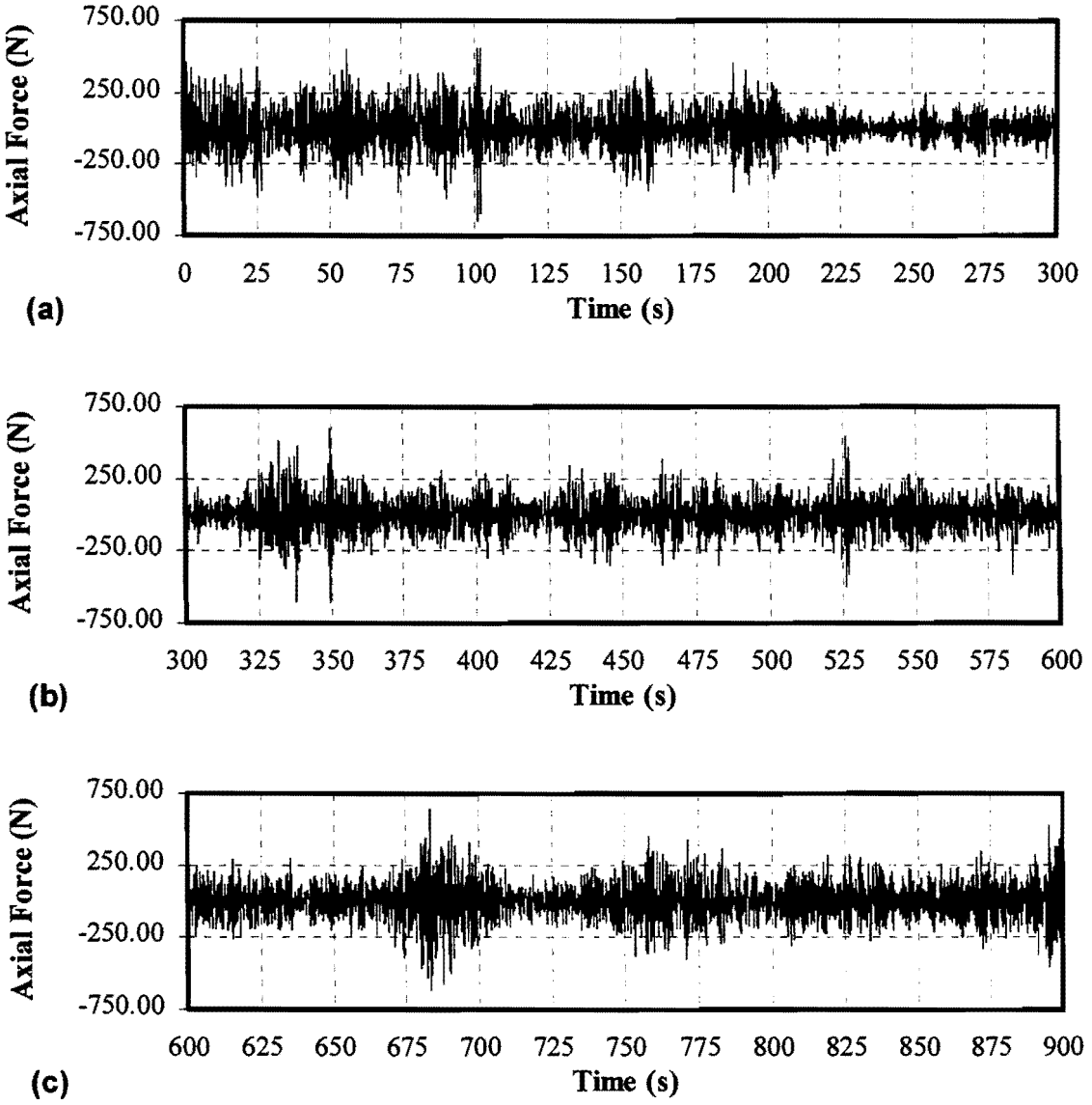

FIG. 111. Actuator Time History for Pole Response to M15H541: (a) 0-300 sec.; (b) 300-600 sec.; and (c) 600-900 sec.

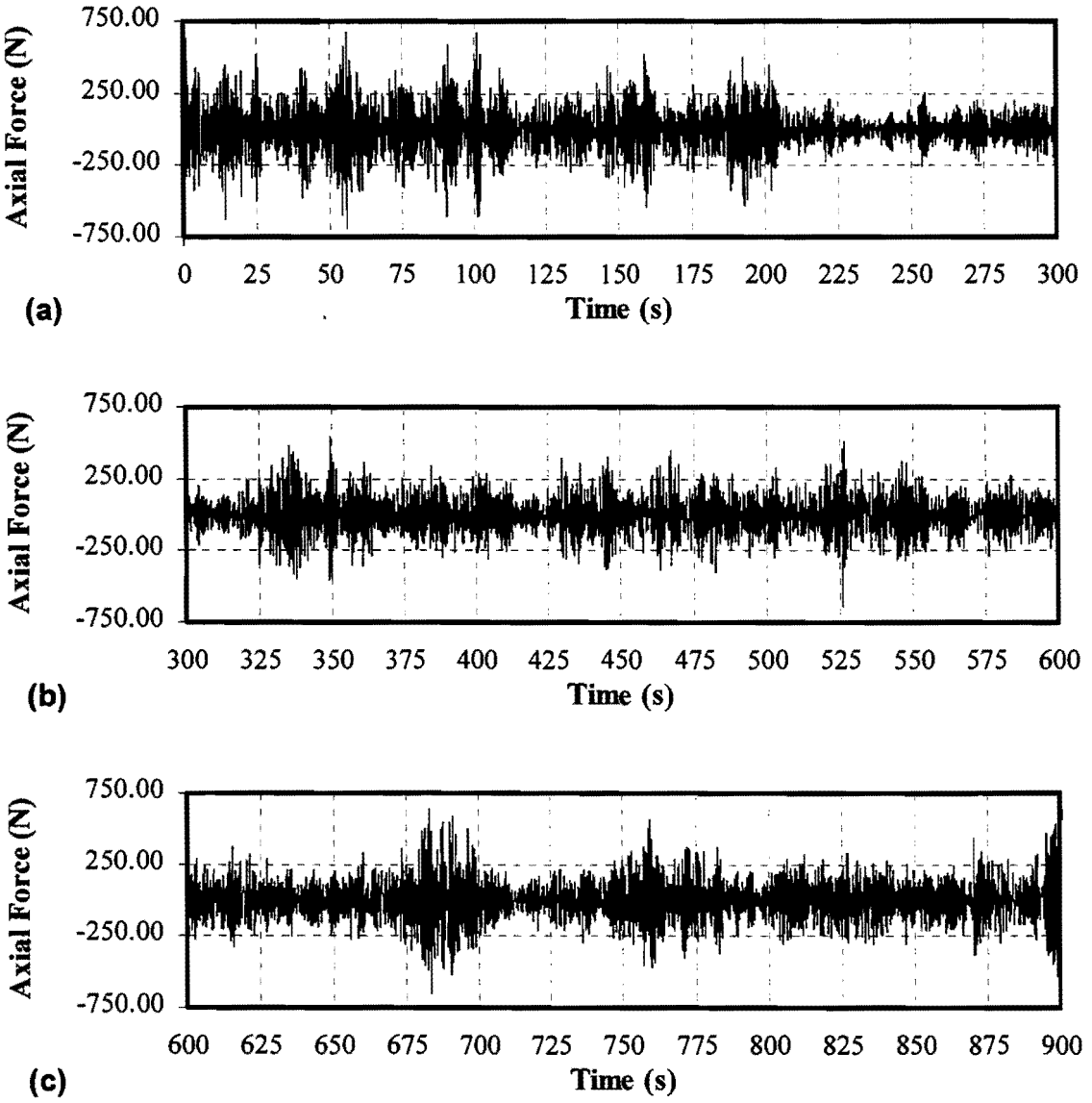

FIG. 112. Actuator Time History for Center Response to M15H541: (a) 0-300 sec.; (b) 300-600 sec.; and (c) 600-900 sec.

5.9 RESULTS OF WIND SIMULATION

Simulation results were encouraging. Both the simulated response in the laboratory and the FEM response time histories had very nearly the same amplitudes and variability (see Figs. 113-118). For instance, in Fig. 113 (a) the first 100 seconds show typical matching of response shape and amplitude for the laboratory and FEM values. Simulation results are presented for both M15H541 and M15H571 in order to show that the transfer functions are

not case specific, but instead are capable of producing actuator time histories to reproduce a large number of responses.

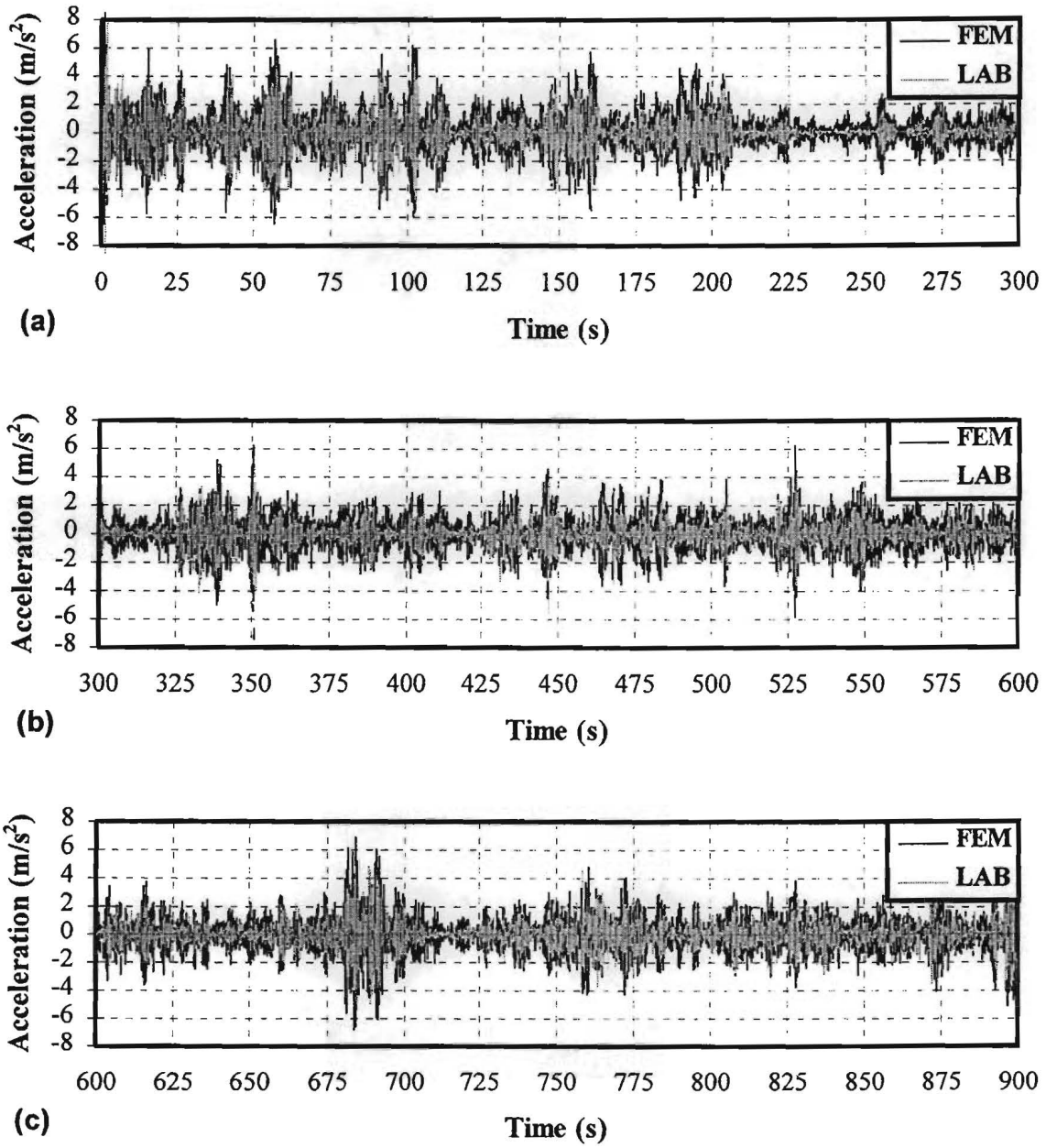

FIG. 113. Laboratory Simulated Response versus FEM for Edge to M15H541: (a) 0-300 sec.; (b) 300-600 sec.; and (c) 600-900 sec.

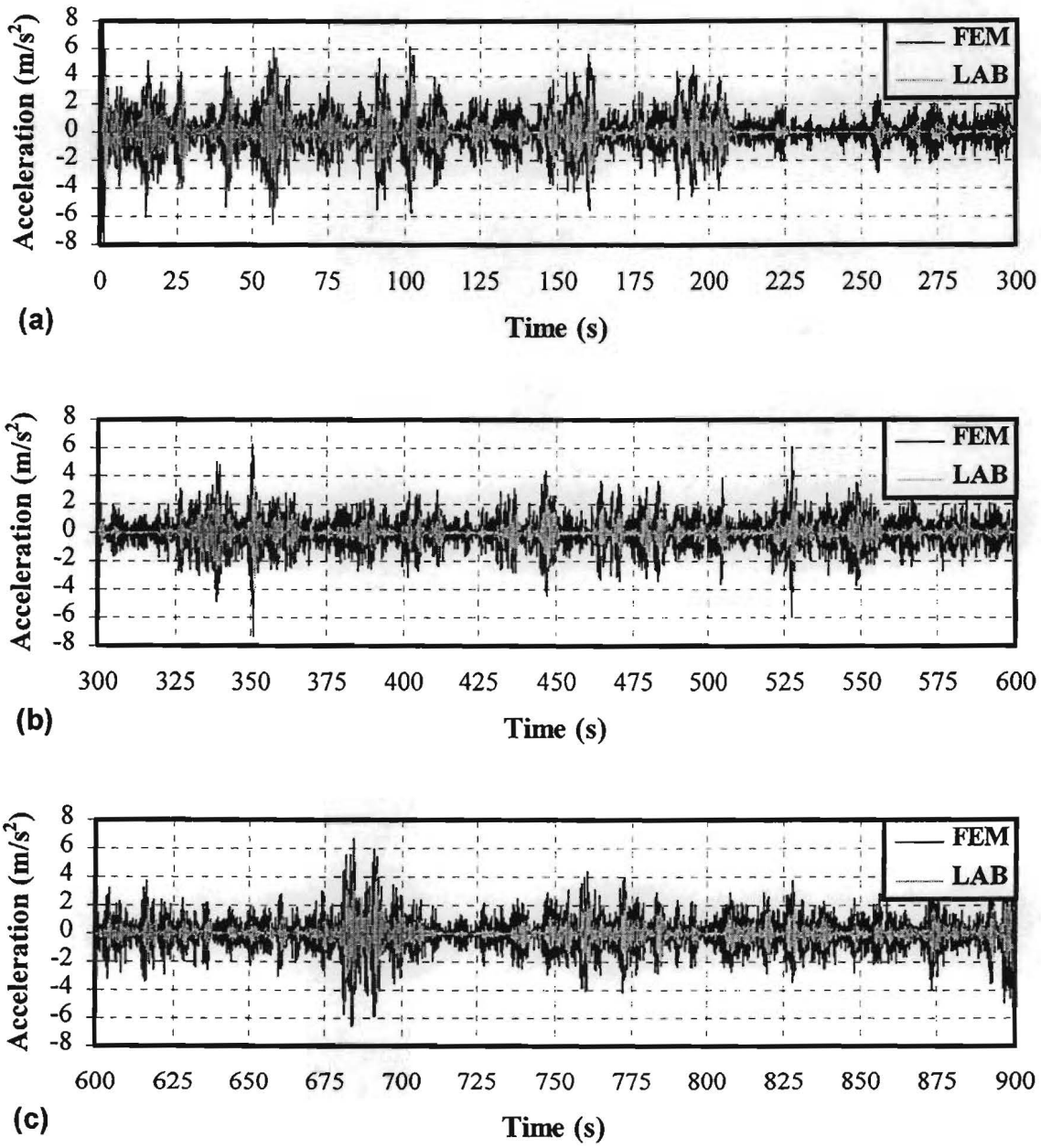

FIG. 114. Laboratory Simulated Response versus FEM for Post to M15H541: (a) 0-300 sec.; (b) 300-600 sec.; and (c) 600-900 sec.

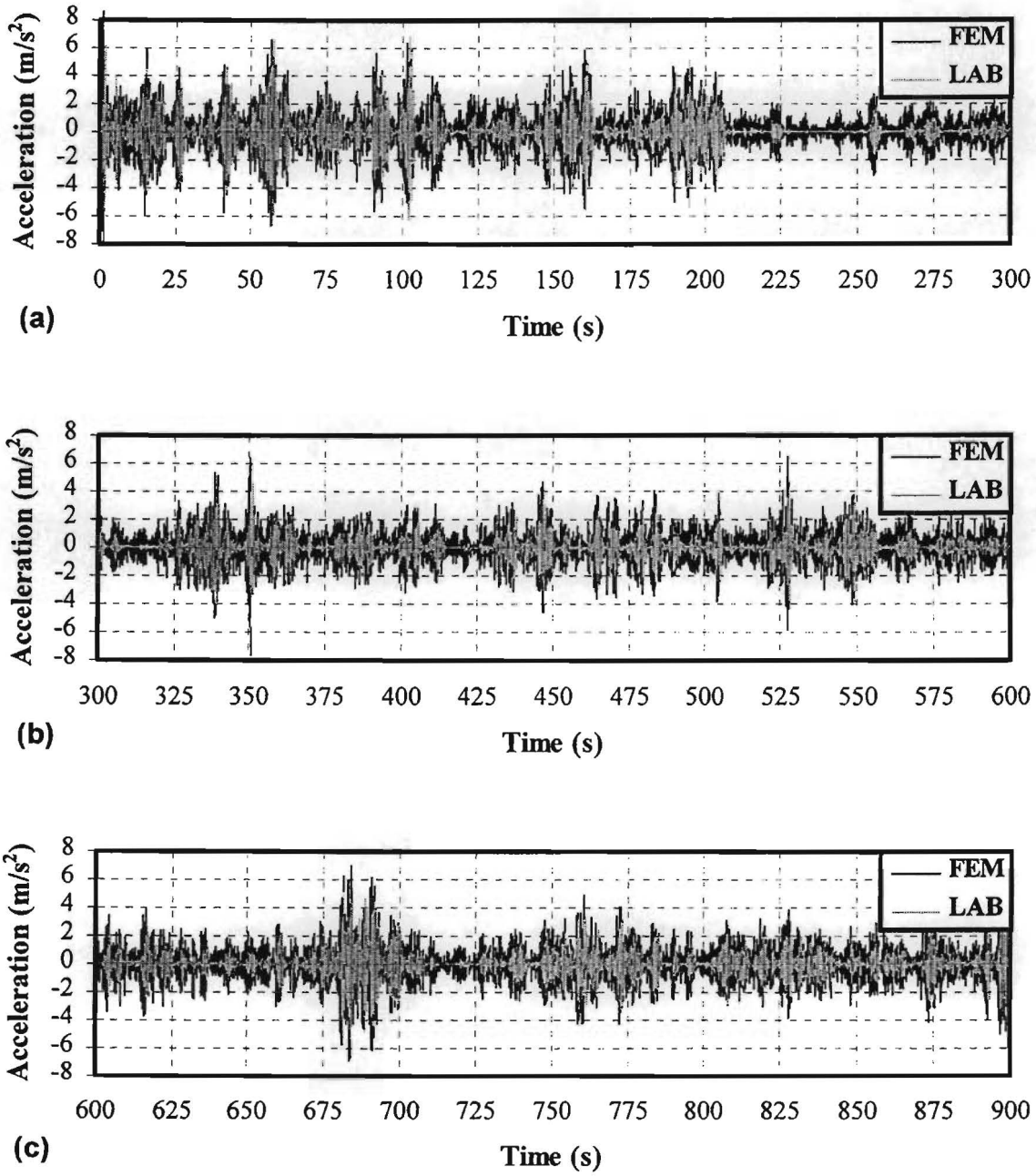

FIG. 115. Laboratory Simulated Response versus FEM for Center to M15H541: (a) 0-300 sec.; (b) 300-600 sec.; and (c) 600-900 sec.

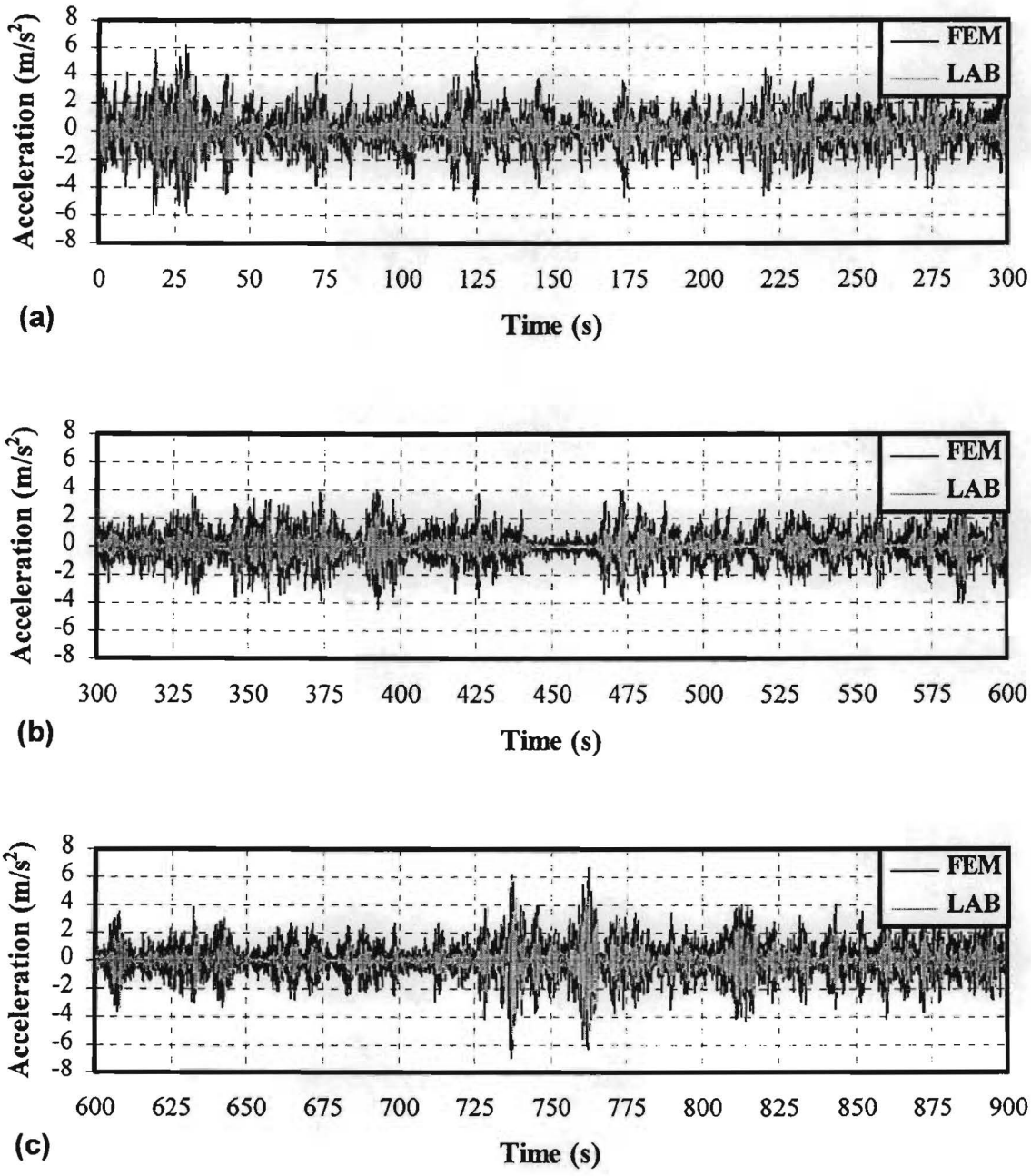

FIG. 116. Laboratory Simulated Response versus FEM for Edge to M15H571: (a) 0-300 sec.; (b) 300-600 sec.; and (c) 600-900 sec.

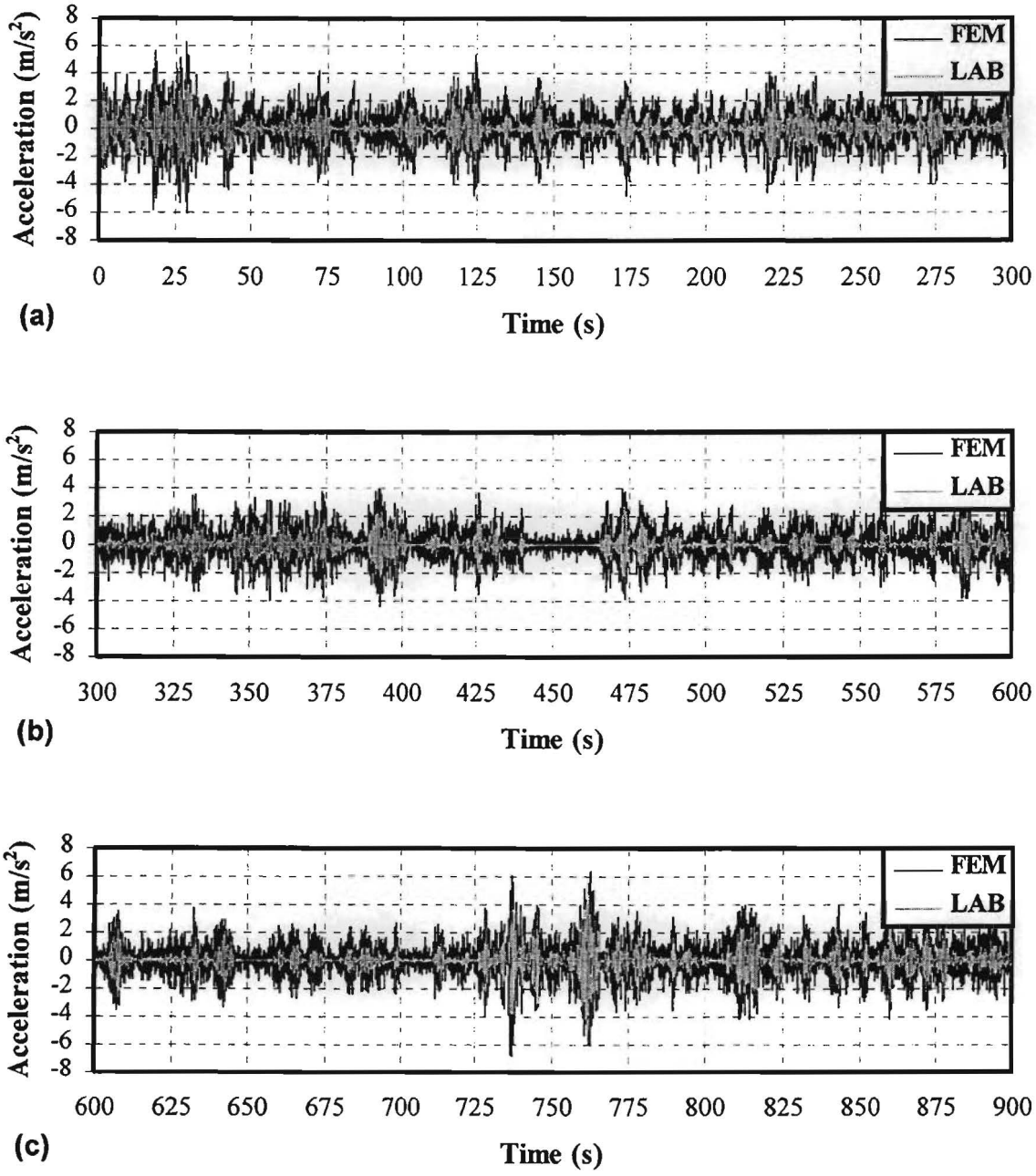

FIG. 117. Laboratory Simulated Response versus FEM for Post to M15H571: (a) 0-300 sec.; (b) 300-600 sec.; and (c) 600-900 sec.

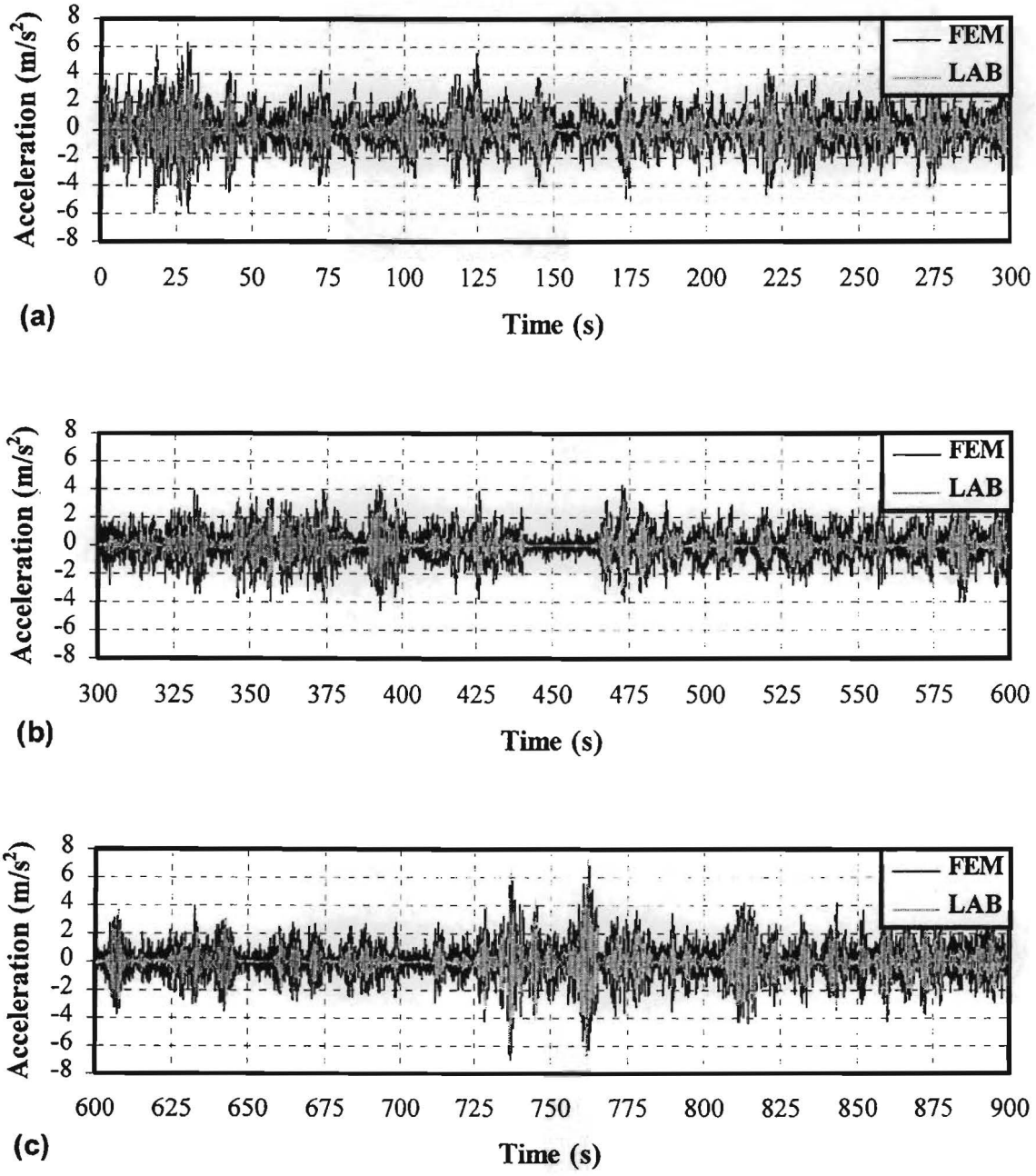

FIG. 118. Laboratory Simulated Response versus FEM for Center to M15H571: (a) 0-300 sec.; (b) 300-600 sec.; and (c) 600-900 sec.

The transfer functions are successful in simulating acceleration responses. Extreme positive accelerations were reproduced to within 20% in 4 out of 6 of the simulations (see Tables 25 and 26). Best results were obtained for simulation of accelerations at the edge of the sign using the M15H541 time history. Internal friction in the actuator caused a reduced level of excitation and the actuator was not be able to overcome the internal friction and excite the structure when actuator forces were low. This limitation was reflected in the differences between the standard deviation of the FEM and laboratory simulations. Comparison of a typical 25 second response shows how well the amplitude and frequency of the response were simulated in the laboratory (see Fig. 119).

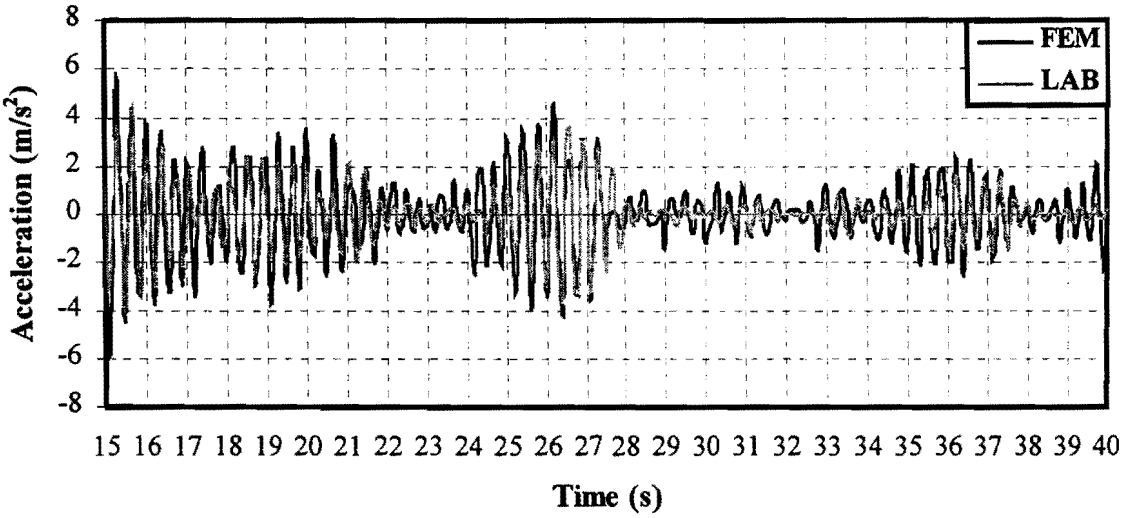

FIG. 119. Typical 25 Second Response

TABLE 25. Simulation Results for M15H541

Parameter (1)	FEM			Laboratory		
	Edge (2)	Post (3)	Center (4)	Edge (5)	Post (6)	Center (7)
Extreme Positive Acceleration	8.20 m/s^2	7.85 m/s^2	8.82 m/s^2	7.81 m/s^2	5.15 m/s^2	7.18 m/s^2
Extreme Negative Acceleration	-8.01 m/s^2	-7.75 m/s^2	-7.87 m/s^2	-6.68 m/s^2	-5.52 m/s^2	-8.04 m/s^2
Standard Deviation	1.47 m/s^2	1.42 m/s^2	1.49 m/s^2	1.03 m/s^2	0.68 m/s^2	0.95 m/s^2

TABLE 26. Simulation Results for M15H571

Parameter (1)	FEM			Laboratory		
	Edge (2)	Post (3)	Center (4)	Edge (5)	Post (6)	Center (7)
Extreme Positive Acceleration	6.75 m/s^2	6.47 m/s^2	6.86 m/s^2	5.75 m/s^2	4.69 m/s^2	7.29 m/s^2
Extreme Negative Acceleration	-6.88 m/s^2	-6.79 m/s^2	-6.94 m/s^2	-5.77 m/s^2	-4.90 m/s^2	-6.75 m/s^2
Standard Deviation	1.46 m/s^2	1.42m/s^2	1.49m/s^2	0.83 m/s^2	0.65 m/s^2	0.93 m/s^2

The procedure outlined in this chapter shows that wind induced structural vibrations may be approximated in a laboratory environment. Applications of this procedure to the design of roadside signs and other more traditional structures are extensive. For example, in recent field experiments conducted by TxDOT, an FRP sign substrate experienced brittle failure due to an impulsive wind load created by high speed passage of a large commercial vehicle. Wind time histories of these impulses could be recorded and simulations could be carried out in a laboratory environment in conjunction with FEA in order to characterize and incorporate these dynamic loads into the design procedure.

6. CONCLUSIONS

6.1 INTRODUCTION

Roadside signs are non-traditional structures, and the need for a formal investigation into their behavior, design, and analysis is extensive. The literature review and complementary investigations have both shown the potential benefit of using reclaimed materials in sign blanks. Moreover, it is apparent that there is a lack of experience pertaining to the design of these medium-sized sign structures with traditional or recycled materials. In the past, traditional wood and aluminum signs have been designed based on experience rather than engineering formulas. When reclaimed materials were initially investigated for use as recycled content sign blanks, failures in field trials of sign installations became a problem. Since the design of signs was not based upon any criteria or formula, it has been difficult to assimilate constructive information from a failed experiment.

In contrast, this study has sought to produce a method by which sign blanks made from recycled materials may be designed according to current engineering practices so that when failures do occur, the method may be refined and more knowledge may be gathered from field tests. As a serendipitous corollary to this approach, sign substrates made from traditional materials such as plywood and aluminum can also benefit from the performance-oriented specifications and design procedures.

6.2 MATERIALS

Concomitant with the development of a design procedure, this report provides information concerning basic mechanical properties and performance criteria of various reclaimed materials and how these materials compare to plywood, the current standard in Texas for medium-sized substrates. After solicitation of candidate materials from a broad range of manufacturers was complete, submitted sample materials were subjected to a series of mechanical tests including flexure, uni-axial tension, creep, and free vibration. Results of mechanical tests on these materials show that some materials, such as the Composite Technologies Corporation (CTC) specimen, have a modulus of elasticity that compares

favorably with plywood. However, the CTC material also shows a lack of ductility in uni-axial tension and relatively low damping properties. Field tests of this material in Utah also showed the potential for brittle cracking at the hardware connections during strong wind events. An alternative material with more ductility and a better ability to dissipate energy may have a lower tendency to exhibit this behavior.

Four materials were submitted for investigation by this study from Pelletech, Inc. These materials exhibited a variety of behaviors. For instance, VIWB is stiff, but also very dense. Like CTC, VIWB exhibits a poor ability to dissipate energy. Unlike CTC and VIWB, GTHW performed well under a broad range of loading and environmental conditions. It is relatively light due to a porous interior matrix that is surrounded by a rigid shell from which the material derives its strength. Although GTHW is one of the least stiff materials tested, it is also very lightweight making it one of the more efficient materials in the study. It exhibits a relatively high percent critical damping of 3.8% and a good level of ductility.

Since GTHW shows promise for use as a sign substrate along state highways, it was chosen as the material for a design example even though the material exhibits a moderate increase in creep at elevated temperatures. It would be important to submit a material such as GTHW to an extended field test so that effects of weathering and ultraviolet light rays can be more carefully evaluated. No extended field tests of materials were conducted in this research program.

An understanding of these fundamental mechanical and dynamic properties provides a base level of knowledge about a particular material so that it may be evaluated, designed, and scrutinized when placed in the field.

6.3 DESIGN PROCEDURE

A rational design procedure based on ASCE 7-95 and various deflection criteria was developed. This procedure, when incorporated with the proposed performance specifications (see Appendix A), provides a method that allows reclaimed materials to be approved for use as sign blanks. The procedure also makes it possible for the design of sign

blanks to become more efficient as more information is gathered on the types of wind and environmental loads to which roadside structures are subjected.

6.4 LABORATORY SIMULATION OF WIND ON SIGN BLANKS

In order to aid future investigations into the behavior of roadside signs under various load conditions, a laboratory procedure has been developed that allows the response of the sign to be closely approximated using an electro-mechanical actuator in a laboratory environment. Results show that acceleration responses for large wind events can be closely approximated in a laboratory environment. Extreme accelerations were reproduced to within 32% while maintaining the trend of the response time history.

6.5 COST

Estimated costs for 1.22 m × 2.44 m sheets of 1.27 cm recycled sign substrates are presented in Table 27. Approximate costs are given for orders ranging by order of magnitude from 1,000 to 1,000,000 sheets. These preliminary estimates of cost are for materials supplied by Pelletech, Inc.

TABLE 27. Approximate Cost of Recycled Content Sign Blanks

	Estimated Cost			
Material Code (1)	1,000 Sheets (2)	10,000 Sheets (3)	100,000 Sheets (4)	1,000,000 Sheets (5)
CMB	$80.80	$75.72	$72.28	$68.90
GTHW	$74.56	$69.87	$66.70	$63.58
SPAB	$145.00	$145.00	$145.00	$145.00
VIWB	$215.00	$215.00	$215.00	$215.00

6.6 CONSIDERATIONS FOR FUTURE STUDY

Recent field tests conducted on fiber-reinforced plastic signs by TxDOT have shown that impulsive wind loads created by large commercial vehicles are substantial enough to produce brittle failure in materials that are being considered for use in sign substrates. Future investigations could provide important information to the extent that they can characterize the nature of these gust events and the responses they produce in roadside signs.

The methods of structural design and analysis incorporated in this report along with careful selection of candidate materials can help develop sign substrates that make judicious use of reclaimed materials.

REFERENCES

AASHTO. (1994). "Standard Specifications for Structural Supports for Highway Signs, Luminaires and Traffic Signals." Washington, D.C.

AASHTO Subcommittee on Bridges and Structures. (1994). "Review of Structural Design Criteria for Noise Walls." Washington, D.C.

ASCE 7-95. (1995). "Minimum Design Loads for Buildings and Other Structures." American Society of Civil Engineers. New York, NY.

ASTM G53-94. (1994). "Practice for Operating Light-Exposure and Water-Exposure Apparatus (Fluorescent UV-Condensation Type) for Exposure of Nonmetallic Materials."

ASTM D638-91. (1991). "Standard Test Methods for Tensile Properties of Plastics."

ASTM D790-92. (1992). "Standard Test Methods for Flexural Properties of Unreinforced and Reinforced Plastics and Electrical Insulating Materials."

Blevins, R. D. (1984). *Applied Fluid Dynamics Handbook*, Van Nostrand Reinhold Co., New York, NY.

Ci65A Xenon Weather-Ometer. Atlas Electric Devices, Inc., Chicago, IL.

Chopra, A. K. (1995). *Dynamics of Structures*, First Edition, Prentice-Hall Co., Englewood Cliffs, NJ.

Clough, R. W. and Penzien, Joseph. (1993). *Dynamics of Structures*, Second Edition, McGraw-Hill Co., New York, NY.

Composite Technologies (1995). "Product Catalogue." Dayton, OH 45404.

FHWA. "Feasibiliy of Using Composite Materials in Construction." Army Corps of Engineers.

Flynn, L. (1993). "Environmental Regs, Issues Impact Industry." *Roads and Bridges* 31(7), 36-38.

Gallagher, J. J. and Donnally, J. L. (1995). "Field Evaluation of Recycled Flat Sheet Sign Substrates." Ohio Department of Transportation. Bureau of Traffic.

Huey, T. Interview.

Ketola, W. D. and Grossman, D. (1994). *Accelerated and Outdoor Durability Testing of Organic Materials*, ASTM, Philadelphia, PA.

Lindeburg, M. R. (1992). *Engineer-in-Training Reference Manual*, Eighth Edition, Professional Publications Co., Belmont, CA.

Lutes, L. D. and Sarkani, S. (1997). *Stochastic Analysis of Structural and Mechanical Vibrations*, First Edition, Prentice-Hall Co., Englewood Cliffs, NJ.

MATLAB®. "Reference Guide." The Math Works, Inc., Natick, MA. 01760.

Ministry of Transportation Ontario. (1993). "Development of Specifications for Plastic Lumber for Use in Highway Applications - Phase I."

Munson, B. R., Young, D. F., and Okiishi, T. H. (1994) *Fundamentals of Fluid Mechanics*, Second Edition, John Wiley and Sons Co., New York, NY.

NSCCRE. (1982). "Survey of Sign Vandalism and Theft in U.S." Chicago, IL.

Oregon Department of Transportation. (1994). "Laboratory Record on Recycling Highway Signs." Salem Sign Shop.

Reichmanis, E. F., Curtis, W., and O'Donnell, J. H. (1993). *Irradiation of Polymeric Materials Processes, Mechanisms, and Applications*, American Chemical Society, Washington, D.C.

Sequentia Incorporated. (1995). "Product Catalogue." Strongsville, OH.

Shephard, F. D. (1989). "Evaluation of Fibreglass Sign Panels." Virginia Department of Transportation.

Signs and Blanks, Inc. (1995). "Practicality and Benefits of Using Recycled 3105-H191 Aluminum Alloy for Ground Level Traffic Control Sign Substrates."

Smith, L. L. (1996). "Wasting No Time. Florida's History of Successful Recycling for Transportation." *TR News*, 184, May-June, 4-7.

Tennessee Department of Transportation. (1995). Personal communication.

Tokarczyk, B. (1996). "Mathematical Modeling of a Tuned Liquid Damper." Thesis to be presented to Texas A&M University. College Station, TX.

Transportation Research Board. (1992). "Maintenance Management of Street and Highway Signs." National Cooperative Highway Research Program, *Report Number 157*, Washington, D.C.

Utah Department of Transportation. (1995). Personal communication.

"Wood/Plastic Composite for Sound Walls." (1993). *Roads and Bridges* 30(11), 28.

APPENDIX A. PERFORMANCE SPECIFICATIONS

TEXAS DEPARTMENT OF TRANSPORTATION

Departmental Materials Specifications: X-X-XXXX

Recycled Content Sign Blanks

SCOPE

Sign panels are designed to serve as substrate for reflective sheeting in the fabrication of traffic signs. The following specifications define general characteristics, mechanical properties, and physical properties. ASTM test procedures are noted for each of the general specifications outlined below.

GENERAL CHARACTERISTICS

Panels will be manufactured from reclaimed materials and will satisfy the following general and specific material specifications. The sign panel shall be stabilized to prevent the release of migrating constituents over time and shall contain no residue release agents on the surface of the blank so that neither migrating constituents nor release agents will be present in amounts that will interfere with any subsequent bonding operation. The panel shall not contain surface imperfections including, but not limited to, visual cracks, pinholes, foreign inclusions, or surface wrinkles, that would impair the designed purpose, alter the specific dimensions, or effect serviceability.

MECHANICAL PROPERTIES

Mechanical properties shall be measured according to the modified ASTM test methods outlined in Chapter 3 (see Table 28).

TABLE 28. Required Mechanical Properties

Property (1)	ASTM Standard Test (2)	Document Section (3)
Tensile Strength	D638	3.3
Tensile Modulus	D638	3.3
Flexural Strength	D790	3.2
Flexural Modulus	D790	3.2
Creep	D2990	3.5
Damping	-	3.4

PRELIMINARY PERFORMANCE REQUIREMENTS

A set of "simple" performance criteria, or preliminary performance requirements, is detailed to aide manufacturers in developing suitable materials without performing expensive mechanical tests or Finite Element Analysis.

Panel Smoothness

Panels shall be manufactured with smooth surfaces on both sides of the panel. Deviations in smoothness may not adversely affect the adhesion of the reflective sheeting, reflectivity of the sheeting, or legibility of the sign.

Adhesion

Adhesiveness shall be checked in accordance to the Texas Department of Transportation Department Materials Specification D-9-8300, section 7, part 3 subpart d, stated as follows: sheeting or sign faces applied (according to manufacturer's instructions) to clean, smooth, paintable surfaces shall adhere so securely at all temperatures between -7° C to 79° C, that it is impossible to peel or pull material from the adhering surfaces in pieces containing areas greater than 1,290 mm^2; adhesion tests will be run no less than 48 hours after application; and reflective sheeting, with pressure sensitive adhesive, shall be aged 36 hours at 60° C.

Impact Resistance

The sign panel shall resist the impact of a 5.25 N ball dropped from 18.3 m in accordance with ASTM D3841.

Creep

A sign panel shall be placed in an outdoor environment and exposed to the suns rays. The substrate shall be leaned against a wall and left exposed for approximately one month. Noticeable out of plane deflections constitute failure.

Workability

Recycled content sign blanks shall be capable of being cut and drilled with wood-working tools.

SECONDARY PERFORMANCE REQUIREMENTS

Secondary performance requirements are to aide in the final selection of a suitable material. No design minimums are given so that a given material with a combination of strengths and weaknesses may still be suitable. For instance, a material with a low modulus of elasticity may have to be quite thick in order to have sufficient strength; however, if the material also has a low unit weight, the substrate may still be quite efficient. As a result the primary emphasis of the specification is on "in place" performance criteria.

Mechanical Tests

The materials must be subjected to the mechanical tests outlined in Table 28 so that a suitable substrate may be designed in accordance to the procedures outlined in this document.

Wind Simulation

The material will be subjected to a wind simulation in a laboratory or through the use of finite element analysis to determine if the material performs satisfactorily. Unsatisfactory performance includes exceeding any of the material yield limit states, cracking at the connections, and excessive vibrations that impair the legibility of the sign.

Thermal Stability

The material shall not show signs of excessive creep or brittle behavior at temperatures between -7° C to 79° C.

Field Testing

All candidate materials must be tested in the field for a period of at least one year. The variability in material properties and related performance necessitate such testing criteria.

APPENDIX B. FORTRAN ROUTINES

1. INTERPOLATION PROGRAM FOR AMPLITUDE OF TRANSFER FUNCTION

```
C    AMPLITUDE INTERPOLATION PROGRAM

C    ******************************************************
C    *                DEFINITION OF VARIABLES             *
C    *                                                    *
C    *          FR1,2=FREQUENCY ARRAY                     *
C    *          LE1,2=AMPLITUDE ARRAY LEFT EDGE           *
C    *          LP1,2= AMPLITUDE ARRAY LEFT POLE          *
C    *          CN1,2= AMPLITUDE ARRAY CENTER             *
C    *          RP1,2= AMPLITUDE ARRAY RIGHT POLE         *
C    *          RE1,2= AMPLITUDE ARRAY RIGHT EDGE         *
C    ******************************************************

C    ********************MAIN PROGRAM*********************
     DIMENSION AMP(5,80), AMP2(5,9000), FR(80), FREQ(9000)

     REAL AMP, AMP2, AMPL, AMPH, FR, FREQ, FREQH, FREQL, STEP1,STEP2
     INTEGER A,B,C,I,J,K,Z
     OPEN (UNIT=5,STATUS='OLD',FILE='TRANOLD.TXT')
     OPEN (UNIT=6,STATUS='NEW',FILE='TRANNEW1.TXT')
     OPEN (UNIT=7,STATUS='NEW',FILE='TRANNEW2.TXT')

C    ************************INPUT*************************
C    READ DATA
     A=0
     DO 10 A = 1,80
        READ(5,*) FR(A), (AMP(B,A),B=1,5)
10   CONTINUE

     CLOSE (5)


C    ************INITIALIZE INTERPOLATION VARIABLES******
     K=1
     STEP1=(1.0/8.0)
     STEP2=(1.0/900.0)
     FREQH=STEP1
     FREQL=0.0
     AMPL=0.0
```

```
C     ***************INTERPOLATION ROUTINE***************
      DO 30 J=1,9000
         FREQ(J)=J*STEP2
         DO 20 Z=1,5
         IF(FREQ(J).GT.FREQH) THEN
           K=K+1
           FREQL=FREQH
           FREQH=FREQH+STEP1
         ENDIF
         IF(K.EQ.1) THEN
          AMPL=0.0
         ELSE
          AMPL=AMP(Z,K-1)
         ENDIF
             AMPH=AMP(Z,K)
             AMP2(Z,J)=(AMPH-AMPL)*((FREQ(J)-FREQL)/STEP1)+AMPL

20           CONTINUE
30       CONTINUE
C     *****************MAKE FFT REFLECTIVE*****************
      K=9001
      DO 36 I=2,4500
        K=K-1
        DO 35 J=1,5
          AMP2(J,K)=AMP2(J,I)
35      CONTINUE
36    CONTINUE

C     ******************BUILD OUTPUT FILE******************

      DO 40 I=1,9000
      WRITE(6,*) FREQ(I),(AMP2(J,I),J=1,3)
      WRITE(7,*) (AMP2(J,I),J=4,5)
40    CONTINUE
      CLOSE (6)
      CLOSE (7)
      END
```

2. INTERPOLATION PROGRAM FOR PHASE OF TRANSFER FUNCTION

```
C    PHASE INTERPOLATION PROGRAM

C    ****************************************************
C    *              DEFINITION OF VARIABLES             *
C    *                                                  *
C    *          FR1,2=FREQUENCY ARRAY                   *
C    *          LE1,2=PHASE ARRAY LEFT EDGE             *
C    *          LP1,2=PHASE ARRAY LEFT POLE             *
C    *          CN1,2=PHASE ARRAY CENTER                *
C    *          RP1,2=PHASE ARRAY RIGHT POLE            *
C    *          RE1,2=PHASE ARRAY RIGHT EDGE            *
C    ****************************************************

C    ******************MAIN PROGRAM******************
     DIMENSION AMP(5,80), AMP2(5,9000), FR(80), FREQ(9000)

     REAL AMP, AMP2, AMPL, AMPH, FR, FREQ, FREQH, FREQL, STEP1,STEP2
     INTEGER A,B,C,I,J,K,Z
     OPEN (UNIT=5,STATUS='OLD',FILE='PHASEOLD.TXT')
     OPEN (UNIT=6,STATUS='NEW',FILE='PHASNEW1.TXT')
     OPEN (UNIT=7,STATUS='NEW',FILE='PHASNEW2.TXT')

C    ***********************INPUT************************
C     READ DATA
     A=0
     DO 10 A = 1,80
        READ(5,*) FR(A), (AMP(B,A),B=1,5)
10    CONTINUE

     CLOSE (5)


C    ********INITIALIZE INTERPOLATION VARIABLES******
K=1
      STEP1=(1.0/8.0)
      STEP2=(1.0/900.0)
      FREQH=STEP1
      FREQL=0.0
      AMPL=0.0
C     *************INTERPOLATION ROUTINE**************
      DO 30 J=1,9000
```

```
          FREQ(J)=J*STEP2
          DO 20 Z=1,5
          IF(FREQ(J).GT.FREQH) THEN
            K=K+1
            FREQL=FREQH
            FREQH=FREQH+STEP1
          ENDIF
          IF(K.EQ.1) THEN
           AMPL=0.0
          ELSE
           AMPL=AMP(Z,K-1)
          ENDIF
              AMPH=AMP(Z,K)
              AMP2(Z,J)=(AMPH-AMPL)*((FREQ(J)-FREQL)/STEP1)+AMPL
20            CONTINUE
30        CONTINUE
C     ************MAKE FFT REFLECTIVE AND CHANGE SIGN******
      K=9001
      DO 36 I=2,4500
        K=K-1
        DO 35 J=1,5
          AMP2(J,K)=-AMP2(J,I)
35      CONTINUE
36    CONTINUE

C     ******************BUILD OUTPUT FILE******************

      DO 40 I=1,9000
      WRITE(6,*) FREQ(I),(AMP2(J,I),J=1,3)
      WRITE(7,*) (AMP2(J,I),J=4,5)
40    CONTINUE
      CLOSE (6)
      CLOSE (7)
      END
```

APPENDIX C. MATLAB SESSION FILES (*.M)

1. MATLAB FILE FOR PERFORMING THE FAST FOURIER TRANSFORM

```
%%%%%%%%%%%%%%% INPUT PARAMETERS %%%%%%%%%%%%%%
load c:\path\filename.inp       % Input files
x=filename(:,:);          clear filename

sr=10;  % Data sampling rate of TT
%frcut=100;    % Frequency to truncate data
% when plotting

%%%%%%%%%%%%%%%%%%%%%%%%%%%%%%%%%%%%%%%%%%%%%%%%%%%%%%%%%%%%%%%%
a=x(:,2);
[nrt,noth]=size(a);
foura=fft(a);
durt=1/sr*nrt; clear nrt
delf=1/durt; clear durt
durf=2*sr/2;
foura=foura';
freq=[delf:delf:durf]';
%%%%%%%%%%%%%%%%%%%%%%%%%%%%%%%%%%%%%%%%%%%%%%%%%%%%%%%%%%%%%%%%
mag=abs(foura);
mag=mag';
ka=figure('Name','Magnitude','Position',[303 650 300 200]);
plot(freq(1:length(freq)),mag(1:length(freq)))
title('Magnitude')
xlabel('Frequency (Hz)')
ylabel('Amplitude')
grid on
ph=angle(foura);
ph=ph';
ka=figure('Name','Phase','Position',[303 320 300 200]);
plot(freq(1:length(freq)),ph(1:length(freq)))
title('Phase')
xlabel('Frequency (Hz)')
ylabel('Amplitude')
grid on
mat=[freq,mag(1:length(freq)),ph(1:length(freq))];
save c:\ben\fromjasn\filename.fft mat -ascii -tabs
```

2. MATLAB FILE FOR PERFORMING THE INVERSE FAST FOURIER TRANSFORM

```
load c:\ben\fromjasn\filename.fft  % Input files
x=filename(:,:);  clear filename

sr=10;  % Data sampling rate of TT
T=[1/sr:1/sr:length(x(:,2))/sr]';
delf=sr/length(x(:,2));
durf=sr/2;

mag=x(:,2);
ph=x(:,3);  clear x

foura1=mag.*exp(i*ph);
foura1=foura1';
a1=real(ifft(foura1))';

kh=figure('Name','Revised Actuator Time History','Position',[703 0 400 400]);
plot(T,a1)
title('Revised Actuator Time History')
xlabel('Time (sec)')
ylabel('Force (N)')
grid on

mat=[T,a1];
save c:\path\filename.tim   mat -ascii -tabs
```